



1 **A review of experimental techniques for aerosol hygroscopicity studies**

2

3 Mingjin Tang,^{1,*} Chak K Chan,^{2,*} Yong Jie Li,³ Hang Su,^{4,5} Qingxin Ma,⁶ Zhijun Wu,⁷ Guohua

4 Zhang,¹ Zhe Wang,⁸ Maofa Ge,⁹ Min Hu,⁷ Hong He,^{6,10,11} Xinming Wang^{1,10,11}

5

6 ¹ State Key Laboratory of Organic Geochemistry and Guangdong Key Laboratory of
7 Environmental Protection and Resources Utilization, Guangzhou Institute of Geochemistry,
8 Chinese Academy of Sciences, Guangzhou 510640, China

9 ² School of Energy and Environment, City University of Hong Kong, Kowloon, Hong Kong,
10 China

11 ³ Department of Civil and Environmental Engineering, Faculty of Science and Technology,
12 University of Macau, Avenida da Universidade, Taipa, Macau, China

13 ⁴ Center for Air Pollution and Climate Change Research (APCC), Institute for Environmental
14 and Climate Research (ECI), Jinan University, Guangzhou 511443, China

15 ⁵ Department of Multiphase Chemistry, Max Planck Institute for Chemistry, Mainz 55118,
16 Germany

17 ⁶ State Key Joint Laboratory of Environment Simulation and Pollution Control, Research
18 Center for Eco-Environmental Sciences, Chinese Academy of Sciences, Beijing 100085, China

19 ⁷ State Key Joint Laboratory of Environmental Simulation and Pollution Control, College of
20 Environmental Sciences and Engineering, Peking University, Beijing 100871, China

21 ⁸ Department of Civil and Environmental Engineering, The Hong Kong Polytechnic University,
22 Hong Kong, China

23 ⁹ State Key Laboratory for Structural Chemistry of Unstable and Stable Species, Institute of
24 Chemistry, Chinese Academy of Sciences, Beijing 100190, China

25 ¹⁰ University of Chinese Academy of Sciences, Beijing 100049, China



26 ¹¹ Center for Excellence in Regional Atmospheric Environment, Institute of Urban
27 Environment, Chinese Academy of Sciences, Xiamen 361021, China

28

29 Correspondence: Mingjin Tang (mingjintang@gig.ac.cn), Chak K. Chan
30 (Chak.K.Chan@cityu.edu.hk)

31

32 **Abstract**

33 Hygroscopicity is one of the most important physicochemical properties of aerosol
34 particles, and also plays indispensable roles in many other scientific and technical fields. A
35 myriad of experimental techniques, which differ in principles, configurations and cost, are
36 available for investigating aerosol hygroscopicity under subsaturated conditions (i.e., relative
37 humidity below 100%). A comprehensive review of these techniques is provided in this paper,
38 in which experimental techniques are broadly classified into four categories, according to the
39 way samples under investigation are prepared. For each technique, we describe its operation
40 principle and typical configuration, use representative examples reported in previous work to
41 illustrate how this technique can help better understand aerosol hygroscopicity, and discuss its
42 advantages and disadvantages. In addition, future directions are outlined and discussed for
43 further technical improvement and instrumental development.

44

45



46 **1 Introduction**

47 Aerosol particles are airborne solid or liquid particles in the size range of a few nanometers
48 to tens of micrometers. They can be emitted directly into the atmosphere (primary particles),
49 and can also be formed in the atmosphere (secondary particles) by chemical transformation of
50 gaseous precursors such as SO₂, NO_x, and volatile organic compounds (Pöschl, 2005; Seinfeld
51 and Pandis, 2016). Aerosol particles are of great concerns due to their environmental, health,
52 climatic and biogeochemical impacts (Finlayson-Pitts and Pitts, 2000; Jickells et al., 2005;
53 Mahowald, 2011; Mahowald et al., 2011; IPCC, 2013; Pöschl and Shiraiwa, 2015; Seinfeld
54 and Pandis, 2016; Shiraiwa et al., 2017b).

55 Water, which can exist in gas, liquid and solid states, is ubiquitous in the troposphere.
56 Interactions of water vapor with aerosol particles largely affect the roles that aerosol particles
57 play in the Earth system. When water vapor is supersaturated (i.e. when relative humidity, RH,
58 is >100%), aerosol particles can act as cloud condensation nuclei (CCN) to form cloud droplets
59 and as ice-nucleating particles (INPs) to form ice crystals (Pruppacher and Klett, 1997;
60 Lohmann and Feichter, 2005; Vali et al., 2015; Lohmann et al., 2016; Tang et al., 2016a; Knopf
61 et al., 2018; Tang et al., 2018). Cloud condensation nucleation and ice nucleation activities of
62 aerosol particles, as well as relevant experimental techniques, have been recently reviewed in
63 several books and review papers (Pruppacher and Klett, 1997; Hoose and Moehler, 2012;
64 Murray et al., 2012; Kreidenweis and Asa-Awuku, 2014; Farmer et al., 2015; Lohmann et al.,
65 2016; Tang et al., 2016a; Kanji et al., 2017), and are thus not further discussed in this paper.

66 When water vapor is unsaturated (i.e. RH <100%), an aerosol particle in equilibrium with
67 the surrounding environment would contain some amount of absorbed or adsorbed water
68 (Martin, 2000; Kreidenweis and Asa-Awuku, 2014; Cheng et al., 2015; Farmer et al., 2015;
69 Seinfeld and Pandis, 2016; Tang et al., 2016a; Freedman, 2017). The amount of water that a
70 particle contains depends on RH, temperature, its chemical composition, size, and etc. The



71 ability of a substance to absorb/adsorb water as a function of RH is typically termed as
72 hygroscopicity (Adams and Merz, 1929; Su et al., 2010; Kreidenweis and Asa-Awuku, 2014;
73 Tang et al., 2016a), and the underlying thermodynamic principles can be found elsewhere
74 (Martin, 2000; Seinfeld and Pandis, 2016). A single-component particle which contains one of
75 water soluble inorganic salts, such as $(\text{NH}_4)_2\text{SO}_4$ and NaCl, is solid at low RH. When RH is
76 increased to the deliquescence relative humidity (DRH), the solid particle will undergo
77 deliquescence to form an aqueous particle, and the aqueous particle at DRH is composed of a
78 saturated solution (Cheng et al., 2015). Further increase in RH would increase the water content
79 of the aqueous droplet, i.e. the aqueous particle would become more diluted as RH increases.
80 During humidification thermodynamics determines phase transition and hygroscopic growth
81 of the particle. During dehumidification, an aqueous particle would not undergo efflorescence to
82 form a solid particle when RH is decreased to below DRH; instead, the aqueous particle would
83 become supersaturated. Only when RH is further decreased to efflorescence relative humidity
84 (ERH), the aqueous particle would undergo crystallization, leading to the formation of a solid
85 particle. Therefore, efflorescence is also kinetically controlled and there is a hysteresis between
86 deliquescence and efflorescence. Deliquescence and efflorescence of multicomponent particles
87 can be more complicated (Seinfeld and Pandis, 2016).

88 It should be pointed out that not all the single-component particles exhibit distinctive
89 deliquescence and efflorescence. Instead, continuous uptake or loss of liquid water is observed
90 during humidification and dehumidification processes for many inorganic and organic particles
91 (Mikhailov et al., 2009; Koop et al., 2011; Shiraiwa et al., 2011). Particles with extremely low
92 hygroscopicity (e.g., mineral dust) will not be deliquesced even at very high RH; instead,
93 adsorbed water will be formed on the particle surface (Tang et al., 2016a). Furthermore, a
94 multicomponent particle which contains some types of organic materials may undergo liquid-
95 liquid phase separation, leading to the formation two coexisting liquid phases in one particles



96 (Mikhailov et al., 2009; You et al., 2012; You et al., 2014; Freedman, 2017; Song et al., 2017;
97 Song et al., 2018). It is conventionally assumed that hygroscopic equilibrium of aerosol
98 particles can be quickly reached. Nevertheless, recent laboratory, field and modeling studies
99 suggested that atmospherically relevant particles can be semi-solid or amorphous solid
100 (Virtanen et al., 2010; Zobrist et al., 2011; Renbaum-Wolff et al., 2013; Shiraiwa et al., 2017a;
101 Reid et al., 2018). The viscosity of these particles can be high enough such that uptake or
102 release of water is largely limited by diffusion of water molecules in the bulk phase of these
103 particles.

104 Hygroscopicity determines the amount of water that a particle contains under a given
105 condition and thereby has several important implications. It affects the size and refractive
106 indices of aerosol particles, affecting their optical properties and consequently their impacts on
107 visibility and direct radiative forcing (Malm and Day, 2001; Chin et al., 2002; Quinn et al.,
108 2005; Hand and Malm, 2007; Cheng et al., 2008; Eichler et al., 2008; Liu et al., 2012; Liu et
109 al., 2013b; Brock et al., 2016b; Titos et al., 2016; Haarig et al., 2017). Hygroscopicity is also
110 closely related to the CCN activity of aerosol particles, affecting their impacts on formation
111 and properties of clouds and thus their indirect radiative forcing (McFiggans et al., 2006;
112 Petters and Kreidenweis, 2007; Reutter et al., 2009; Kreidenweis and Asa-Awuku, 2014;
113 Farmer et al., 2015). Aerosol liquid water and/or surface-adsorbed water, largely controlled by
114 hygroscopicity, determines heterogeneous and multiphase reactions of aerosol particles via
115 several mechanisms, as revealed by recent studies (Bertram and Thornton, 2009; Shiraiwa et
116 al., 2011; Rubasinghege and Grassian, 2013; Cheng et al., 2016; Wang et al., 2016; Tang et al.,
117 2017; Mu et al., 2018; Wu et al., 2018). In addition, hygroscopicity significantly impacts dry
118 and wet deposition rates of aerosol particles and thus their lifetimes, spatiotemporal distribution
119 and environmental and health effects (Fan et al., 2004; Wang et al., 2014a). For primary
120 biological aerosols in specific, changes in their atmospheric transport behavior have important



121 implications for the spread of plants and microbes and therefore the evolution of ecosystems
122 (Brown and Hovmoller, 2002; Després et al., 2012; Fisher et al., 2012; Fröhlich-Nowoisky et
123 al., 2016).

124 Atmospheric aerosol is only one of many fields in which hygroscopicity is of great interest.
125 Hygroscopicity is closely linked to water activities and thermodynamics of solutions (Atkins,
126 1998). It also determines the amount of surface-adsorbed water and surface reactivity of
127 various solid materials, and has been widely investigated in surface science and heterogeneous
128 catalysis (Miranda et al., 1998; Ewing, 2006; Yamamoto et al., 2010b; Chen et al., 2012;
129 Rubasinghege and Grassian, 2013; Liu et al., 2017). Hygroscopicity is related to the possible
130 existence of liquid water in some hyperarid environments (such as Mars and the Atacama
131 Desert on earth) (Martin-Torres et al., 2015): while pure liquid water is not stable in these
132 environments, the deliquescence of some salts, such as chlorides and perchlorates, can occur
133 at RH significantly below 100% and lead to the formation of aqueous solutions (Gough et al.,
134 2011; Gough et al., 2016; Gu et al., 2017a; Jia et al., 2018). Hygroscopic properties
135 significantly affect transport and deposition of inhaled aerosol particles in the respiratory tract,
136 therefore playing an important role in the health impact of ambient aerosols as well as efficacy
137 and side effects of aerosolized pharmaceuticals (Hickey and Martonen, 1993; Robinson and
138 Yu, 1998; Carvalho et al., 2011; Hofmann, 2011; Haddrell et al., 2014; Winkler-Heil et al.,
139 2014; Darquenne et al., 2016; Davidson et al., 2017; Winkler-Heil et al., 2017). Impacts of
140 moisture and implications of hygroscopicity have been well documented for physical and
141 chemical stability of pharmaceuticals (Ahlneck and Zografis, 1990; Chan et al., 1997; Peng et
142 al., 2000; Newman et al., 2008; Mauer and Taylor, 2010b; Tong et al., 2010a; Feth et al., 2011)
143 as well as food ingredients and blends (Mauer and Taylor, 2010a; Allan and Mauer, 2016), and
144 large efforts have been made in pharmaceutical and food industry to prevent relevant products
145 from deliquescence. Corrosion and degradation of various constructions and buildings depend



146 largely on RH, and as a result both chemical inertness and hygroscopicity of materials used
147 should be taken into account (Schindelholz et al., 2014a; Schindelholz et al., 2014b; Vainio et
148 al., 2016); in addition, deposition of particles of different compositions has also been shown to
149 affect the extent of corrosion of mild steel (Lau et al., 2008).

150 As summarized in this paper, a number of experimental techniques, which differ largely
151 in principles, configurations and cost, have been developed to investigate hygroscopic
152 properties of atmospherically relevant particles. Hygroscopic properties investigated at <100%
153 RH typically include the amount of water absorbed/adsorbed by particles as a function of RH,
154 as well as DRH and ERH if they exist. Techniques employed to investigate aerosol
155 hygroscopicity under supersaturation, commonly termed as CCN activity, are relatively less
156 diverse, and interested readers are referred to relevant literature (Nenes et al., 2001; Roberts
157 and Nenes, 2005; Kreidenweis and Asa-Awuku, 2014) for further information. In addition,
158 technique used to study ice nucleation have been discussed in a number of recent papers
159 (DeMott et al., 2011; Murray et al., 2012; Ladino et al., 2013; DeMott et al., 2018) and as a
160 result are not further discussed here.

161 Several review papers and book chapters have discussed some of these techniques used to
162 investigate aerosol hygroscopicity. For example, Kreidenweis and Asa-Awuku (2014)
163 discussed a few widely used techniques for aerosol hygroscopicity measurements, and Tang et
164 al. (2016) summarized in brief experimental techniques used to investigate water adsorption
165 and hygroscopicity of mineral dust particles. There are also a few review papers focused on a
166 specific technique or a specific category of techniques. For example, Swietlicki et al. (2008)
167 reviewed aerosol hygroscopicity measured in various environments using humidity-tandem
168 differential mobility analysers, and provided a nice overview of this technique; application of
169 single particle levitation techniques to investigate properties and processes of aerosol particles,
170 including aerosol hygroscopicity, was reviewed by Krieger et al. (2012); Titos et al. (2016)



171 reviewed techniques used to investigate the effect of hygroscopic growth on aerosol light
172 scattering, and Ault and Axson (2017) summarized and discussed recent advancements in
173 spectroscopic and microscopic methods for characterization of aerosol composition and
174 physicochemical properties.

175 Nevertheless, to our knowledge there is hitherto no paper or book which covers most of
176 (if not all) experimental techniques used for hygroscopicity measurements. This paper aims at
177 providing the first comprehensive review in this field. For each technique, we first introduce
178 its operation principle and typical configurations, and then use exemplary results to illustrate
179 how this technique can help better understand hygroscopic properties. According to the way
180 samples under investigation are prepared, experimental techniques covered in this paper are
181 classified into four categories, which are discussed in Sections 2-5. In Section 2, we discuss
182 experimental techniques applied to bulk solutions. Experimental techniques for particles
183 deposited on substrates, levitated single particles and aerosol particles are reviewed in Sections
184 3-5, respectively. Remote sensing techniques can also be employed to retrieve aerosol
185 hygroscopicity (Ferrare et al., 1998; Feingold and Morley, 2003; Pahlow et al., 2006; Schuster
186 et al., 2009; Li et al., 2013; Lv et al., 2017; Bedoya-Velasquez et al., 2018; Fernandez et al.,
187 2018); however, they are not covered in this paper because we intend to focus on in-situ
188 techniques and application of remote sensing to investigate aerosol hygroscopicity has been
189 discussed very recently in a book chapter (Kreidenweis and Asa-Awuku, 2014). In addition,
190 techniques for measuring CCN and IN activities of aerosol particles are not covered in the
191 present paper, and interested readers are referred to relevant literature (Roberts and Nenes,
192 2005; Lance et al., 2006; Petters et al., 2007; Good et al., 2010a; DeMott et al., 2011; Latham
193 and Nenes, 2011; Hiranuma et al., 2015; Wex et al., 2015).



194 **2 Bulk solution-based techniques**

195 In principle, the hygroscopicity of a compound can be determined by measuring the water
196 vapor pressure of air over (i.e. in equilibrium with) the aqueous solution at a given
197 concentration (Pitzer, 1991; Rard and Clegg, 1997). Experimental data can then be used to
198 derive water-to-solute ratios as a function of RH for aqueous solutions, and the RH over the
199 saturated solution can generally be regarded as the DRH. Experimental methods based on this
200 principle have been widely used since the early 20th century (or probably even earlier) (Adams
201 and Merz, 1929; Hepburn, 1932) and are still being used (Königsberger et al., 2007; Sadeghi
202 and Shahebrahimi, 2011; Golabiazar and Sadeghi, 2014) to investigate thermodynamic
203 properties of aqueous solutions. In general, these methods can be further classified to two
204 categories, i.e. isopiestic and nonisopiestic methods (Rard and Clegg, 1997).

205 **2.1 The isopiestic method**

206 The isopiestic method was described in a number of previous studies (Spedding et al., 1976;
207 Rard and Miller, 1981; Pitzer, 1991; Hefter et al., 1997; Rard and Clegg, 1997; Königsberger
208 et al., 2007), and a brief introduction is provided herein. For a typical experiment, two open
209 vessels which contain a reference solution and a sample solution are housed in a sealed chamber
210 with temperature being well controlled, and water vapor will be transferred between the two
211 solutions until an equilibrium is reached. For the reference solution, its water activity should
212 be well documented as a function of concentration. When the equilibrium is reached, the water
213 activity of the sample solution is equal to that of the reference solution. If we measure the
214 concentrations of the two solutions in equilibrium, the water activity of the sample solution at
215 a given concentration can then be determined.

216 **2.2 Nonisopiestic techniques**

217 The water vapor pressure over (or the water activity of) an aqueous solution can be
218 determined using a number of methods (Rard and Clegg, 1997), including but not limited to (i)



235 The RH of air over 10 mL aqueous solutions which were contained in sealed test tubes
236 kept at constant temperatures were measured by Tolbert and coworkers (Brooks et al., 2002;
237 Wise et al., 2003) to investigate water activities as a function of solution concentration. In the
238 first study (Brooks et al., 2002), RH over saturated solutions were measured for $(\text{NH}_4)_2\text{SO}_4$,
239 several dicarboxylic acids, as well as mixtures of $(\text{NH}_4)_2\text{SO}_4$ with individual dicarboxylic acids
240 to determine their DRH. As shown in Fig. 1, the DRH values of $(\text{NH}_4)_2\text{SO}_4$ measured by
241 Brooks et al. (2002) agreed well with those reported in previous studies (Cziczo et al., 1997;
242 Tabazadeh and Toon, 1998; Cziczo and Abbatt, 1999; Onasch et al., 1999; Braban et al., 2001)
243 for temperature ranging from ~250 to ~300 K, confirming that the simple technique could
244 determine DRH in a reliable manner. It was further found that the presence of water soluble
245 dicarboxylic acids would reduce the DRH of $(\text{NH}_4)_2\text{SO}_4$, whereas the presence of less soluble
246 dicarboxylic acids had no measurable effects (Brooks et al., 2002). In a following study (Wise
247 et al., 2003), RH of air over eutonic mixtures of $(\text{NH}_4)_2\text{SO}_4$ /dicarboxylic acids were measured
248 at 25 °C to investigate the effect of organic acids on hygroscopic growth of $(\text{NH}_4)_2\text{SO}_4$. The
249 presence of water soluble dicarboxylic acids reduced hygroscopic growth of $(\text{NH}_4)_2\text{SO}_4$, while
250 the effect of less soluble dicarboxylic acids were found to be negligible (Wise et al., 2003).

251 Water activity meters, which measure the dew point temperature of the air in equilibrium
252 with an aqueous sample, are commercially available (Maffia and Meirelles, 2001; Marcolli et
253 al., 2004; Salcedo, 2006). For example, water activities meters were employed by Salcedo
254 (2006) and Maffia and Meirelles (2001) to study hygroscopic properties of organic acids and
255 their mixtures with $(\text{NH}_4)_2\text{SO}_4$ and NH_4HSO_4 at 25 °C.

256 **2.3 Discussion**

257 Bulk solution-based techniques have the advantage of being inherently accurate and very
258 simple, while one major drawback is that these measurement cycles can be very time-
259 consuming, typically taking days up to months to reach the equilibrium (Königsberger et al.,



260 2007). Particle water content can be quantitatively determined for unsaturated solutions,
261 whereas no information can be provided for supersaturated solutions. Bulk solution-based
262 methods do not require particle sphericity assumption to derive particle water content, but
263 cannot be used to study water adsorption. Generally speaking, while these techniques are useful
264 for understanding properties of deliquesced particles, they are not applicable for direct
265 measurements of ambient aerosol particles.

266 **3 Particles deposited on substrates**

267 In this section we review and discuss techniques which can be used to investigate
268 hygroscopic properties of particles (either particle ensembles or individual particles) deposited
269 on substrates. This section is further divided to five parts: techniques for which changes in
270 water vapor and particle mass are measured to investigate particle hygroscopicity are reviewed
271 in Sections 3.1 and 3.2, and microscopic and spectroscopic tools employed to investigate
272 particle hygroscopicity are reviewed in Sections 3.3 and 3.4. Measurements of change in
273 electrical conductivity for understanding hygroscopic properties of particles are briefly
274 discussed in Section 3.5.

275 **3.1 Measurement of water vapor**

276 Particles would absorb/adsorb water vapor from the gas phase to reach a new equilibrium
277 as RH increases, while water vapor will be released if RH decreases. Measurement of change
278 in water vapor can be used to investigate hygroscopic properties. Exposure of water vapor to
279 particles can be achieved either in a static cell or in a flow cell.

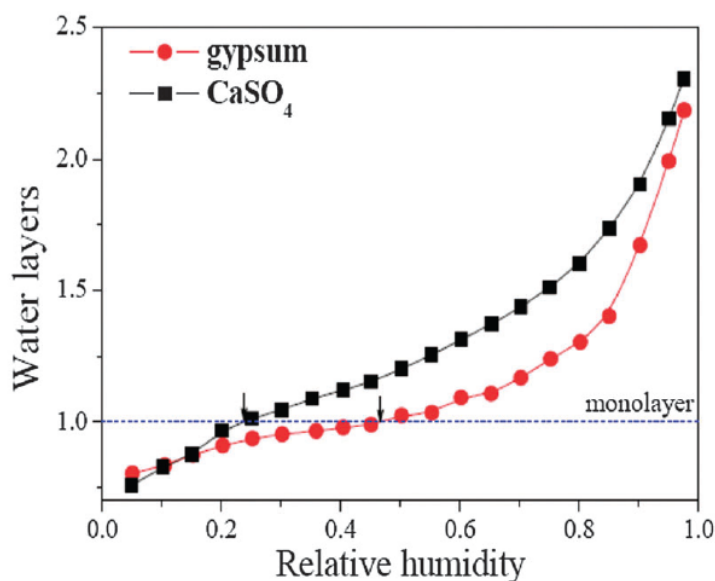
280 **3.1.1 Physisorption analyser**

281 When exposed to water vapor, particles will absorb/adsorb water vapor, leading to
282 depletion of water vapor in the system. The amount of water absorbed/adsorbed by particles
283 can be determined from the measured change in water vapor pressure (if the volume remains
284 constant), and the RH can be calculated from the final water vapor pressure when the



285 equilibrium is reached. The amount of water associated with particles can be determined as a
286 function of RH by varying the initial water vapor pressure.

287 Commercial instruments, usually designed to measure the Brunauer-Emmett-Teller (BET)
288 surface areas using nitrogen or helium (Torrent et al., 1990), have been utilized to investigate
289 hygroscopic properties of atmospherically relevant particles (Ma et al., 2010b; Ma et al., 2012b;
290 Hung et al., 2015). For example, Ma et al. (2010b) integrated an AUTOSORB-1-C instrument
291 (Quantachrome, US) with a water vapor generator, and employed this apparatus to investigate
292 hygroscopic properties of NaCl, NH_4NO_3 and $(\text{NH}_4)_2\text{SO}_4$. The measured DRH values and mass
293 hygroscopic factors were found to agree very well with those reported in literature (Ma et al.,
294 2010b). This method has proved to be very sensitive; as shown in Fig. 2, change in adsorbed
295 water as small as <0.5 monolayer can be reliably quantified (Ma et al., 2013a). In addition to
296 CaSO_4 and gypsum, this instrument was also employed to investigate hygroscopic properties
297 of fresh and aged Al_2O_3 , MgO and CaCO_3 particles (Ma et al., 2012a).



298



299 **Figure 2.** Water adsorption isotherms of CaSO_4 (black square) and gypsum ($\text{CaSO}_4 \cdot 2\text{H}_2\text{O}$, red
300 circle) at 278 K. Reprinted with permission by Ma et al. (2013a). Copyright 2013 the PCCP
301 Owner Societies.

302

303 A similar instrument (Micromeritics ASAP 2020) was employed by Hung et al. (2015) to
304 examine the hygroscopicity of black carbon, kaolinite and montmorillonite particles at 301 K,
305 and a sensitivity of sub-monolayers of adsorbed water could be achieved. Assuming a dry
306 particle diameter of 200 nm, the single hygroscopicity parameters, κ , were determined to be
307 ~ 0.002 for montmorillonite and < 0.001 for both black carbon and kaolinite (Hung et al., 2015).

308 This technique is able to quantify particle water content for unsaturated samples, and is
309 sensitive enough to measure adsorbed water; however, it cannot be (at least has not been) used
310 to examine supersaturated samples. This technique, which is independent on particle size and
311 morphology, can also been used to investigate hygroscopic properties of ambient aerosol
312 particles in an offline manner. For example, a physisorption analyser was used to study
313 hygroscopic properties of ambient aerosol particles collected in Beijing during an Asian dust
314 storm, and one monolayer of adsorbed water was formed on these particles at 46% RH (Ma et
315 al., 2012b).

316 3.1.2 Katharometer

317 The katharometer, also known as the thermal conductivity detector, can be used to measure
318 water vapor concentration. Lee and co-workers employed a katharometer to investigate liquid
319 water content of aerosol particles collected on filters (Lee and Hsu, 1998; Lee and Hsu, 2000;
320 Lee and Chang, 2002). In this setup (Lee and Chang, 2002), aerosol particles were collected
321 on a Teflon filter and then equilibrated with a helium flow at a given RH; after the equilibrium
322 was reached, the particle-loaded filter was purged with a dry helium flow, which was
323 subsequently directed to a katharometer to measure the water vapor concentration. As a result,



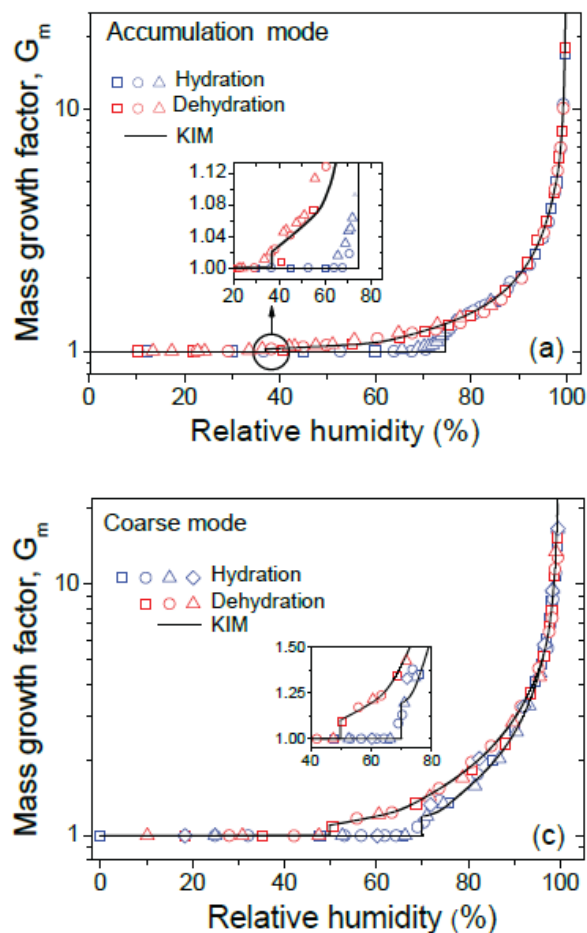
324 the liquid water content associated with particles at a given RH could be quantified. The
325 performance of this new method was systematically examined (Lee and Hsu, 1998; Lee and
326 Hsu, 2000; Lee and Chang, 2002), and the measured water-to-solute ratios at different RH
327 during both humidification and dehumidification processes were found to agree well with those
328 reported in literature for several compounds, including NaCl, NH₄Cl, Na₂SO₄, (NH₄)₂SO₄ and
329 NH₄NO₃.

330 Mikhailov et al. (2011, 2013) also developed a katharometer-based method to investigate
331 aerosol hygroscopicity. The instrument, called filter-based differential hygroscopicity analyser
332 (FDHA), are described elsewhere (Mikhailov et al., 2011), and a brief introduction is provided
333 here. In this apparatus, a humidified helium flow was split to two identical flows which were
334 then passed through a pair of differential measurement cells: the reference cell contained a
335 blank filter, and the sample cell contained a filter laden with particles (typically less than 0.1
336 mg). The difference in water vapor concentrations in these two cells, caused by
337 absorption/adsorption of water by particles loaded on the filter, was measured using a
338 differential katharometer, and the amount of water taken up by particles could be quantified by
339 integration of the katharometer signals over time. This instrument could measure hygroscopic
340 growth at very high RH (up to 99%).

341 Hygroscopic properties of (NH₄)₂SO₄, NaCl, levoglucosan, malonic acid, and mixed
342 (NH₄)₂SO₄/malonic acid particles were examined using FDHA at different RH during
343 humidification and dehumidification (Mikhailov et al., 2013), and the measured mass growth
344 factors agreed well with those reported in literature. This instrument was further employed to
345 investigate hygroscopic properties of particles collected from a pristine tropical rainforest (near
346 Manaus, Brazil) (Mikhailov et al., 2013), a suburban boreal forest site (near the city of St.
347 Petersburg, Russia) (Mikhailov et al., 2013) and a remote boreal site (the Zotino Tall Tower
348 Observatory, ZOTTO) in Siberia (Mikhailov et al., 2015). Fig. 3 displays the measured



349 hygroscopic properties of aerosol particles collected at the ZOTTO site. As shown in Fig. 3,
350 both supermicrometer and submicrometer particles started to uptake substantial amount of
351 water at ~70% RH; nevertheless, efflorescence took place at different RH, with ERH being
352 ~35% RH for submicrometer particles and ~50% RH for supermicrometer particles (Mikhailov
353 et al., 2015). It was suggested that the observed difference in ERH could be explained by the
354 difference in organic contents in submicrometer and supermicrometer particles (Mikhailov et
355 al., 2015): submicrometer particles contained larger fractions of organic materials,
356 consequently leading to the reduction of ERH.



357



358 **Figure 3.** Mass growth factors of particles collected at the ZOTTO site in Serbia in June 2013:
359 (upper panel) accumulation mode; (lower panel) coarse mode. The solid curves represents
360 simulations using the κ_m -interaction model (KIM). Reprinted with permission by Mikhailov et
361 al. (2015). Copyright 2015 Copernicus Publications.

362

363 The katharometer-based technique can be used to determine particle water content for
364 unsaturated and supersaturated samples, independent of particle size and morphology (Lee and
365 Chang, 2002; Mikhailov et al., 2013). It has also been successfully used as an offline method
366 to investigate hygroscopic properties of ambient aerosol particles (Mikhailov et al., 2013;
367 Mikhailov et al., 2015). It remains to be tested whether this technique is sensitive enough to
368 investigate water adsorption of a few monolayers or less.

369 3.1.3 Knudsen cell reactor

370 Knudsen cell reactors are low-pressure reactors widely used to investigate heterogeneous
371 uptake of trace gases (Al-Abadleh and Grassian, 2000; Karagulian and Rossi, 2005; Karagulian
372 et al., 2006; Wagner et al., 2008; Liu et al., 2009; Zhou et al., 2012). This technique was also
373 employed in several studies to explore water adsorption by particles with atmospheric
374 relevance (Rogaski et al., 1997; Seisel et al., 2004; Seisel et al., 2005). For example, the initial
375 uptake coefficient was reported to be 0.042 ± 0.007 for uptake of water vapor by Saharan dust
376 at 298 K (Seisel et al., 2004). Another study (Rogaski et al., 1997) found that pretreatment with
377 SO_2 , HNO_3 and H_2SO_4 could significantly increase water uptake by amorphous carbon.
378 Knudsen cell reactors are normally operated in the molecular flow regime, and thus water vapor
379 pressure used in these experiments is extremely low. As a result, although these measurements
380 can provide mechanistic insights into the interaction of water vapor with particles at the
381 molecular level, limited information on aerosol hygroscopicity under atmospheric conditions
382 can be provided.



383 **3.2 Measurement of sample mass**

384 Aerosol hygroscopicity can be quantitatively determined by measuring the mass of
385 particles as a function of RH under isotherm conditions. This can be achieved by several types
386 of experimental techniques, as introduced below.

387 **3.2.1 Analytical balance**

388 In a simple manner, the change in particle mass due to water uptake can be measured using
389 an analytical balance under well controlled conditions (Hänel, 1976; McInnes et al., 1996;
390 Hitzenberger et al., 1997; Diehl et al., 2001). For example, Diehl et al. (2001) investigated
391 hygroscopic properties of ten pollen species at room temperature, using an analytical balance
392 housed in a humidification chamber. The mass of pollen samples were measured at 0, (73±4)
393 and (95±2)% RH. The average ratios of the mass of adsorbed water to dry mass increased from
394 around 0.1 at 73% RH to ~3 at 95% RH (Diehl et al., 2001), suggesting that pollen samples
395 can adsorb substantial amount of water at elevated RH.

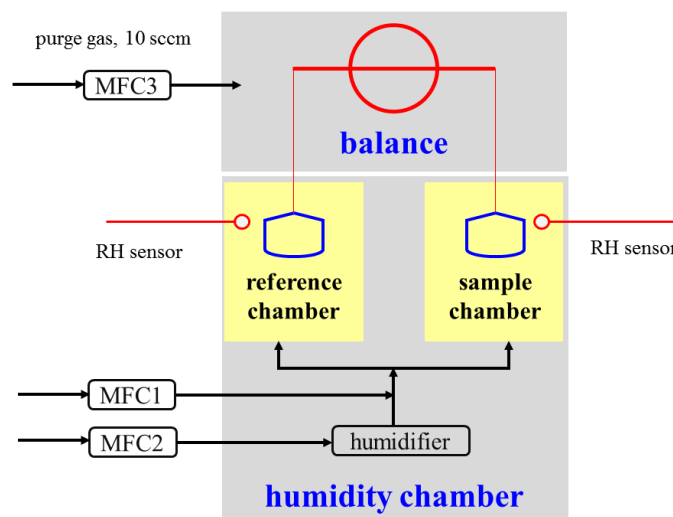
396 Analytical balance was also employed to investigate hygroscopic properties of ambient
397 aerosol particles. McInnes et al. (1996) employed an analytical balance to explore the
398 hygroscopic properties of submicrometer marine aerosol particles collected on filters, and
399 found that liquid water accounted for up to 9% of the dry particle mass at 35% RH and up to
400 29% of the dry particle mass at 47% RH. In another study (Hitzenberger et al., 1997), size-
401 segregated aerosol particles were collected on aluminum foils using a nine-stage cascade
402 impactor in downtown Vienna, and their hygroscopic properties were examined using an
403 analytic balance. Aerosol hygroscopicity was found to be strongly size dependent
404 (Hitzenberger et al., 1997), and the mass ratios of particles at 90% RH to that at dry condition
405 were found to be 2.35-2.6 for particles in the accumulation mode and 1.16-1.33 for those in the
406 coarse mode.



407 **3.2.2 Thermogravimetric analysis**

408 Similar to humidity-controlled analytical balance, thermogravimetric analysers (TGA) can
409 directly measure the mass change of particle samples at different temperature to investigate
410 aerosol hygroscopicity. Commercial TGA instruments are typically integrated with automated
411 systems for humidity generation and control. They can control temperature and RH very
412 precisely, and are very sensitive in mass measurement (typically down to 1 μg or even better).

413 Thermogravimetric analysers, sometimes also called vapor sorption analysers (VSA), have
414 been employed by several groups to investigate hygroscopic properties of atmospherically
415 relevant particles. For example, water uptake by CaCO_3 and Arizona test dust was measured at
416 room temperature using a Mettler-Toledo TGA with an accuracy of 1 μg in mass measurement
417 (Gustafsson et al., 2005), and about 4 monolayers of adsorbed water were formed at 80% RH
418 for both mineral dust samples. A similar instrument was utilized to determine the DRH of
419 dicarboxylic acids and their sodium salts at different temperatures (Beyer et al., 2014;
420 Schroeder and Beyer, 2016), and the DRH was found to decrease with temperature for malonic
421 acid, from 80.2% at 277 K to 69.5% at 303 K (Beyer et al., 2014). This method was also used
422 to probe water adsorption by different soot particles (Popovitcheva et al., 2001; Popovitcheva
423 et al., 2008a; Popovitcheva et al., 2008b), although no details of the instrument used were
424 provided. It is worth noting that TGA and/or VSA have been widely used to investigate
425 hygroscopic properties of pharmaceutical materials. For example, at room temperature
426 anhydrous theophylline was observed to transform to hydrate at 62% RH, and its DRH was
427 determined to be 99% (Chen et al., 2010).



428

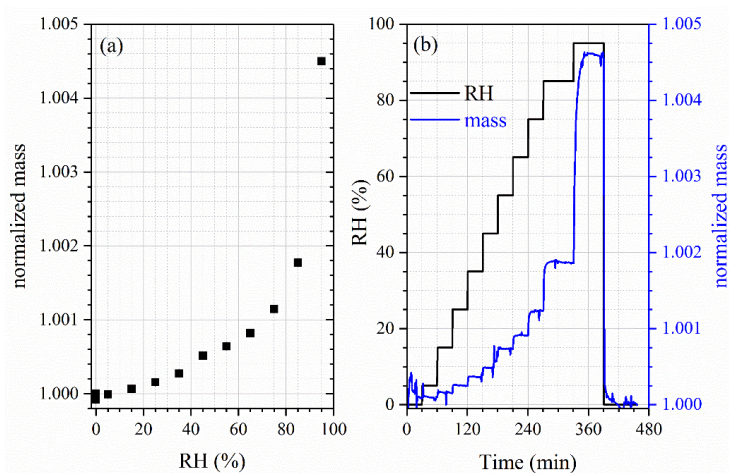
429 **Figure 4.** Schematic diagram of a vapor sorption analyser (Q5000SA, TA Instruments, New
430 Castle, DE, USA). Three mass flow controllers were used (MFC1: the dry flow; MFC2: the
431 humidified flow; MFC3: the dry flow to purge the balance). Reprint with permission by Gu et
432 al. (2017b). Copyright 2017 Copernicus Publications.

433

434 Very recently, Tang and coworkers systematically evaluated the performance of a vapor
435 sorption analyser to investigate hygroscopic properties of particles of atmospheric relevance
436 (Gu et al., 2017b). The instrument, with its schematic diagram shown in Fig. 4, has two sample
437 crucibles housed in a temperature- and humidity-regulated chamber, and one crucible is empty
438 so that the background is simultaneously measured and subtracted. DRH values of six
439 compounds, including $(\text{NH}_4)_2\text{SO}_4$ and NaCl, were determined at different temperatures (5-30
440 °C) and found to agree well with literature values. In addition, the mass change as a function
441 of RH (up to 90%), relative to that at 0% RH, was also found to agree well with those calculated
442 using the E-AIM model (Clegg et al., 1998) for $(\text{NH}_4)_2\text{SO}_4$ and NaCl at 5 and 25 °C. Therefore,
443 it can be concluded that the vapor sorption analyser is a reliable technique to study hygroscopic
444 properties of atmospherically relevant particles.



445 The vapor sorption analyzer was used to examine hygroscopicity of $\text{CaSO}_4 \cdot 2\text{H}_2\text{O}$ at 25 °C
446 (Gu et al., 2017b), and the results are displayed in Fig. 5. The hygroscopicity of $\text{CaSO}_4 \cdot 2\text{H}_2\text{O}$
447 was found to be very low, and the sample mass was only increased by <0.5% when RH was
448 increased from 0 to 95%. This instrument was very sensitive to the change in sample mass due
449 to water uptake; for example, as shown in Fig. 5b, a relative mass change of <0.025% within 6
450 h could be accurately determined. This instrument was further employed to investigate
451 hygroscopic properties of perchlorates (Gu et al., 2017a; Jia et al., 2018), Ca- and Mg-
452 containing salts (Guo et al., 2019), and primary biological particles (Tang et al., 2019), which
453 play significant roles in the environments of the earth and the Mars. To our knowledge, the
454 VSA technique has not yet been used to explore hygroscopic properties of ambient aerosol
455 particles.



456
457 **Figure 5.** Sample mass of $\text{CaSO}_4 \cdot 2\text{H}_2\text{O}$ (relative to that of 0% RH) as a function of RH at 25
458 °C, measured using a vapor sorption analyzer. (a) Change of sample mass with RH up to 95%;
459 (b) change of sample mass and RH with experimental time. Reprint with permission by Gu et
460 al. (2017b). Copyright 2017 Copernicus Publications.



461 3.2.3 Quartz crystal microbalance

462 It was proposed in 1959 (Sauerbrey, 1959) that a film attached to the electrodes of a
463 piezoelectric quartz resonator would cause a decrease in the resonance frequency, given by Eq.
464 (1):

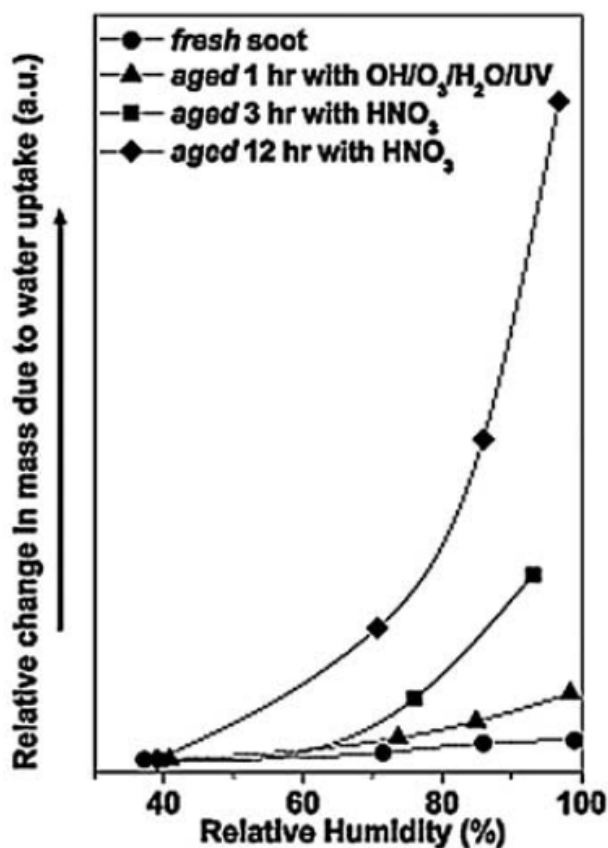
$$465 \quad \Delta f = -C_f \cdot \Delta m \quad (1)$$

466 where Δf is the change in resonance frequency, Δm is the mass of the film, and C_f is a constant
467 specific for the quartz resonator and can be experimentally calibrated. Eq. (1), known as the
468 Sauerbrey equation, forms the basis for using the piezoelectric quartz resonator as a
469 microbalance, which is usually called quartz crystal microbalance (QCM). QCM is a highly
470 sensitive technique for particle mass measurement, and could be extended to investigate aerosol
471 hygroscopicity. In a typical experiment, a particle film is first coupled to the quartz crystal, and
472 RH is then varied with the resonance frequency being simultaneously recorded. According to
473 Eq. (1), change in the mass of the particle film, due to change in RH, is proportional to the
474 change in resonance frequency. Hygroscopicity measurements only need the information of
475 relative mass change (relative to that under dry conditions), and as a result, knowledge of C_f is
476 not required. QCM has a very high sensitivity in mass measurement, and it has been reported
477 that the change in mass on the order of a few percent of a monolayer can be reliably determined
478 (Tsionsky and Gileadi, 1994).

479 A QCM was used to measure the DRH of a number of inorganic and organic salts,
480 including NaCl, $(\text{NH}_4)_2\text{SO}_4$, CH_3COONa and CH_3COOK (Arenas et al., 2012), and the
481 measured values agreed very well with those reported in previous work. Several studies
482 (Thomas et al., 1999; Demou et al., 2003; Asad et al., 2004a; Liu et al., 2016) have utilized
483 QCM to explore hygroscopic properties of organic compounds of atmospheric interest. For
484 example, Demou et al. (2003) quantitatively determined the amount of water taken up by
485 dodecane, 1-octanol, octanoic acid, 1,5-pentanediol, 1,8-octanediol and malonic acid at room



486 temperature. The DRH was measured to be ~72% for malonic acid and ~95% for 1,8-octanediol,
487 and in general compounds with higher oxidation state showed higher hygroscopicity (Demou
488 et al., 2003). Another study (Asad et al., 2004a) found that exposure to O_3 would substantially
489 increase the hygroscopicity of oleic acid. Using a QCM, Zuberi et al. (2005) explored the effect
490 of heterogeneous reactions on hygroscopic properties of soot particles. As shown in Fig. 6,
491 while water adsorption was very limited for fresh soot particles, hygroscopicity of soot particles
492 was significantly increased after heterogeneous reactions with OH/O_3 and HNO_3 (Zuberi et al.,
493 2005).



494



495 **Figure 6.** Water uptake (quantified as the ratio of mass of water taken up to that of dry particle
496 mass) of fresh and aged soot particles. Reprinted with permission by Zuberi et al. (2005).
497 Copyright 2005 John Wiley & Son, Inc.

498

499 QCM has also been applied to study hygroscopic properties of mineral dust particles,
500 including oxides (Schuttlefield et al., 2007a), clay minerals (Schuttlefield et al., 2007b;
501 Yeşilbaş and Boily, 2016) and authentic dust samples (Navea et al., 2010; Yeşilbaş and Boily,
502 2016). For example, Yeşilbaş and Boily (2016) measured the amount of water taken up by 21
503 different types of mineral particles up to 70% RH at 25 °C, and found that particle size played
504 a critical role in water adsorption by these minerals. At 70% RH, submicrometer-sized particles
505 could adsorb up to ~5 monolayers of water, while the amount of water adsorbed by micrometer-
506 sized particles can reach several thousand monolayers (Yeşilbaş and Boily, 2016). Another
507 study (Hatch et al., 2008) suggested that ~3 monolayers of adsorbed water was formed on
508 CaCO₃ particles at 78% RH, and internal mixing with humic and fulvic acids could
509 substantially increase the hygroscopicity of CaCO₃.

510 It should be pointed out (as often not fully considered) that a few assumptions are required
511 for the Sauerbrey equation to be valid (Rodahl and Kasemo, 1996), including: (i) the film
512 deposited on the quartz crystal is rigid, i.e. internal friction is negligible; (ii) the film is perfectly
513 coupled to the quartz crystal, i.e. there is no slip between the film and the crystal. The Sauerbrey
514 equation may not hold if these conditions are not fulfilled, and the stiffness of the particle film
515 would significantly affect the quartz resonator response (Dybwad, 1985; Pomorska et al., 2010;
516 Vittorias et al., 2010; Arenas et al., 2012). Rodal and Kasemo (1996) suggested that the
517 Sauerbrey equation can offer reliable mass change measurement only if the film is thin enough
518 and does not slide on the QCM electrode. In addition, as supersaturated films formed on the



519 quartz crystal are unstable, QCM may not be able to explore hygroscopic properties of
520 supersaturated samples.

521 Piezoelectric bulk wave resonators, which work in a way similar to the QCM, have been
522 used for monitoring aerosol mass concentrations (Thomas et al., 2016; Wasisto et al., 2016).
523 When particles are deposited onto the resonator surface, the resonance frequency will be
524 linearly reduced with the particle mass. Very recently a new method based on piezoelectric
525 bulk wave resonators was developed to investigate aerosol hygroscopicity (Zielinski et al.,
526 2018). Aerosol particles were first collected on the resonator surface and then exposed to
527 changing RH. Measured DRH and ERH values were found to agree with literature for NaCl
528 and $(\text{NH}_4)_2\text{SO}_4$; in addition, good consistency between experimentally measured and E-AIM
529 predicted hygroscopic growth curves was found for NaCl, $(\text{NH}_4)_2\text{SO}_4$ and NaCl/malonic acid
530 mixture (Zielinski et al., 2018). Therefore, this technique appears to be a very promising
531 method for aerosol hygroscopicity measurements.

532 **3.2.4 Beta gauge and TEOM**

533 In addition to the gravimetric method, the beta gauge method is widely used to measure
534 aerosol mass concentrations in a semi-continuous way (Courtney et al., 1982; Chow, 1995;
535 McMurry, 2000; Solomon and Sioutas, 2008; Kulkarni et al., 2011). A beta gauge measures
536 the attenuation of beta particles emitted from a radioactive source through a particle-loaded
537 filter, and if properly calibrated, attenuation of beta particles through the filter can be used to
538 quantify the mass of particles loaded on the filter (McMurry, 2000). The mass of aerosol
539 particles, after being collected on a filter, was measured at different RH in a closed chamber
540 using a beta gauge to determine the aerosol liquid water content (Speer et al., 1997). Laboratory
541 evaluation showed that the liquid water content of $(\text{NH}_4)_2\text{SO}_4$ determined using this method
542 agreed well with those measured gravimetrically (Speer et al., 1997), and when compared to
543 humidification, a hysteresis was found during dehumidification for $(\text{NH}_4)_2\text{SO}_4$. The ability to



544 observe hysteresis is related to the use of hydrophobic substrate (for example, Teflon is usually
545 a good option) in particle sampling. In addition, the beta gauge method was preliminarily
546 employed to explore hygroscopic properties of submicrometer ambient aerosol particles (Speer
547 et al., 1997). Further tests with other compounds, in addition to $(\text{NH}_4)_2\text{SO}_4$, are required to
548 validate the robustness and reliability of this method.

549 Another widely-employed semi-continuous technique for aerosol mass measurement is
550 tapered-element oscillating microbalance (TEOM) (Patashnick and Rupprecht, 1991; Chow et
551 al., 2008; Solomon and Sioutas, 2008; Kulkarni et al., 2011). In a typical TEOM instrument,
552 the wide end of a tapered hollow tube is mounted on a base plate, and its narrow end is coupled
553 to a filter used to collect aerosol particles (Kulkarni et al., 2011). The oscillation frequency
554 of the tapered hollow tube depends on the mass of particles collected on the filter and can be
555 used to measure particle mass if properly calibrated (Kulkarni et al., 2011). Rogers et al. (1998)
556 explored the possibility of using TEOM to measure aerosol liquid water content. Increase in
557 particle mass was observed when a humid particle-free air flow was passed through a particle-
558 loaded filter in the TEOM, and the particle mass started to decrease after a dry particle-free air
559 was introduced (Rogers et al., 1998). This suggested that TEOM had the potential to examine
560 hygroscopic properties of aerosol particles, though further experimental evaluation is needed
561 to assess its performance.

562 **3.2.5 Discussion**

563 All the techniques discussed in Section 3.2 determine particle water content through direct
564 measurement of sample mass or properties that are related to the sample mass, and hence there
565 is no requirement on particle shape. Some of these techniques, such as thermogravimetric
566 analysis (Gustafsson et al., 2005) and quartz crystal microbalance (Schuttlefield et al., 2007a;
567 Yeşilbaş and Boily, 2016), are sensitive enough to investigate water adsorption down to one or
568 a few monolayers, while other techniques, such as the analytic balance, may not be sensitive



569 enough for this application. If particles are supported on proper substrates (such as hydrophobic
570 films), these techniques can be used to investigate hygroscopic properties of supersaturated
571 samples, as demonstrated for the beta gauge method (Speer et al., 1997) and the piezoelectric
572 bulk wave resonators (Zielinski et al., 2018). Nevertheless, supersaturated solutions formed in
573 majority of these applications may not be stable enough for hygroscopic growth measurements,
574 and as a result measurements have been rarely reported for supersaturated samples. In principle
575 these techniques can all be used offline to investigate ambient aerosol particles if samples with
576 enough mass can be collected. Analytical balance (McInnes et al., 1996; Hitznerberger et al.,
577 1997) and the beta gauge method (Speer et al., 1997) have been used to explore hygroscopic
578 properties of ambient aerosols; to our knowledge, application of thermogravimetric analysis,
579 quartz crystal microbalance, TOEM and piezoelectric bulk wave resonators to ambient samples
580 is yet to be demonstrated.

581 **3.3 Microscopic techniques**

582 Deliquescence and efflorescence can be monitored using a number of microscopic
583 methods, as discussed in this section. Furthermore, change in particle size at different RH, as
584 measured microscopically, can be used to determine hygroscopic growth factors.

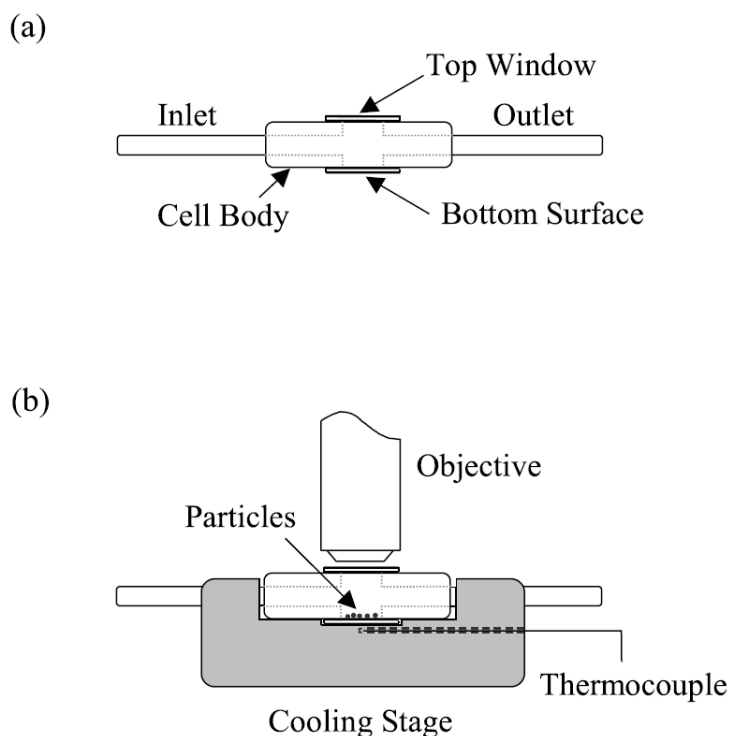
585 **3.3.1 Optical microscopy**

586 Optical microscopy was employed to investigate phase transition of atmospheric particles
587 as early as in 1950s (Twomey, 1953; Twomey, 1954). In these two studies (Twomey, 1953;
588 Twomey, 1954), a large number of aerosol particles collected in Sydney were found to
589 deliquesce at 71-75% RH, implying that they consisted mainly of sea salt. Since then, optical
590 microscopy has been widely used to study hygroscopic properties of atmospherically relevant
591 particles, and herein we only introduce representative studies conducted in the last two decades.

592 Bertram and co-workers (Parsons et al., 2004a; Parsons et al., 2004b; Parsons et al., 2006)
593 developed a flow cell-optical microscope apparatus to investigate phase transitions of



594 individual particles deposited on glass slides coated with hydrophobic films. As show in Fig.
595 7, the glass slide was placed in a flow cell mounted on a cooling stage for temperature
596 regulation. A dry nitrogen flow was mixed with a humidified nitrogen flow and then delivered
597 into the flow cell through the inlet, and the two flows were regulated using two mass flow
598 controllers to adjust water vapor pressure (and thus RH) in the flow cell. Phase transitions of
599 particles deposited on the glass slide were monitored using a microscope, and particle images
600 were recorded using a CCD camera.



601

602 **Figure 7.** Schematic diagram of the flow cell-optical microscope apparatus developed by
603 Bertram and co-workers to investigate particle phase transitions: (a) side view of the flow cell;
604 (b) side view of the entire apparatus. Particles were deposited on a glass slide placed on the
605 bottom of the flow cell, which was mounted on a cooling stage. Objective: objective lens of



606 the microscope. Reprint with permission by Parsons et al. (2004b). Copyright 2004 John Wiley
607 & Sons, Inc.

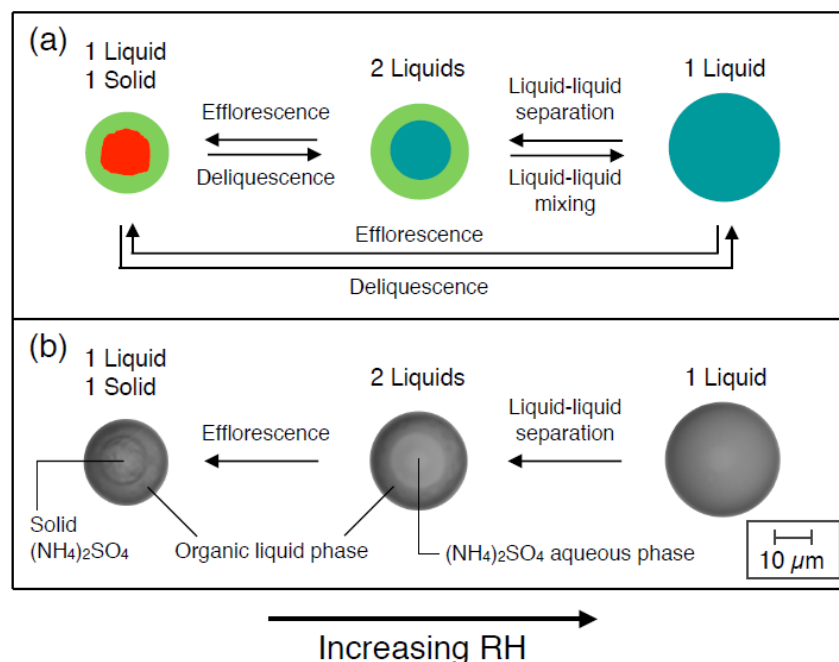
608

609 The performance of this apparatus was evaluated by measuring DRH of $(\text{NH}_4)_2\text{SO}_4$
610 particles from ~260 to 300 K (Parsons et al., 2004b), and the measured DRH agreed well with
611 those reported in literature. This setup was then used to investigate the deliquescence of
612 malonic, succinic, glutaric and adipic acid particles from 243 to 293 K (Parsons et al., 2004b)
613 and deliquescence and crystallization of $(\text{NH}_4)_2\text{SO}_4$ and NaCl particles internally mixed with
614 organic compounds (Pant et al., 2004; Parsons et al., 2004a). It was found that if $(\text{NH}_4)_2\text{SO}_4$ or
615 NaCl particles contained substantial amounts of organic materials, their DRH would be
616 significantly reduced and these particles were more likely to be aqueous in the troposphere
617 (Pant et al., 2004). A similar instrument was employed to investigate deliquescence and
618 efflorescence of HIO_3 and I_2O_5 particles (Kumar et al., 2010), and the DRH at 293 K were
619 reported to be 81% for HIO_3 and 85% for I_2O_5 .

620 As illustrated by Fig. 8a, besides deliquescence and efflorescence, atmospheric aerosols
621 can also undergo liquid-liquid phase separation (LLPS), leading to coexistence of two liquid
622 phases (Bertram et al., 2011; You et al., 2012; You et al., 2014; Freedman, 2017). LLPS can
623 impact the direct and indirect radiative forcing of atmospheric aerosol particles as well as their
624 heterogeneous reactivity, and therefore has received increasing attention in the last several
625 years (You et al., 2012; Freedman, 2017). Optical microscopy has played an important role in
626 understanding LLPS of atmospherically relevant particles (Bertram et al., 2011; You et al.,
627 2012; You et al., 2014). Fig. 8b shows optical microscopic images of an internally mixed
628 particle during an experiment in which RH was decreased while temperature was kept at ~291
629 K (Bertram et al., 2011), and the particle contained $(\text{NH}_4)_2\text{SO}_4$ and 1,2,6-trihydroxyhexane
630 with a mass ratio of 1:2.1. As shown in Fig. 8b, at high RH the particle existed as an aqueous



631 droplet, and LLPS happened when RH was decreased, leading to the formation of two liquid
632 phases; efflorescence took place with further decrease in RH, leading to the formation of a solid
633 $(\text{NH}_4)_2\text{SO}_4$ core coated with an organic liquid layer.



634
635 **Figure 8.** (a) Some of the phase transitions which may occur for internally mixed atmospheric
636 particles consisting of $(\text{NH}_4)_2\text{SO}_4$ and organic materials. Aqua represents an aqueous phase,
637 green represents a liquid phase of organic material, and red presents a solid phase of $(\text{NH}_4)_2\text{SO}_4$.
638 (b) Optical microscopic images of a particle which contained $(\text{NH}_4)_2\text{SO}_4$ and 1,2,6-
639 trihydroxyhexane with a mass ratio of 1:2.1, during an experiment in which temperature was
640 kept at around 291 K while RH was decreased. Reprint with permission by Bertram et al. (2011).
641 Copyright 2011 Copernicus Publications.

642

643 In addition to identification of phase transitions, analysis of optical microscopic images
644 recorded can also be used to determine particle size change and as a result hygroscopic growth
645 factors (Ahn et al., 2010; Eom et al., 2014; Gupta et al., 2015). For instance, Ahn et al. (2010)



646 employed an optical microscope to investigate hygroscopic properties of NaCl, KCl,
647 (NH₄)₂SO₄ and Na₂SO₄ particles collected on TEM grids, and found that their measured
648 hygroscopic growth factors agreed well with those reported in literature for all the four types
649 of particles examined. A following study (Eom et al., 2014) compared the influence of six types
650 of supporting substrates (including TEM grid, Parafilm-M, aluminum foil, Ag foil, silicon
651 wafer and cover glass) on hygroscopicity measurements using optical microscopy, and
652 concluded that TEM grids were the most suitable substrate for this application. Optical
653 microscopy was also used to study hygroscopic properties of MgCl₂ and NaCl-MgCl₂ mixed
654 particles (Gupta et al., 2015), and hygroscopic properties (including DRH and growth factors)
655 of these particles were found to differ significantly from NaCl. Since MgCl₂ is an important
656 component in sea salt aerosol, this work can have significant implications for hygroscopicity
657 and thus climatic impacts of sea salt aerosol (Zieger et al., 2017).

658 Optical microscopy can be (and has been widely) coupled to suitable spectroscopic
659 techniques such as FTIR (Liu et al., 2008a), Raman spectroscopy (Liu et al., 2008c) and
660 fluorescence (Montgomery et al., 2015), and if so chemical information can be simultaneously
661 provided.

662 **3.3.2 Electron microscopy**

663 Electron microscopy has been widely used in laboratory and field studies to examine
664 composition, mixing state and morphology of atmospheric particles, as summarized by a few
665 excellent review articles (Prather et al., 2008; Posfai and Buseck, 2010; Li et al., 2015; Ault
666 and Axson, 2017). Herein we discuss exemplary studies to illustrate how electron microscopy
667 can help improve our knowledge of aerosol hygroscopicity. This section is further divided to
668 two parts, i.e. scanning electron microscopy (SEM) and transmission electron microscopy
669 (TEM).

670 **3.3.2.1 SEM**

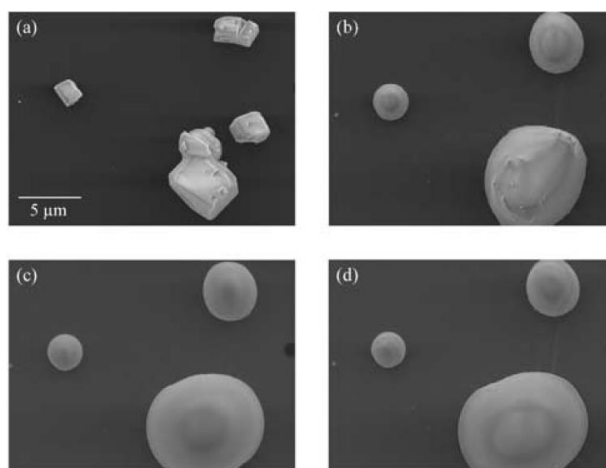
671 Ebert et al. (2002) developed an environmental scanning electron microscope (ESEM)
672 technique to explore hygroscopic properties of individual particles, and the instrument they
673 used had a spatial resolution of 8-15 nm. Changes in particle morphology could be used to
674 identify phase transitions (deliquescence and efflorescence), and growth factors could be
675 derived from observed change in particles size at different RH. Their measured DRH and
676 hygroscopic growth factors (Ebert et al., 2002) were in good agreement with results reported
677 by previous literature for NaCl, (NH₄)₂SO₄, Na₂SO₄ and NH₄NO₃. However, ERH could not
678 be accurately determined due to the influence of the substrate onto which particles under
679 investigation were deposited (Ebert et al., 2002).

680 ESEM, coupled to energy disperse X-ray analysis (EDX), was employed to investigate
681 hygroscopic properties of a wide range of atmospheric particles, including (NH₄)₂SO₄
682 (Matsumura and Hayashi, 2007), sea spray (Hoffman et al., 2004), aerosol particles collected
683 in nickel refineries (Inerle-Hof et al., 2007), agricultural aerosol (Hiranuma et al., 2008), pollen
684 (Pope, 2010; Griffiths et al., 2012) and protein (Gomery et al., 2013). For example, Hoffman
685 et al. (2004) found that both NaNO₃ and NaNO₃/NaCl particles existed as amorphous solids
686 even at very low RH and exhibit continuous hygroscopic growth, instead of having clear DRH;
687 furthermore, EDX analysis showed that Cl was enriched in the core of dried NaCl/NaNO₃
688 particles (Hoffman et al., 2004), implying that during dehumidification NaCl started to
689 crystalline first because of its lower solubility. This finding may have important implications
690 for chemical and radiative properties of marine aerosol particles (Quinn et al., 2015). In another
691 study (Pope, 2010), ESEM observations revealed that birch pollen gains swelled internally but
692 did not take up water on the surface significantly even at 93% RH; however, liquid water could
693 be observed on the particle surface when RH was >95%. Hiranuma et al. (2008) found that
694 most of aerosol particles collected at a cattle feedlot in the Texas did not take up significant



695 amount of water at 96% RH, though a small fraction of coarse particles became deliquesced at
696 ~75% RH and their sizes were doubled at 96% RH compared to their original sizes.

697 SEM/EDX was utilized by Krueger et al. (2003) to monitor changes in phase, morphology
698 and composition of individual mineral dust particles after heterogeneous reaction with gaseous
699 HNO₃. For the first time, laboratory work showed that solid mineral dust particles could be
700 transformed to aqueous droplets due to heterogeneous reactions (Krueger et al., 2003). As
701 displayed in [Fig. 9](#), solid CaCO₃ particles were converted to spherical droplets as
702 heterogeneous reaction with gaseous HNO₃ proceeded (Krueger et al., 2003), and this was
703 caused by the formation of Ca(NO₃)₂ which had very low DRH (Al-Abadleh et al., 2003; Kelly
704 and Wexler, 2005). A following study (Krueger et al., 2004) examined heterogeneous reactions
705 of HNO₃ with mineral dust samples collected from four different regions, using SEM/EDX. It
706 was suggested that calcite and dolomite particles exhibited large reactivity towards HNO₃ and
707 could be transformed to aqueous droplets, while no morphological change was observed for
708 gypsum, aluminum silicate clay and quartz particles after exposure to HNO₃ (Krueger et al.,
709 2004).



710



711 **Figure 9.** SEM images of CaCO_3 particles before and after exposure to 26 ppbv gaseous HNO_3
712 at ~41% RH. (a): Before exposure; (b) exposure for 1 h; (c) exposure for 2 h; (d) exposure for
713 4 h. Reprint with permission by Krueger et al. (2003). Copyright 2003 John Wiley & Sons, Inc.

714

715 The new laboratory discovery by Krueger et al. (2003) has been supported by a number of
716 field measurements (Li et al., 2015; Tang et al., 2016a), and in some of which SEM was also
717 utilized. For example, Laskin et al. (Laskin et al., 2005) provided the first evidence
718 demonstrating that in the ambient air solid nonspherical CaCO_3 particles could be transformed
719 to aqueous droplets which contained $\text{Ca}(\text{NO}_3)_2$ formed in heterogeneous reaction with nitrogen
720 oxides. ESEM was also applied to examine mineral dust particles collected in Beijing (Matsuki
721 et al., 2005) and southwestern Japan (Shi et al., 2008), and both studies found that some Ca-
722 containing particles existed in aqueous state even at RH as low as 15% because heterogeneous
723 reactions with nitrogen oxides converted CaCO_3 to $\text{Ca}(\text{NO}_3)_2$. Similarly, it was shown by
724 SEM/EDX measurements (Tobo et al., 2010; Tobo et al., 2012) that Ca-containing mineral
725 dust particles in remote marine troposphere were transformed to aqueous droplets, because
726 CaCl_2 was formed in heterogeneous reaction of CaCO_3 with HCl.

727 3.3.2.2 TEM

728 Compared to SEM, transmission electron microscopy (TEM) has better spatial resolution
729 and can resolve features down to one nanometer or even smaller. TEM and AFM (atomic force
730 microscopy) were employed by Buseck and colleagues (Posfai et al., 1998) to examine ambient
731 particles collected on TEM grids under vacuum and ambient conditions. It was found that
732 particle volumes were up to four times larger under ambient conditions, compared to vacuum
733 conditions. Several years later Buseck and co-workers (Wise et al., 2005) developed an
734 environmental transmission electron microscope (ETEM) which enabled individual particles
735 to be characterized under environmental conditions. The performance of this instrument was



736 validated by measuring DRH and ERH of NaBr, CsCl, NaCl, (NH₄)₂SO₄ and KBr particles in
737 the size range of 0.1-1 μm, and good agreement was found between their measured values and
738 these reported by previous work for all the five compounds investigated (Wise et al., 2005).

739 The ETEM technique was further employed to investigate hygroscopic properties of a
740 wide range of atmospheric particles, including NaCl-containing particles (Semeniuk et al.,
741 2007b; Wise et al., 2007), biomass burning particles (Semeniuk et al., 2007a) and potassium
742 salts (Freney et al., 2009). The DRH of NaCl particles internally mixed with insoluble materials
743 was determined to be ~76% (equal to that for pure NaCl), while internal mixing with other
744 soluble compounds (e.g., NaNO₃) would reduce the DRH (Wise et al., 2007). DRH and ERH
745 were reported to be 85 and 56% for KCl and 96 and 60% for K₂SO₄, while KNO₃ displayed
746 continuous hygroscopic growth (Freney et al., 2009); in addition, deliquescence and
747 efflorescence of internally mixed KCl/KNO₃ and KCl/K₂SO₄ were also examined (Freney et
748 al., 2009). In another study (Adachi et al., 2011), aerosol particles, mainly being sulfate
749 internally mixed with weakly hygroscopic organic materials, were collected at Mexico City
750 and their hygroscopic properties were investigated using ETEM. It was found that only the
751 sulfate part was deliquesced at elevated RH, while the entire particles containing deliquesced
752 sulfate did not necessarily become spherical. It was further suggested that the actual light
753 scattering ability was 50% larger than that estimated by Mie theory which assumes particle
754 sphericity (Adachi et al., 2011).

755 Recently cryogenic TEM has been deployed to explore morphology, hygroscopic
756 properties and chemical composition of atmospheric particles (Veghte et al., 2014; Patterson
757 et al., 2016). For example, it was observed that most nascent sea spray aerosol particles were
758 homogeneous aqueous droplets, and upon exposure to low RH they would be quickly
759 reorganized and undergo phase separation (Patterson et al., 2016).



760 **3.3.3 Atomic force microscopy**

761 Atomic force microscopy (AFM) is a widely used technique in surface chemistry and
762 surface science. Compared to other microscopic techniques (e.g., optical microscopy, FTIR
763 microscopy, TEM and SEM), AFM has several unique advantages. It does not require vacuum
764 condition, and thus can be operated under environmental conditions; in addition, it has a high
765 spatial resolution down to the nanometer level, and offers three-dimensional imaging (Morris
766 et al., 2016).

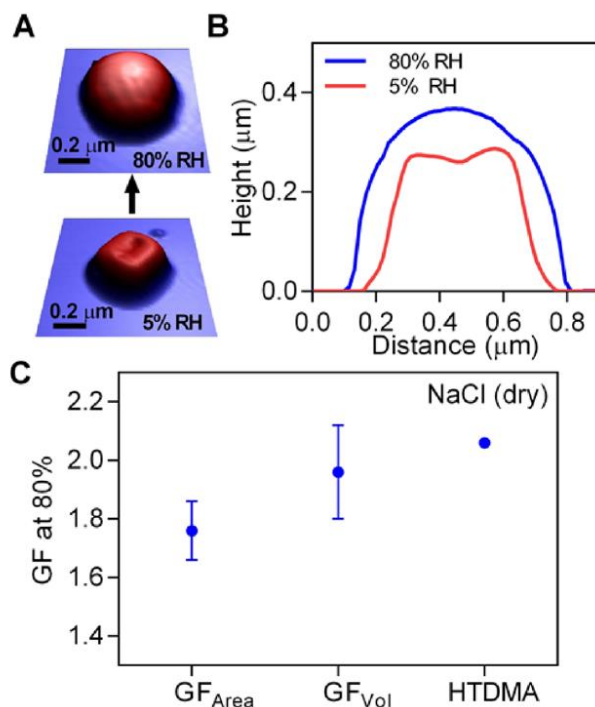
767 In the past two decades, AFM has been gradually utilized in atmospheric chemistry to
768 observe three-dimensional morphology of aerosol particles, and its application in atmospheric
769 chemistry started with observation of surfaces of single crystals with atmospheric relevance.
770 For example, AFM was employed to study the (100) cleavage surface of NaCl during exposure
771 to water vapor (Dai et al., 1997). A uniform layer of water was formed on the surface and
772 surface steps started to evolve slowly at ~35% RH; when RH increased to ~73%
773 (approximately the DRH of NaCl), the step structure disappeared abruptly due to deliquescence
774 of the surface (Dai et al., 1997). This pioneering work demonstrated that AFM had the potential
775 to be used to determine DRH of hygroscopic salts, in addition to providing rich information of
776 surface structure change during exposure to water vapor. AFM was later used to observe
777 MgO(100) and CaCO₃(1014) surface during exposure to water vapor and gaseous nitric acid
778 (Krueger et al., 2005). Instabilities of oscillations in AFM images were observed, indicating
779 that deliquescence of nitrate salts, which were formed in to heterogeneous reaction with nitric
780 acid, occurred at elevated RH (Krueger et al., 2005).

781 To our knowledge, AFM was successfully used in 1995 to characterize aerosol particles
782 collected using a low-pressure impactor (Friedbacher et al., 1995). Three years later, Posfai et
783 al. (1998) used AFM to examine individual particles collected above the North Atlantic Ocean
784 at different RH. The particle volume was observed to be four times larger under ambient



785 conditions (measured by AFM) compared to that in the vacuum (measured by TEM) (Posfai et
786 al., 1998). Another study (Wittmaack and Strigl, 2005) used AFM to measure height-to-
787 diameter ratios of ambient particles, and concluded that some particles may exist in the
788 supersaturated metastable state at around 50% RH. Non-contact environmental AFM was used
789 to examine uptake of water vapor by NaCl nanoparticles at RH below DRH (Bruzewicz et al.,
790 2011). NaCl nanoparticles started to adsorb water at RH well below its DRH (75%), and a
791 liquid-like surface layer with thickness of 2-5 nm was formed at 70% RH, suggesting that
792 deliquescence of NaCl nanoparticles was much more complicated than an abrupt first-order
793 phase transition.

794 Very recently Tivanski and co-workers (Ghorai et al., 2014; Laskina et al., 2015b; Morris
795 et al., 2015; Morris et al., 2016) developed an AFM-based method to investigate hygroscopicity
796 of particles deposited on substrates, and systematically evaluated its performance by measuring
797 hygroscopic growth factors of NaCl, malonic acid and binary mixture of NaCl with malonic or
798 nonanoic acid. It was found that hygroscopic growth factors derived from 3D volume
799 equivalent diameters always agreed well with H-TDMA results; however, hygroscopic growth
800 factors derived from 2D area equivalent diameters showed significant deviation from H-TDMA
801 results for some types of particles (Morris et al., 2016). An example is displayed in [Fig. 10](#),
802 suggesting that at 80% RH, the hygroscopic growth factor of NaCl particles derived from the
803 volume-equivalent diameter was equal to that determined using H-TDMA, significantly larger
804 than that derived from area-equivalent diameter. Such deviation was caused by anisotropic
805 growth of particles (Morris et al., 2016), and the extent of deviation depended on the particle
806 composition and their hydrate state at the time when they were collected on the substrate.



807

808 **Figure 10.** AFM measurements of hygroscopicity of NaCl particles. (A) 3D AFM images of a
809 NaCl particle at 5 and 80% RH; (B) Cross section of the particles at 5% (red) and 80% (blue)
810 RH; (C) Comparison of hygroscopic growth factors derived from changes in mobility diameter
811 (measured using H-TDMA), area equivalent diameter (measured using AFM) and volume
812 equivalent diameter (measured using AFM). Reprint with permission by Morris et al. (2016).
813 Copyright 2016 American Chemical Society.

814

815 In addition to hygroscopicity measurement, AFM were used in several studies to
816 characterize morphology, structure and other physicochemical properties of atmospheric
817 particles (Lehmpuhl et al., 1999; Freedman et al., 2010; Laskina et al., 2015a). For example,
818 AFM measurements found that organic and soot particles would shrink after interactions with
819 O₃ while inorganic particles remained unchanged (Lehmpuhl et al., 1999). Freedman et al.
820 (2010) employed AFM coupled to Raman microscopy to characterize atmospheric particles



821 under ambient conditions, and observed core-shell structure for some organic particles. A
822 recent study (Laskina et al., 2015a) characterized particles collected on substrates using AFM,
823 Raman microscopy and SEM, and suggested that microscopy techniques operated under
824 ambient conditions would offer the most relevant and robust information on particle size and
825 morphology. Conventional AFM offers no chemical information; however, it can be (and has
826 already been) coupled to spectroscopic techniques (such as FTIR) (Dazzi et al., 2012; Ault and
827 Axson, 2017; Dazzi and Prater, 2017), enabling detailed physical and chemical properties to
828 be provided with high spatial resolution. Very recently, the peak force infrared microscopy, a
829 type of scanning probe microscopy, was developed to investigate IR absorption and mechanical
830 properties of ambient aerosol particles (Wang et al., 2017b), and a spatial resolution of 10 nm
831 could be achieved.

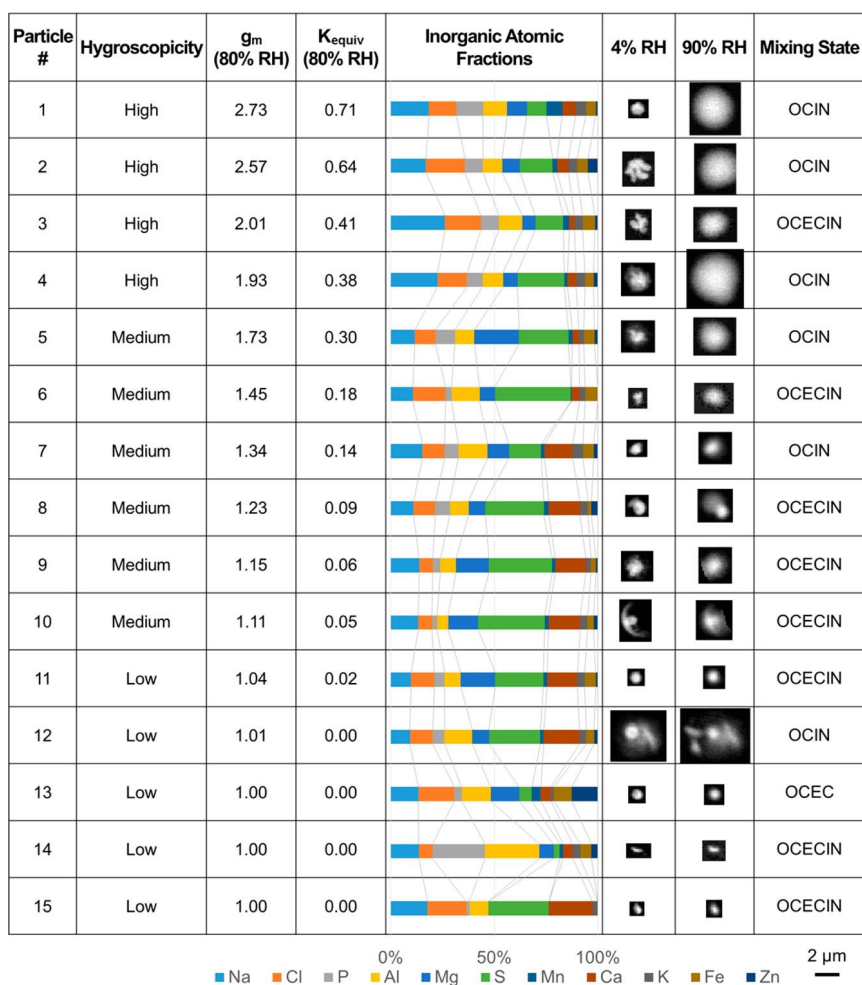
832 3.3.4 X-ray microscopy

833 Scanning transmission X-ray microscopy (STXM) is a novel technique which can provide
834 spatial distribution of physical, chemical and morphological information of individual particles
835 (de Smit et al., 2008), and has been recently employed to investigate atmospheric particles
836 (Ault and Axson, 2017). For example, Ghorai and Tivanski (2010) developed a STXM-based
837 method to study hygroscopic growth of individual submicrometer particles, and proposed a
838 method to quantify the mass of water associated with individual particles at a given RH. DRH
839 and ERH values of NaCl, NaBr, and NaNO₃, determined using STXM (Ghorai and Tivanski,
840 2010), agreed very well with previous results, and mass hygroscopic growth factors were also
841 reported for these particles. In a following study (Ghorai et al., 2011), STXM was used to
842 investigate hygroscopic growth of individual malonic acid; in addition to measured mass
843 hygroscopic growth factors, near-edge X-ray absorption fine structure spectroscopy (NEXAFS)
844 acquired using STXM suggested that keto-enol tautomerism occurred for deliquesced malonic



845 acid particles (Ghorai et al., 2011). The keto-enol equilibrium constants were found to vary
846 with RH, with enol formation favored at high RH (Ghorai et al., 2011).

847 Hygroscopic growth of submicrometer $(\text{NH}_4)_2\text{SO}_4$, measured using STXM/NEXAFS
848 (Zelenay et al., 2011a), agreed well with previous studies; furthermore, analysis of STXM
849 images and NEXAFS spectra suggested that phase separation occurred for internally mixed
850 $(\text{NH}_4)_2\text{SO}_4$ -adipic acid particles, and adipic acid was partially enclosed by $(\text{NH}_4)_2\text{SO}_4$ at high
851 RH (Zelenay et al., 2011a). An environmental chamber was constructed to be directly coupled
852 to a STXM instrument (Kelly et al., 2013), and this set-up was utilized to explore hygroscopic
853 properties of NaCl, NaBr, KCl, $(\text{NH}_4)_2\text{SO}_4$, levoglucosan and fructose (Piens et al., 2016).
854 Measured mass hygroscopic growth factors were compared with those predicted by a
855 thermodynamic model (AIOMFAC) (Zuend et al., 2011), and good agreement between
856 measurement and prediction was found for all the compounds investigated (Piens et al., 2016).
857 In another study, Zelenay et al. (2010b) utilized STXM/NEXAFS to investigate hygroscopic
858 properties of submicrometer tannic acid and Suwannee River Fulvic acid used as proxies for
859 humic-like substance found in atmospheric aerosol. Both compounds exhibited continuous
860 water uptake, and at 90% RH around one water molecule was associated with each oxygen
861 atoms contained by tannic acid while approximately two water molecules were associated with
862 each oxygen atoms contained by Suwannee River Fulvic acid (Zelenay et al., 2011b).



863

864 **Figure 11.** Hygroscopicity, mass growth factors at 80% RH (g_m), single hygroscopicity
 865 parameters (K_{equiv}), inorganic atomic fractions, STXM images (acquired at 4 and 90% RH) and
 866 mixing state for 15 aerosol particles examined. Reprint with permission by Piens et al. (2016).
 867 Copyright 2016 American Chemical Society.

868

869 STXM/NEXAFS has already been applied to explore hygroscopicity of ambient particles.
 870 For example, Pöhlker et al. (2014) collected aerosol particles from the Amazonian forest during
 871 periods with anthropogenic impacts, and then analyzed these particles using STXM-NEXAFS



872 at different RH. Substantial changes in particle microstructure were observed upon dehydration,
873 very likely caused by efflorescence and crystallization of sulfate salts (Pöhlker et al., 2014).
874 Piens et al. (2016) employed STXM-NEXAFS to examine hygroscopicity of atmospheric
875 particles collected from the Department of Energy's Atmospheric Radiation Monitoring site in
876 the Southern Great Plains. As shown in [Fig. 11](#), compared to particles with medium and low
877 hygroscopicity, particles with high hygroscopicity always contained larger fractions of Na and
878 Cl (Piens et al., 2016).

879 3.3.5 Discussion

880 Hygroscopicity measurements using microscopic techniques typically rely on changes in
881 particle diameter measured microscopically. Therefore, it would be non-trivial for these
882 techniques to quantify hygroscopic growth factors for non-spherical particles. In addition, these
883 techniques may not be sensitive enough to investigate water adsorption. Since single particles
884 deposited on supporting substances are usually examined, these techniques can be employed
885 to investigate supersaturated samples if proper supporting substances are used. They have also
886 been widely used to explore hygroscopic properties of ambient aerosol particles which were
887 collected on proper substances. As discussed in Section 3.4, microscopic techniques can be and
888 have widely been coupled to spectroscopic tools, and if so chemical information could be
889 simultaneously provided;

890 3.4 Spectroscopic techniques

891 Interaction with water vapor would lead to changes in composition and chemical
892 environment of particles under examination, and these changes can be monitored using
893 spectroscopic techniques to understand hygroscopic properties of atmospherically relevant
894 particles.



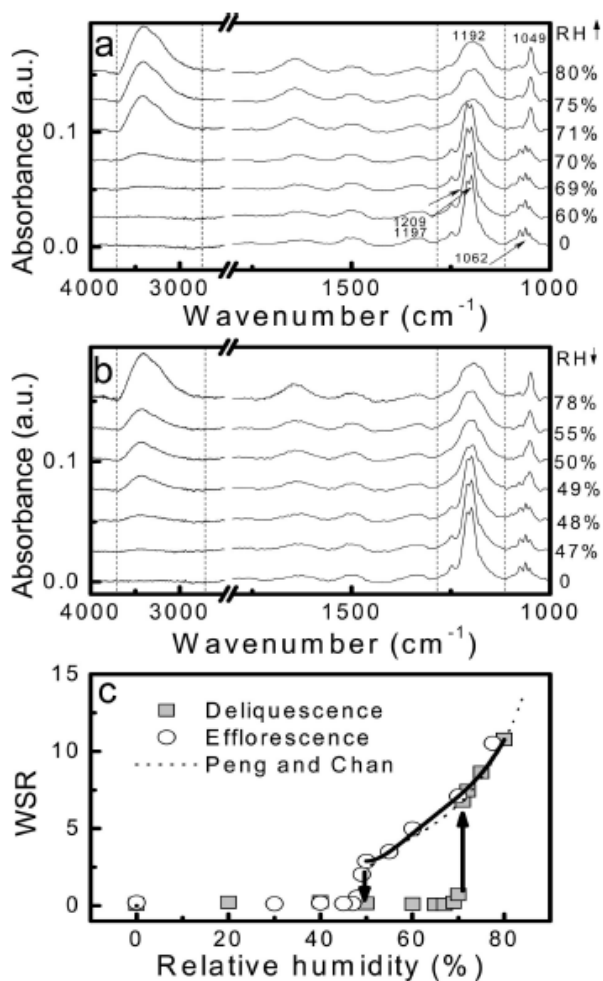
895 **3.4.1 Fourier transform infrared spectroscopy**

896 Fourier transform infrared spectroscopy (FTIR), a vibrational absorption spectroscopy, has
897 been widely employed in laboratory (Goodman et al., 2000; Eliason et al., 2003; Asad et al.,
898 2004b; Hung et al., 2005; Najera et al., 2009; Li et al., 2010; Tan et al., 2016; Tang et al., 2016b)
899 and field work (Maria et al., 2002; Russell et al., 2011; Takahama et al., 2013; Kuzmiakova et
900 al., 2016; Takahama et al., 2016; Takahama et al., 2019) to characterize chemical composition
901 of aerosol particles. It can also be used in aerosol hygroscopicity studies. When water is
902 adsorbed or absorbed by particles, change in IR absorption of particles under investigation due
903 to water uptake can be recorded as a function of RH, and therefore hygroscopic properties of
904 these particles can be characterized. One advantage of FTIR is that it can be coupled with a
905 range of accessories to form different experimental configurations, including transmission
906 FTIR (Cziczo et al., 1997; Braban et al., 2001; Goodman et al., 2001; Zhao et al., 2006; Song
907 and Boily, 2013; Leng et al., 2015; Zawadowicz et al., 2015), attenuated total reflection-FTIR
908 (ATR-FTIR) (Schuttlefield et al., 2007a; Navea et al., 2010; Hatch et al., 2011; Zeng et al.,
909 2014; Zhang et al., 2014a; Yeşilbaş and Boily, 2016; Navea et al., 2017; Gao et al., 2018),
910 diffuse reflectance infrared Fourier transform spectroscopy (DRIFTS) (Gustafsson et al., 2005;
911 Ma et al., 2010a; Joshi et al., 2017; Ibrahim et al., 2018) and micro-FTIR for which FTIR is
912 coupled with a microscope (Liu et al., 2008b; Liu and Laskin, 2009). Particles under
913 investigation are typically deposited on proper substrates, though aerosol particles can also be
914 studied using transmission FTIR (Cziczo et al., 1997; Cziczo and Abbatt, 2000; Zhao et al.,
915 2006; Zawadowicz et al., 2015). FTIR has been used in a large number of studies to investigate
916 hygroscopic properties of atmospherically relevant particles, and herein we only introduce and
917 highlight a few representative examples.

918 Micro-FTIR was employed to investigate hygroscopic properties of $\text{CH}_3\text{SO}_3\text{Na}$ particles
919 (Liu and Laskin, 2009) and NH_4NO_3 (Wu et al., 2007). [Fig. 12a](#) shows IR spectra of $\text{CH}_3\text{SO}_3\text{Na}$



920 particles during humidification, and no significant change in IR spectra was observed when
921 RH was increased from 0 to 70%; however, when RH was increased to 71%, IR absorption
922 attributed to the $\nu(\text{H}_2\text{O})$ band (at $\sim 3400\text{ cm}^{-1}$) became very evident and its intensity increased
923 with further increase in RH, indicating that the deliquescence of $\text{CH}_3\text{SO}_3\text{Na}$ particles occurred
924 at 71% RH. In addition, at $<71\%$ RH two groups of narrow and structured bands, typically
925 observed for crystalline samples, were observed for $\text{CH}_3\text{SO}_3\text{Na}$ particles. The first one,
926 centered at ~ 1197 and 1209 cm^{-1} , was attributed to asymmetrical stretching of $\nu_8(-\text{SO}_3^-)$, and
927 the other one, centered at 1062 cm^{-1} , was attributed to symmetrical stretching of $\nu_3(-\text{SO}_3^-)$.
928 When RH was increased to 71%, both bands were significantly broaden and shifted to lower
929 wavelengths, further confirming that DRH of $\text{CH}_3\text{SO}_3\text{Na}$ particles was $\sim 71\%$. IR spectra of
930 $\text{CH}_3\text{SO}_3\text{Na}$ particles during dehumidification are displayed in [Fig. 12b](#). Complete
931 disappearance of IR absorption at $\sim 3400\text{ cm}^{-1}$ and significant change in shape and position of
932 IR peaks of $\nu_8(-\text{SO}_3^-)$ and $\nu_3(-\text{SO}_3^-)$ were observed when RH was decreased from 49 to 48%,
933 suggesting that the ERH of $\text{CH}_3\text{SO}_3\text{Na}$ was around 48%.



934

935 **Figure 12.** (a) FTIR spectra of CH₃SO₃Na particles during humidification. (b) FTIR spectra of936 CH₃SO₃Na particles during dehumidification. (c) Water-to-solute ratios (WSR) of CH₃SO₃Na

937 particles as a function of RH: comparison between WSR measured by Liu and Laskin (2009)

938 using micro-FTIR to those determined by Peng and Chan (2001b) using electrodynamic

939 balance. Reprinted with permission by Liu et al. (2009). Copyright 2009 American Chemical

940 Society.

941

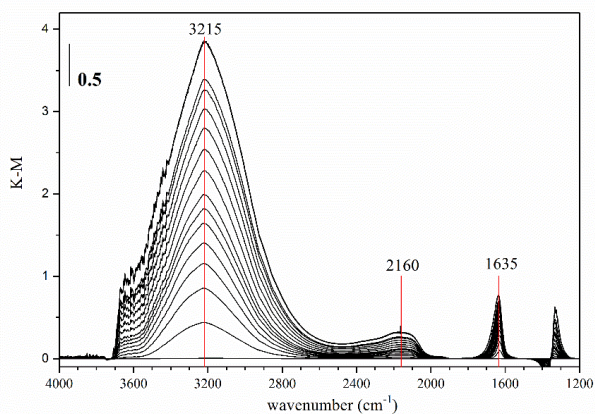


942 FTIR spectra can also be used to investigate hygroscopic growth quantitatively if IR
943 absorbance can be calibrated. In the work by Liu and Laskin (2009), the absorbance ratio of
944 $\nu(\text{H}_2\text{O})$ (at $\sim 3400\text{ cm}^{-1}$) to $\nu_8(-\text{SO}_3^-)$ (at $\sim 1192\text{ cm}^{-1}$) was calibrated and then used to calculate
945 water-to-solute ratios (WSR, defined as mole ratios of H_2O to CH_3SO_3^-) of aqueous $\text{CH}_3\text{SO}_3\text{Na}$
946 particles. As shown in Fig. 12c, WSR values determined using FTIR (Liu and Laskin, 2009)
947 agreed well with those reported in a previous study (Peng and Chan, 2001b) using the
948 electrodynamic balance (EDB). In another study (Liu et al., 2008b), DRH, ERH and WSR
949 measured using micro-FTIR were found to agree well with those reported in literature for NaCl,
950 NaNO_3 and $(\text{NH}_4)_2\text{SO}_4$ particles. ATR-FTIR can be used in a similar way to micro-FTIR to
951 investigate phase transitions and WSR of atmospherically relevant particles, and has been
952 applied to a number of compounds, including NaCl (Schuttlefield et al., 2007a; Zeng et al.,
953 2014), NaNO_3 (Tong et al., 2010b; Zhang et al., 2014a), Na_2SO_4 (Tong et al., 2010b), NH_4NO_3
954 (Schuttlefield et al., 2007a), $(\text{NH}_4)_2\text{SO}_4$ (Schuttlefield et al., 2007a), $\text{CH}_3\text{SO}_3\text{Na}$ (Zeng et al.,
955 2014), sodium formate (Gao et al., 2018), sodium acetate (Gao et al., 2018), and etc.

956 In addition, ATR-FTIR (Schuttlefield et al., 2007a; Schuttlefield et al., 2007b; Hatch et al.,
957 2011; Navea et al., 2017), DRIFTS (Ma et al., 2010a; Joshi et al., 2017; Ibrahim et al., 2018)
958 and transmission FTIR (Goodman et al., 2001) have been employed to investigate water
959 adsorption by insoluble particles, such as mineral dust. [Fig. 13](#) displays IR spectra of adsorbed
960 water on SiO_2 at different RH, as measured using DRIFTS at $30\text{ }^\circ\text{C}$. As shown in [Fig. 13](#), two
961 intensive peaks appeared in IR spectra at elevated RH (Ma et al., 2010a), one at $2600\text{-}3800$
962 cm^{-1} attributed to the O-H stretching mode and the other one at $\sim 1630\text{-}1650\text{ cm}^{-1}$ attributed to
963 the bending mode of H-O-H. Both peaks can be used to quantify the amount of adsorbed water,
964 though surface OH groups may also contribute to the IR absorbance at $\sim 3400\text{ cm}^{-1}$ (Goodman
965 et al., 2001; Tang et al., 2016a). The intensity of the third peak at $2100\text{-}2200\text{ cm}^{-1}$, attributed
966 to the association mode of H-O-H, was much smaller (Ma et al., 2010a). It is possible but non-



967 trivial to convert IR absorbance to the amount of adsorbed water, and the procedure used can
968 be found elsewhere (Goodman et al., 2001; Ma et al., 2010a; Joshi et al., 2017; Ibrahim et al.,
969 2018). It was found that the three-parameter BET equation (Joyner et al., 1945) could well
970 describe water adsorption as a function of RH on mineral oxides (such as SiO₂, TiO₂, Al₂O₃,
971 MgO and etc.) (Goodman et al., 2001; Ma et al., 2010a; Joshi et al., 2017), authentic mineral
972 dust from different sources (Joshi et al., 2017; Ibrahim et al., 2018) and Icelandic volcanic ash
973 (Joshi et al., 2017). Another study (Hatch et al., 2011) suggested that compared to the two-
974 parameter BET equation, the Freundlich adsorption isotherm could better approximate the
975 amount of water adsorbed by kaolinite, illite, and montmorillonite at different RH.



976

977 **Figure 13.** IR spectra of adsorbed water on SiO₂ at 30 °C, as measured using DRIFTS at
978 different RH. Reprint (with modification) with permission by Ma et al. (2010a). Copyright
979 2011 Elsevier.

980

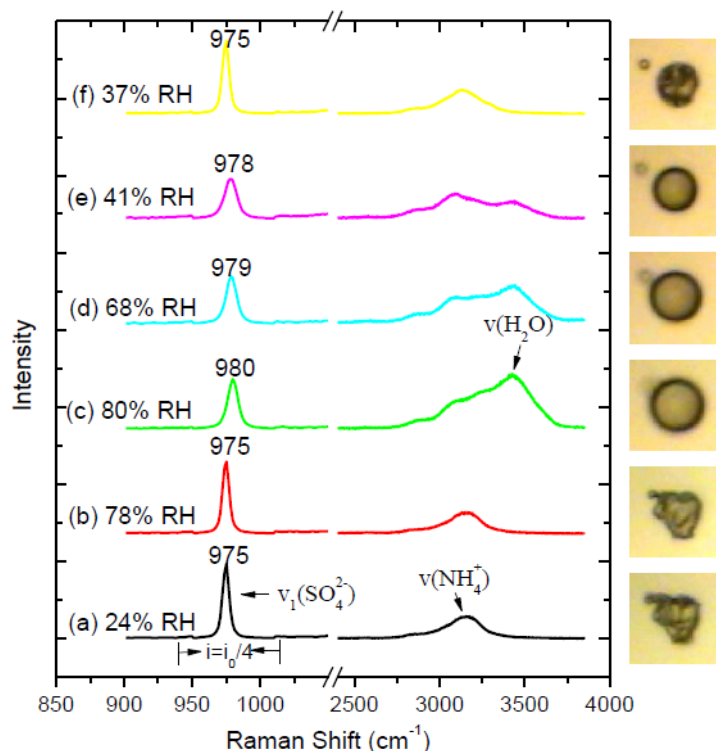
981 **3.4.2 Raman spectroscopy**

982 Raman spectroscopy is complementary to infrared spectroscopy. Bands which are weak in
983 infrared spectroscopy can be strong in Raman spectroscopy, and vice versa. Compared to
984 infrared spectroscopy, Raman spectroscopy is much less sensitive to H₂O, despite that
985 symmetric stretching vibration of H₂O is Raman active, and this characteristic limits



986 application on Raman spectroscopy in exploring particles with low hygroscopicity. Meanwhile,
987 Raman spectroscopy is very sensitive to crystalline structures, making it very useful to
988 investigate particle phase transition. For example, Raman spectroscopy was employed to probe
989 phase transformation of levitated $(\text{NH}_4)_2\text{SO}_4$, Na_2SO_4 , LiClO_4 , $\text{Sr}(\text{NO}_3)_2$, KHSO_4 , RbHSO_4
990 and NH_4HSO_4 microparticles (Tang et al., 1995), and the occurrence of metastable solid states
991 was observed under ambient conditions for Na_2SO_4 , LiClO_4 , $\text{Sr}(\text{NO}_3)_2$ and bisulfates. Raman
992 spectroscopy was also used to investigate hygroscopic properties of supersaturated droplets
993 (Zhang and Chan, 2000; Zhang and Chan, 2002b), such as $(\text{NH}_4)_2\text{SO}_4$ and MgSO_4 .

994 For regular spherical droplets, their Raman spectra may overlap with strong morphology-
995 dependent resonances (Zhang and Chan, 2002b). Nevertheless, if individual droplets were
996 deposited on proper substrates, Raman spectra with high quality (i.e. high signal-to-noise ratios)
997 could be obtained using confocal micro-Raman spectroscopy (Wang et al., 2005; Li et al.,
998 2006). For example, micro-Raman spectrometry was successfully used to investigate
999 hygroscopic properties of $(\text{NH}_4)_2\text{SO}_4$, $\text{Ca}(\text{NO}_3)_2$ and NO_2 -aged $\text{Ca}(\text{NO}_3)_2$ particles deposited
1000 on fluorinated ethylene propylene slides (Liu et al., 2008c; Zhao, 2010). Herein we use
1001 $(\text{NH}_4)_2\text{SO}_4$ as an example to illustrate how Raman spectroscopy can be used to determine
1002 hygroscopic properties of atmospherically relevant particles. [Fig. 14](#) shows Raman spectra and
1003 microscopic images of an $(\text{NH}_4)_2\text{SO}_4$ particle at different RH during humidification and
1004 dehumidification processes (Zhao, 2010). When RH was increased to 80% during
1005 humidification, the Raman peak centered at $\sim 3450\text{ cm}^{-1}$, attributed to the stretching vibration
1006 of H_2O , started to become evident; whereas during dehumidification this peak disappeared
1007 when RH was decreased to 37%. This suggested that deliquescence and efflorescence of
1008 $(\text{NH}_4)_2\text{SO}_4$ took place at 80 and 37% RH, respectively.



1009

1010 **Figure 14.** Raman spectra and microscopic images of an $(\text{NH}_4)_2\text{SO}_4$ particle during
1011 humidification (a-c) and dehumidification (c-f). Reprint with permission by Liu (2008).

1012 Copyright 2008 Peking University.

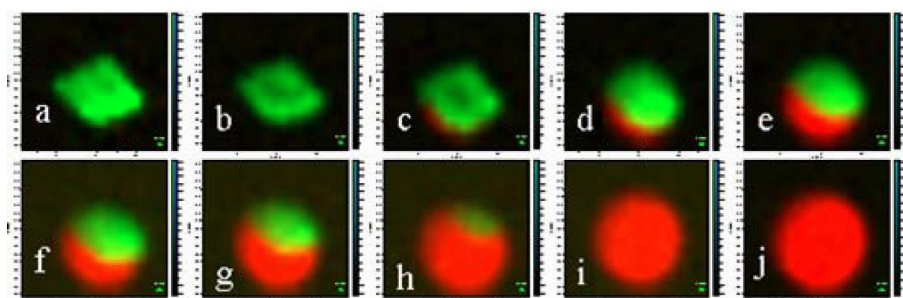
1013

1014 As discussed in previous work (Ling and Chan, 2007; Liu et al., 2008c; Zhao, 2010), the
1015 occurrence of deliquescence and efflorescence of $(\text{NH}_4)_2\text{SO}_4$ could also be identified from the
1016 change in position and full width at half maxima (FWHM) of the Raman peak at 970-980 cm^{-1}
1017 (due to symmetrical stretching of sulfate, $\nu_1\text{-SO}_4^{2-}$). As shown in [Fig. 14](#), during humidification
1018 $\nu_1\text{-SO}_4^{2-}$ was shifted from 975 to 980 cm^{-1} when RH was increased to 80%, and meanwhile its
1019 FWHM increased from 6 to 9 cm^{-1} , implying the occurrence of deliquescence. For comparison,
1020 during dehumidification when RH was decreased to 37%, $\nu_1\text{-SO}_4^{2-}$ was shifted from 978-980
1021 to 975 cm^{-1} and the corresponding FWHM decreased from ~ 10 to 6 cm^{-1} , suggesting that



1022 efflorescence took place at ~37% RH. Phase transitions could be further inferred from
1023 microscopic images (Liu et al., 2008c; Zhao, 2010). Fig. 14 shows that the particle under
1024 investigation became spherical when it was deliquesced (at 80% RH), and became irregular
1025 when efflorescence occurred (at ~37% RH).

1026 The peak intensity ratio of stretching vibration of H₂O to symmetrical stretching of sulfate
1027 is proportional to the molar ratio of H₂O to sulfate in the solution, and could be used to quantify
1028 the water-to-solute ratios (WSR) in aqueous (NH₄)₂SO₄ droplets if properly calibrated (Liu et
1029 al., 2008c). WSR values determined using Raman spectroscopy (Liu et al., 2008c) were found
1030 to agree well with those reported in literature as a function of RH for (NH₄)₂SO₄ and Ca(NO₃)₂
1031 during humidification and dehumidification processes (Stokes and Robinson, 1948; Tang and
1032 Munkelwitz, 1994; Clegg et al., 1998; Kelly and Wexler, 2005). In addition, Liu et al. (2008c)
1033 employed micro-Raman spectroscopy to study heterogeneous reaction of CaCO₃ with NO₂,
1034 and revealed that solid CaCO₃ particles were converted to aqueous droplets after heterogeneous
1035 reaction with NO₂, due to the formation of Ca(NO₃)₂.

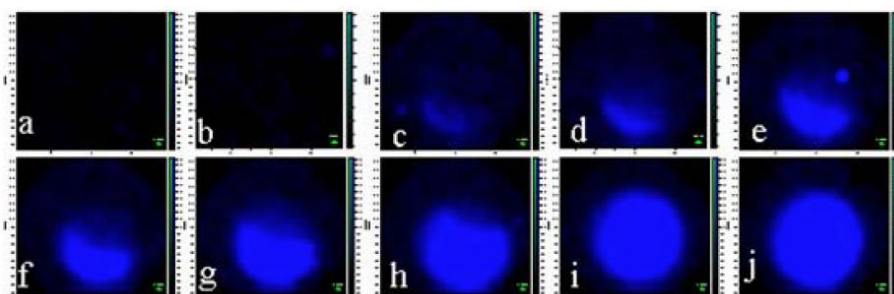


1036
1037 **Figure 15.** Spatial distribution of nitrate (red) and carbonate (green) for a CaCO₃ particle
1038 during heterogeneous reaction with 50 ppmv NO₂ at 40% RH. The reaction time was 0 (a), 10
1039 (b), 23 (c), 38 (d), 58 (e), 64.5 (f), 77.5 (g), 105 (h), 119 (i) and 126 min (j). Reprint with
1040 permission by Zhao et al. (2010). Copyright 2010 Peking University.

1041



1042 Raman microscopy was further used to map spatial distribution of chemical composition
1043 of individual CaCO_3 particles during heterogeneous reaction with 50 ppmv NO_2 at 40% RH
1044 (Zhao, 2010), and the results are displayed in Fig. 15-16. As the reaction proceeded, the spatial
1045 coverage decreased with time for carbonate and increased for nitrate (Fig. 15), suggesting that
1046 CaCO_3 was converted to $\text{Ca}(\text{NO}_3)_2$ upon exposure to NO_2 . Meanwhile, the spatial coverage of
1047 particle water also increased with time (Fig. 16), and its spatial distribution overlapped well
1048 with that of nitrate, suggesting that the increase in particle water content was caused by the
1049 formation of hygroscopic $\text{Ca}(\text{NO}_3)_2$. In addition, microscopic images revealed that the particle
1050 size increased with reaction time, suggesting that hygroscopicity of the particle under
1051 investigation increased as heterogeneous reaction with NO_2 proceeded.



1052
1053 **Figure 16.** Spatial distribution of particle water content for a CaCO_3 particle during
1054 heterogeneous reaction with 50 ppmv NO_2 at 40% RH. The reaction time was 0 (a), 10 (b), 23
1055 (c), 38 (d), 58 (e), 64.5 (f), 77.5 (g), 105 (h), 119 (i) and 126 min (j). Reprint with permission
1056 by Zhao et al. (2010). Copyright 2010 Peking University.

1057

1058 Raman spectroscopy has been employed in a number of studies to investigate hygroscopic
1059 properties of organic aerosols and mixed particles (Ling and Chan, 2007; Ling and Chan, 2008;
1060 Yeung et al., 2009; Yeung and Chan, 2010; Yeung et al., 2010; Ma and He, 2012; Ma et al.,
1061 2013a; Ma et al., 2013b). During humidification-dehumidification processes, oxalic acid was
1062 converted to oxalate when mixed with NaCl (Ma et al., 2013b) or $\text{Ca}(\text{NO}_3)_2$ (Ma and He, 2012),



1063 and such conversion would lead to significant change in hygroscopic properties of mixed
1064 particles. When a hygroscopic sulfate, such as $(\text{NH}_4)_2\text{SO}_4$ or Na_2SO_4 , was mixed with a
1065 hygroscopic calcium salt, such as $\text{Ca}(\text{NO}_3)_2$ or CaCl_2 , gypsum, the hygroscopicity of which
1066 was very limited, would be formed by humidification. Raman spectroscopy was also used to
1067 explore hygroscopic properties of $\text{NH}_4\text{NO}_3/(\text{NH}_4)_2\text{SO}_4$ mixed particles (Ling and Chan, 2007),
1068 and the formation of double-salts, including $3(\text{NH}_4\text{NO}_3)\cdot(\text{NH}_4)_2\text{SO}_4$ and
1069 $2(\text{NH}_4\text{NO}_3)\cdot(\text{NH}_4)_2\text{SO}_4$, was observed for the first time during crystallization. The effect of
1070 malonic, glutaric and succinic acids on the hygroscopic properties of $(\text{NH}_4)_2\text{SO}_4$ particles were
1071 explored using Raman spectroscopy (Ling and Chan, 2008). Partial crystallization of
1072 $(\text{NH}_4)_2\text{SO}_4$ /malonic acid droplets took place at 16% RH, while $(\text{NH}_4)_2\text{SO}_4$ /glutaric acid and
1073 $(\text{NH}_4)_2\text{SO}_4$ /succinic acid particles became completely effloresced at ~30% RH. In addition,
1074 partial deliquescence with solid inclusions was observed at 10-79% RH for $(\text{NH}_4)_2\text{SO}_4$ /malonic
1075 acid, 70-80% for $(\text{NH}_4)_2\text{SO}_4$ /glutaric acid, and 80-90% RH for $(\text{NH}_4)_2\text{SO}_4$ /succinic acid
1076 particles.

1077 3.4.3 Fluorescence spectroscopy

1078 Water molecules in aqueous solutions can exist in two states, i.e. solvated water which
1079 interacts directly with ions, and free water which interacts with other water molecules. Chan
1080 and co-workers (Choi et al., 2004; Choi and Chan, 2005) developed a method to explore the
1081 state of water molecules in single droplets levitated in an EDB. Pyranine, a water soluble dye,
1082 was added into the droplets. When excited by radiation at ~345 nm, Pyranine would emit
1083 fluorescence, and the spectra peaked at ~440 nm (attributed to the presence of solvated water)
1084 and ~510 nm (attributed to the presence of free water). The amounts of solvated and free water
1085 can be derived by combining mass hygroscopic growth factors (determined using the EDB)
1086 and the ratio of fluorescence intensity at 440 nm to that at 510 nm (Choi et al., 2004). It was
1087 found that for NaCl, Na_2SO_4 and $(\text{NH}_4)_2\text{SO}_4$, efflorescence of supersaturated droplets occurred



1088 when the amount of solvated water was equal to that of free water (Choi et al., 2004; Choi and
1089 Chan, 2005). Imaging analysis further revealed that solvated and free water were
1090 homogeneously distributed in the droplets for some types of droplets, e.g., MgSO_4 , but
1091 heterogeneously distributed for other types of droplets, such as NaCl and Na_2SO_4 (Choi and
1092 Chan, 2005).

1093 In another study (Montgomery et al., 2015), fluorescence microscopy was used to monitor
1094 structural change of particle aggregates with RH. In this work NaCl particle aggregates were
1095 collected on wire meshes and then coated with Rhodamine which would generate fluorescence.
1096 Particle aggregates collapsed and became more compact when RH was increased from 0 to 52%
1097 (Montgomery et al., 2015), lower than the DRH of NaCl (~75%). Hosny et al. (2013) developed
1098 fluorescence lifetime imaging microscopy (FLIM) to determine viscosity of individual
1099 particles via measuring viscosity dependent fluorescence lifetime of fluorescent molecular
1100 rotors. The viscosity of a particles is of interest because it is closely related to the phase state
1101 of the particle and largely determines diffusion in the particle (Koop et al., 2011; Reid et al.,
1102 2018). FLIM was used to investigate the viscosity of ozonated oleic acid particles and
1103 secondary organic particles formed by myrcene ozonolysis, and their viscosity was observed
1104 to increase largely with decreasing RH and increasing extent in oxidative aging (Hosny et al.,
1105 2016).

1106 **3.4.4 Other surface characterization techniques**

1107 In addition to spectroscopic and microscopic methods discussed in Sections 3.3 and 3.4,
1108 there are a number of other surface characterization techniques which can be used to explore
1109 water adsorption on surfaces, e.g., sum frequency generation spectroscopy (Ma et al., 2004;
1110 Liu et al., 2005; Jubb et al., 2012; Ault et al., 2013), atmospheric pressure X-ray photoelectron
1111 spectroscopy (Ketteler et al., 2007; Salmeron and Schlogl, 2008; Yamamoto et al., 2010a),
1112 scanning tunneling microscopy (Wendt et al., 2006; He et al., 2009), and etc. These techniques,



1113 which are able to provide fundamental and mechanistic insights into water-surface interactions,
1114 have mainly been applied to surfaces of single crystals, and their usefulness for particles with
1115 direct atmospheric relevance is yet to be demonstrated. As a result, these techniques are not
1116 further discussed here, and readers are referred to aforementioned literature and references
1117 therein for more details.

1118 **3.4.5 Discussion**

1119 Infrared and Raman spectroscopy can be used to quantify particle water content for
1120 unsaturated and supersaturated samples, with no restriction imposed by particle shape or
1121 morphology. Infrared spectroscopy is very sensitive to adsorbed water and has been widely
1122 used to investigate water adsorption (Tang et al., 2016a), as discussed in Section 3.3.1. In
1123 contrast, Raman spectroscopy is not sensitive enough to detect adsorbed water; nevertheless,
1124 recent work (Gen and Chan, 2017) showed that electrospray surface enhanced Raman
1125 spectroscopy was able to detect surface adsorbed water. One important advantage for infrared
1126 and Raman spectroscopy is that simultaneous measurement of chemical composition can be
1127 provided; therefore, they have been coupled to other techniques (such as optical microscope,
1128 electrodynamic balance, and etc.) to further understand hygroscopic properties of
1129 atmospherically relevant particles, as discussed in Sections 3.3, 3.4, 4.1 and 4.2. Infrared and
1130 Raman spectroscopy have been widely employed to characterize ambient aerosol particles
1131 collected on proper substrates, and therefore they can be used to explore hygroscopic properties
1132 of ambient particles in an offline manner.

1133 **3.5 Measurement of electrical properties**

1134 Deliquescence of ionic solids would lead to significant increase in electrical conductivity
1135 and vice versa efflorescence of electrolyte solutions to ionic solids would cause large decrease
1136 in electrical conductivity. Therefore, relative changes in electrical conductivity/impedance can
1137 be used to identify the occurrence of deliquescence and efflorescence (Yang et al., 2006; He et



1138 al., 2008; Schindelholz et al., 2014a; Schindelholz et al., 2014c). For example, in one study
1139 (Schindelholz et al., 2014c) micrometer-sized particles were deposited on an interdigitated
1140 microelectrode sensor housed in an environmental chamber, and the electrical impedance was
1141 detected online while RH in the chamber was varied. The measured DRH and ERH using this
1142 method were found to agree well with literature values for several compounds, e.g., NaCl,
1143 NaBr and KCl (Schindelholz et al., 2014c). In another study (He et al., 2008), the electrical
1144 conductivity and capacitance of a single droplet were measured as different RH to investigate
1145 hygroscopic properties of NaClO₄ particles. Overall, this method has not been widely applied
1146 to study atmospherically relevant particles and thus is not further discussed herein.

1147 **4 Levitated single particles**

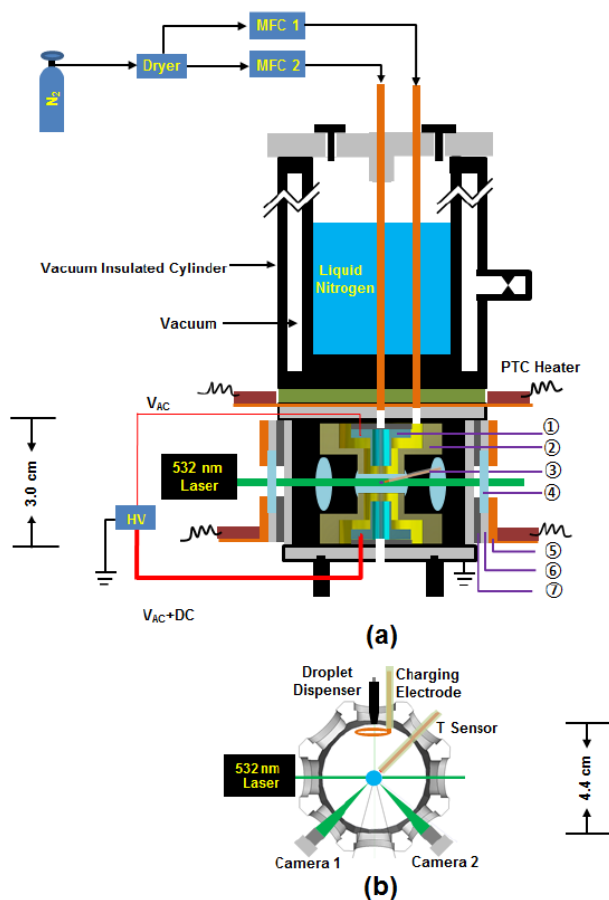
1148 Single particle levitation techniques can be broadly classified into three groups (Krieger et
1149 al., 2012), including electrodynamic balance, optical levitation and acoustic levitation. These
1150 techniques have been widely used to investigate chemical and physical transformation of
1151 atmospherically relevant particles (Lee et al., 2008; Krieger et al., 2012). Herein we introduce
1152 basic principles of each techniques and illustrate how they can help understand aerosol
1153 hygroscopicity via discussing representative studies.

1154 **4.1 Electrodynamic balance**

1155 The electrodynamic balance (EDB) technique has been widely used in the last several
1156 decades, and diameters of particles which can be levitated by EDB are typically in the range of
1157 1-100 μm (Davis, 1997; Davis, 2011). The principle, configuration and operation of EDB have
1158 been extensively documented elsewhere (Reid and Sayer, 2003; Lee et al., 2008; Davis, 2011;
1159 Krieger et al., 2012), and hence are not described in detail here. In brief, a particle can be
1160 levitated and trapped at the null point of the EDB chamber when the AC and DC electric fields
1161 surrounding the particle are properly adjusted. The schematic diagram of a low-temperature
1162 EDB (Tong et al., 2015) is shown in [Fig. 17](#). The main body of the EDB was an octagonal



1163 aluminum chamber with an optical window on each side. Two cold nitrogen flows, which were
1164 first passed through copper tubes immersed in a liquid nitrogen Dewar, were fed into the
1165 chamber to cool the EDB. Temperature at the null point where a particle was trapped was
1166 further regulated using a PTC heater, and temperature and RH inside the chamber were
1167 monitored online. A continuous-wave laser at 532 nm was used to illuminate the trapped
1168 particle, and the scattered light was measured at an angle of 21° to determine the particle size.



1169
1170 **Figure 17.** Schematic diagram of a cold electrodynamic balance. (a) Side view of this set-up:
1171 1) inner electrode; 2) outer electrode; 3) temperature and RH sensors; 4) glass optical window;
1172 5) heating jacket; 6) optical window holder; 7) rubber insulator. (b) Top view of this set-up:
1173 droplets were generated using a droplet dispenser and charged using a charging electrode, and



1174 one of them may be trapped at the null point. A 532 nm laser was used to illuminate the trapped
1175 particle, and two cameras were used to observe the particle and record the scattered light.
1176 Reprint with permission by Tong et al. (2015). Copyright 2015 Copernicus Publications.

1177

1178 In the absence of other forces, the gravitational force of the particle trapped in the EDB is
1179 equal to the balancing electrostatic force, given by Eq. (2) (Pope et al., 2010a; Davis, 2011):

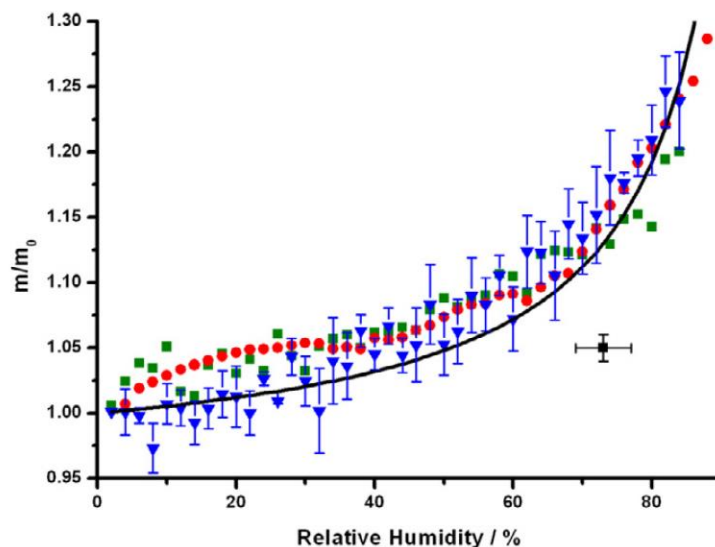
$$1180 \quad mg = nqC \frac{V_{DC}}{z} \quad (2)$$

1181 where m is the particles mass, g is the gravitational constant, n is the number of elementary
1182 charges present on the particles, q is the elementary charge, z is the distance between the two
1183 electrodes, C is a constant dependent on the geometrical configuration of the EDB, and V_{DC} is
1184 the DC voltage required to levitate the particle. Eq. (2) suggests that as long as the charge
1185 present on the trapped particle remains constant, the mass of the particle is proportional to the
1186 DC voltage required to balance its gravitational force. Therefore, the relative mass change of
1187 the particle due to any physical or chemical processing can be quantified by measurement of
1188 the DC voltage. Haddrell et al. (Haddrell et al., 2012) discussed conditions when the
1189 assumption of constant charge may fail and proposed experimental strategies to minimize its
1190 occurrence.

1191 In hygroscopicity studies, the relative mass change of the trapped particle (typically
1192 relative to that under dry condition) during humidification and dehumidification can be
1193 determined to obtain mass hygroscopic growth factors (Peng et al., 2001; Pope et al., 2010a;
1194 Haddrell et al., 2014; Steimer et al., 2015). For example, EDB has been used to measure DRH,
1195 ERH and mass hygroscopic growth factors for a number of inorganic (Tang and Munkelwitz,
1196 1994; Tang and Fung, 1997; Tang et al., 1997; Zhang and Chan, 2002a; Zhang and Chan, 2003;
1197 Hargreaves et al., 2010b), organic (Peng and Chan, 2001a; Peng et al., 2001; Choi and Chan,
1198 2002a; Pope et al., 2010a; Steimer et al., 2015) and mixed inorganic/organic particles (Choi



1199 and Chan, 2002b; Zardini et al., 2008; Pope et al., 2010a) of atmospheric relevance. In addition,
1200 water uptake by different types of pollen was measured as a function of RH using an EDB
1201 (Pope, 2010; Griffiths et al., 2012). As displayed in Fig. 17, pollen grains were found to be
1202 moderately hygroscopic, and the mass of water taken up at 90% RH was around 30% of the
1203 dry mass (Pope, 2010). It was further found that hygroscopic growth of pollen species could
1204 be described by the κ -Kohler theory, with κ values falling in the range of 0.05-0.1 (Pope, 2010).
1205 In another two studies (Haddrell et al., 2013; Haddrell et al., 2014), EDB was utilized to explore
1206 hygroscopic growth of several pharmaceutically relevant formulations, and the results can help
1207 better understand where medical aerosol particles would deposit in our inhalation system.



1208
1209 **Figure 18.** Mass hygroscopic growth factors (defined as the ratio of the particle mass at a given
1210 RH to the dry particle mass) of *Salix caprea* (red circle), *Betula occidentalis* (blue triangle),
1211 and *Narcissus* sp. (green square). For clarity only the error bars ($\pm 1 \sigma$) are shown for *Betula*
1212 *occidentalis*, and the mass hygroscopic growth factors have similar uncertainties for the other
1213 two pollen species. The black square represents water uptake reported by Diehl et al. (2001),
1214 and the black curve represents the fitted mass hygroscopic growth curve using the κ -Kohler
1215 theory. Reprint with permission by Pope (2010). Copyright 2010 IOP Publishing Ltd.



1216

1217 Light scattering techniques can be used to measure optical properties of single particles
1218 levitated in an EDB. For example, Tang and co-workers (Tang and Munkelwitz, 1994; Tang,
1219 1997; Tang and Fung, 1997; Tang et al., 1997) measured the intensity of elastically scattered
1220 light from a levitated particle which was illuminated by a He-Ne laser beam, and managed to
1221 retrieve its diameter and refractive index as a function of RH using the Mie theory. Since the
1222 relative mass change was also determined at the same time, change in particle density with RH
1223 could also be determined (Tang and Munkelwitz, 1994; Tang et al., 1997). In addition,
1224 spectroscopic techniques have been frequently coupled to EDB in order that chemical
1225 information could be simultaneously provided. For example, Chan and colleagues (Zhang and
1226 Chan, 2002a; Zhang and Chan, 2003; Lee et al., 2008) directed a laser beam with a wavelength
1227 of 514.5 nm to the trapped particle in the EDB and measured the resulting Raman signals with
1228 a CCD detector. This configuration enabled change in particle composition and hygroscopicity
1229 due to heterogeneous reactions to be monitored online in a simultaneous manner (Lee and Chan,
1230 2007; Lee et al., 2008). Experimental work in which EDB was coupled to fluorescence
1231 spectroscopy has also been reported (Choi et al., 2004; Choi and Chan, 2005).

1232 In addition to hygroscopicity research, EDB have also been used in a number of studies
1233 (Reid and Sayer, 2003; Lee et al., 2008; Pope et al., 2010b; Davis, 2011; Krieger et al., 2012;
1234 Bilde et al., 2015b) to investigate other physicochemical properties (including vapor pressure,
1235 mass accommodation coefficients, evaporation coefficients, gas phase diffusion coefficients,
1236 and etc.) and chemical reactions of atmospheric particles.

1237 **4.2 Optical levitation**

1238 Trapping and manipulation of atoms, molecules, nanostructures and particles have been
1239 widely used in a number of scientific fields (Ashkin, 2000; McGloin, 2006; Mitchem and Reid,
1240 2008; Krieger et al., 2012; Lehmuskero et al., 2015; Spesyvtseva and Dholakia, 2016; Gong et



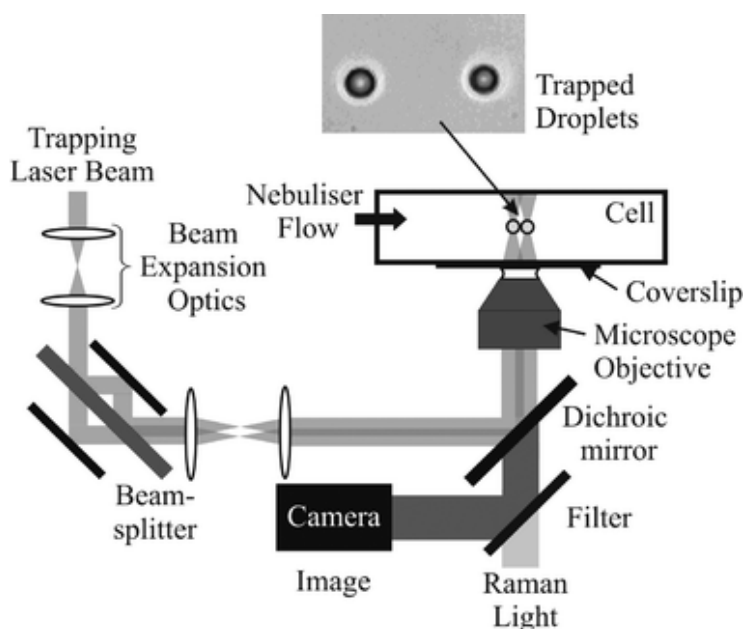
1241 al., 2018). The effects of radiation pressure on microscopic particles were first demonstrated
1242 in 1970 (Ashkin, 1970). After that, levitation of solid particles and liquid droplets in air using
1243 a vertically propagating weakly focused laser beam was achieved (Ashkin and Dziedzic, 1971;
1244 Ashkin and Dziedzic, 1975). Applications of optical levitation to particles of atmospheric
1245 relevance have been previously reviewed (Mitchem and Reid, 2008; Wills et al., 2009; Krieger
1246 et al., 2012), and very recently general applications related to trapping single particles in air
1247 have also been summarized (Gong et al., 2018).

1248 Interaction of an incident laser beam with a particle consists of two forces: (i) a scattering
1249 force that results from the transfer of momentum to the dielectric particle from backscattered
1250 photons, and (ii) a gradient force that depends on the gradient of the electromagnetic field
1251 associated with the optical beam. The first type of force exerts a push on the particle, while the
1252 second type exerts a pull (Krieger et al., 2012). Utilization of either of these two forces as the
1253 primary force to trap particles leads to two types of optical levitation techniques, i.e. optical
1254 levitation trap and optical tweezers. In an optical levitation trap, the laser beam is mildly
1255 focused and the particle adopts a stable position within the divergent beam above the focus,
1256 where the downward gravitational force is exactly balanced by the upward scattering force
1257 (Wills et al., 2009). Droplets of 20-100 μm in diameter can be trapped with active
1258 compensating adjustment of light intensity with respect to changes in droplet size (Krieger et
1259 al., 2012); nevertheless, optical levitation traps are intrinsically delicate and unstable (Wills et
1260 al., 2009). Optical tweezers effectively create a strong intensity gradient in three dimensions,
1261 by amplifying the gradient force using a microscope objective lens to tightly focus the trapping
1262 laser beam. The gradient force leads to strong transverse and axial restoring forces that are
1263 many orders of magnitude larger than the gravitational force of the particle (Wills et al., 2009),
1264 restoring the particle to the region with the highest light intensity (Krieger et al., 2012).
1265 Therefore, particles can be captured and held tightly against the scattering and gravitational



1266 forces, allowing true 3-dimensional confinement of particles with diameters of 1-10 μm
1267 (Krieger et al., 2012).

1268 Different laser beams have been used as incident light sources. In optical levitation traps,
1269 mildly focused Gaussian beams (Ashkin and Dziedzic, 1975), counter-propagating Gaussian
1270 beams (Ashkin, 2000) and a Gaussian beam plus a Bessel beam (Davis et al., 2015a) can be
1271 used to trap single particles. In optical tweezers, particles can be trapped with a single laser
1272 beam (Magome et al., 2003; Mitchem et al., 2006a) or in a dual-trap configuration with two (or
1273 split) laser beams (Fallman and Axner, 1997; Buajarern et al., 2006; Butler et al., 2008), and
1274 counter-propagating Bessel beams have also been used (Lu et al., 2014). Fig. 19 shows a typical
1275 experimental setup for a dual-trap configuration of optical tweezers in which droplets were
1276 generated using a nebulizer and then introduced into the trapping cell (Butler et al., 2008). A
1277 laser beam at 532 nm was used as the trapping light and focused by an oil immersion objective
1278 to create a working distance of $\sim 130 \mu\text{m}$. A beam splitter was then used to create two parallel
1279 trapping beams that could be translated independently over distances of $>50 \mu\text{m}$, allowing
1280 individual manipulation or probing of two separate particles in close range.



1281

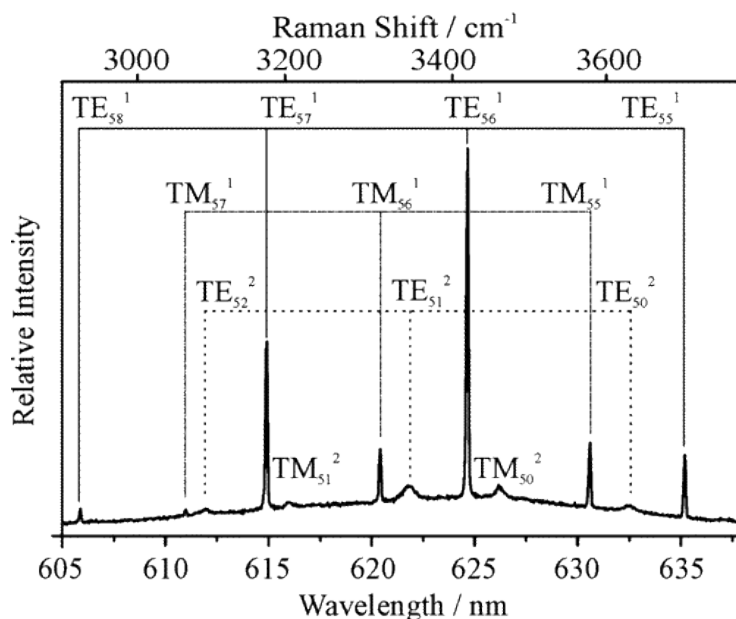
1282 **Figure 19.** Schematic diagram of the dual trap configuration of the optical tweezers. Reprint
1283 with permission by Butler et al. (2008). Copyright 2008 Royal Society of Chemistry.

1284

1285 When a single particle is optically trapped, it can be characterized by a number of
1286 techniques. Direct imaging is the most straightforward one, and bright field imaging can be
1287 used to determine particle size with an accuracy of $\pm 0.2 \mu\text{m}$ (Burnham and McGloin, 2009).
1288 However, this method suffers from low accuracy in size measurement due to the dependence
1289 of the axial position on laser power (Knox et al., 2007). Spectroscopy, especially Raman
1290 spectroscopy, is more accurate in particle size measurement (Wills et al., 2009) and can also
1291 offer compositional information (Reid et al., 2007). Known as cavity-enhanced Raman
1292 spectroscopy, spectra recorded from optically trapped particles comprise of spontaneous and
1293 stimulated Raman scattering (Mitchem et al., 2006a; Wills et al., 2009). Spontaneous Raman
1294 scattering can be used to investigate changes in OH stretching vibrations ($2900\text{-}3700 \text{ cm}^{-1}$) of
1295 particulate water during hygroscopic growth as well as hydrogen bonding environments within



1296 the particle. On the other hand, stimulated Raman scattering can be strongly amplified (by a
1297 factor of >10) (Mitchem et al., 2006a), but it occurs only at distinct wavelengths that are
1298 commensurate with whispering gallery modes (WGMs). This stimulated Raman scattering
1299 under WGMs, as shown in Fig. 20, is also commonly referred to as morphology-dependent
1300 resonances or cavity resonances (Mitchem et al., 2006a). Using the stimulated Raman spectra,
1301 one can achieve a sizing accuracy of ± 2 nm that is only limited by spectral dispersion of the
1302 spectrograph (Mitchem et al., 2006a; Mitchem and Reid, 2008). Other techniques have also
1303 been coupled with optical levitation, including elastic (Mie) scattering (Ward et al., 2008), light
1304 absorption (Knox and Reid, 2008), and so on.



1305
1306 **Figure 20.** An example of Raman scattering from a trapped water droplet, illuminated at 514.5
1307 nm. Stimulated Raman scattering is observed at wavelengths commensurate with whispering
1308 gallery modes. The resonant modes can be assigned by comparison with Mie scattering
1309 calculations, and the droplet radius can then be derived. Reprint with permission by Mitchem
1310 et al. (2006a). Copyright 2006 American Chemical Society.
1311



1312 There are a number of studies in which optical levitation techniques were employed to
1313 investigate hygroscopic properties of atmospheric particles. Based on an early design (Hopkins
1314 et al., 2004), Mitchem et al. (2006a) investigated hygroscopic growth of a NaCl particle trapped
1315 by optical tweezers for RH >80% by characterizing spontaneous and stimulated Raman
1316 scattering. Changes in the OH stretching band of the particle were observed as RH increased,
1317 and size measurement was achieved with an accuracy of a few nanometre and a time resolution
1318 of 1 s. The measured equilibrium sizes agreed well with these predicted using the Köhler theory,
1319 and the largest uncertainties came from the error in RH measurement with a capacitive sensor
1320 ($\pm 2\%$ for RH below 90%) (Mitchem et al., 2006a). The change in the OH stretching band was
1321 also used to probe the formation and destruction of hydrogen bonding in a trapped NaCl particle
1322 at different RH (Treuel et al., 2010).

1323 A dual-trap configuration of optical tweezers, in which two particles could be levitated
1324 simultaneously (as shown in [Fig. 19](#)), was employed to investigate hygroscopic properties of
1325 individual particles (Butler et al., 2008). In this setup, the first particle with well-known
1326 hygroscopicity (in this case, NaCl) served as an accurate RH probe ($\pm 0.09\%$ even for
1327 RH >90%), while the second particle (NaCl/glutaric acid, for example) was interrogated for its
1328 hygroscopic properties as an “unknown” particle. Excellent agreement between experimental
1329 measurement and prediction using the Köhler theory was achieved (Butler et al., 2008).
1330 Hygroscopic properties of inorganic/organic mixed particles, including NaCl/glutaric acid and
1331 $(\text{NH}_4)_2\text{SO}_4$ /glutaric acid mixtures with different mass ratios, were further studied using this
1332 comparative approach (Hanford et al., 2008). Measured equilibrium sizes of those
1333 inorganic/organic mixed particles were found to agree well with theoretical predictions,
1334 demonstrating the robustness of this approach for hygroscopicity study at the high RH (>97%).

1335 Using the dual-trap configuration, hygroscopic properties of NaCl and $(\text{NH}_4)_2\text{SO}_4$ were
1336 measured at low RH (down to 80%) (Walker et al., 2010). The usage of NaCl as a reference



1337 particle could reduce the errors associated with the measured equilibrium wet size of
1338 $(\text{NH}_4)_2\text{SO}_4$ to $<0.2\%$; for comparison, the errors could be as large as $\pm 5\%$ when a capacitance
1339 RH probe was used. The difference between the measured and modelled growth factors was
1340 found to be in the range of 0.1-0.3% for $(\text{NH}_4)_2\text{SO}_4$ in the medium RH region (84 – 96% RH)
1341 (Walker et al., 2010). In a following study (Hargreaves et al., 2010a), the dual-trap
1342 configuration was utilized to investigate hygroscopic properties of NaCl at 45-75% RH, and
1343 growth factors of NaCl measured by this (Hargreaves et al., 2010a) and previous studies (Butler
1344 et al., 2008; Hanford et al., 2008) were found to be in excellent agreement with those predicted
1345 (Clegg and Wexler, 2011) for RH in the range of 45-99%.

1346 Optical levitation can also be used to explore phase transitions and surface hydration. For
1347 example, liquid to solid phase transitions were observed for the $(\text{NH}_4)_2\text{SO}_4$ /glycerol/ H_2O
1348 system via morphology-dependent resonances and Raman spectroscopy (Trunk et al., 1997),
1349 and Raman spectroscopy revealed the presence of adsorbed water on the surface of optically
1350 levitated mineral oxide particles at different RH (Rkiouak et al., 2014). In addition, optical
1351 tweezers were utilized to investigate efflorescence and deliquescence of a number of inorganic
1352 salts (Davis et al., 2015a). Compared to deliquescence, efflorescence usually occurs for a lower
1353 RH (Martin, 2000). Immersion of solid particles (e.g., mineral dust) in aqueous droplets would
1354 cause efflorescence to take place at higher RH, as observed in previous work (Han et al., 2002;
1355 Pant et al., 2006). Recently optical levitation was employed to explore efflorescence of
1356 supersaturated aqueous droplets induced by collision with solid particles (Davis et al., 2015a;
1357 Davis et al., 2015b). It was found that upon collision with several different types of solid
1358 particles, including NaCl, KCl, $(\text{NH}_4)_2\text{SO}_4$, Na_2SO_4 , and etc., aqueous NH_4NO_3 , $(\text{NH}_4)_2\text{SO}_4$
1359 and NaCl droplets would effloresce at RH significantly higher than those for homogeneous
1360 efflorescence (Davis et al., 2015b).



1361 Kinetics of water uptake by aerosol particles can also be studied using optical levitation
1362 techniques. For example, hygroscopic properties of NaCl particles coated with oleic acid was
1363 examined using optical tweezers (Dennis-Smith et al., 2012). It was observed that
1364 efflorescence and deliquescence behavior of the NaCl particle and the timescales to reach re-
1365 equilibrium were not affected by the presence of oleic acid; furthermore, heterogeneous
1366 oxidation by O₃ was found to increase the hygroscopicity of oleic acid in the NaCl-oleic acid
1367 mixed particle (Dennis-Smith et al., 2012). In another study (Tong et al., 2011), optical
1368 tweezers were employed to explore the timescales for mass transfer of water in glassy aerosol
1369 particles. It was found that the half-time for re-equilibration after RH change could increase
1370 from tens and hundreds of seconds (RH above glass transition) to >1000 seconds (RH below
1371 glass transition) for sucrose-water, raffinose-water and sucrose-NaCl-water systems.

1372 Particle viscosity determines diffusion coefficients of water molecules in the particles,
1373 affecting water uptake kinetics (Reid et al., 2018). A novel microrheological method, which
1374 employed holographic aerosol optical tweezers, has been developed to measure particle
1375 viscosity in the range of 10⁻³ to 10⁹ Pa S (Power et al., 2013). In brief, coalescence between
1376 two airborne particles, with volumes smaller than 500 femtolitres, was initiated using the
1377 optical tweezers, and the time required by the coalesced particle to relax to a sphere was
1378 measured to infer particle viscosity. More details of this method can be found elsewhere (Power
1379 et al., 2013; Song et al., 2016).

1380 In addition, optical levitation techniques have also been employed to investigate a myriad
1381 of heterogeneous processes, including evaporation of volatile/semi-volatile species, mixing of
1382 inorganic/organic particles and heterogeneous reactions (Mitchem et al., 2006b; Buajarern et
1383 al., 2007; Tang et al., 2014; Jones et al., 2015; Gorkowski et al., 2016; Cai and Zhang, 2017).
1384 Optical tweezers have recently become commercially available, and commercial instruments



1385 have been used to investigate physicochemical properties and processes of atmospherically
1386 relevant particles (Davies and Wilson, 2016; Haddrell et al., 2017).

1387 **4.3 Acoustic levitation**

1388 Inside a typical acoustic levitator, high frequency sound wave, generated using a
1389 piezoelectric oscillator (also called radiator), is reflected by a concave reflector. Standing
1390 waves can be generated in the space between the radiator and the reflector if the radiator and
1391 the reflector are properly positioned. Droplets with diameters ranging from tens of micrometers
1392 to a few millimeters can then be trapped in the vertical position near one of these existing wave
1393 nodes. Detailed description of this technique can be found elsewhere (Kavouras and Krammer,
1394 2003b; Ettner et al., 2004; Mason et al., 2008). The size of the levitated particle can be
1395 characterized using a camera, and spectroscopic techniques, such as FTIR and Raman
1396 spectroscopy, can be coupled to the acoustic levitator so that chemical information can be
1397 simultaneously provided (Brotton and Kaiser, 2013).

1398 Acoustic levitation has been used in a variety of research fields to investigate interactions
1399 of single solid/liquid particles with different gases (Kavouras and Krammer, 2003a; Mason et
1400 al., 2008; Schenk et al., 2012), including water vapor. For example, Schenk et al. (2012) used
1401 an acoustic levitator to measure hygroscopicity of imidazolium-based ionic liquids, and low
1402 temperature acoustic levitation was developed to study homogeneous and heterogeneous
1403 freezing of aqueous droplets (Ettner et al., 2004; Diehl et al., 2009; Diehl et al., 2014). Particles
1404 which can be acoustically levitated are typically $>20\ \mu\text{m}$ (Mason et al., 2008; Krieger et al.,
1405 2012), while most of atmospheric aerosol particles are significantly smaller (Seinfeld and
1406 Pandis, 2016). Therefore, compared to the other two levitation techniques (i.e. EDB and optical
1407 levitation), acoustic levitation is much less widely utilized in atmospheric chemistry (Krieger
1408 et al., 2012).



1409 **4.4 Discussion**

1410 Both EDB and optical levitation can measure liquid water content for unsaturated and
1411 supersaturated samples, as particles used in these experiments are free of contact with other
1412 substances. EDB measures relative mass change to quantify aerosol liquid water content, and
1413 thus there is no constrain on particle shape; whereas for optical levitation, particle diameter
1414 change is usually measured optically, and particles under investigation need to be spherical.
1415 Both techniques may not be sensitive enough to study water adsorption. To our knowledge,
1416 they have not been used to investigate hygroscopic properties of ambient aerosol particles,
1417 though in principle they both have the capacity. One reason is that particles that can be explored
1418 using these techniques are usually one order of magnitude larger than those typically found in
1419 the troposphere. Another reason could be that only one particle can be examined in each
1420 experiment, while there are numerous aerosol particles in the ambient air. One unique
1421 advantage of these two techniques is that size, chemical composition and optical properties of
1422 levitated particles can be obtained in an online and noninvasive manner, making them very
1423 valuable to explore aerosol properties and processes at the fundamental level (Lee et al., 2008;
1424 Krieger et al., 2012).

1425 **5 Aerosol particles**

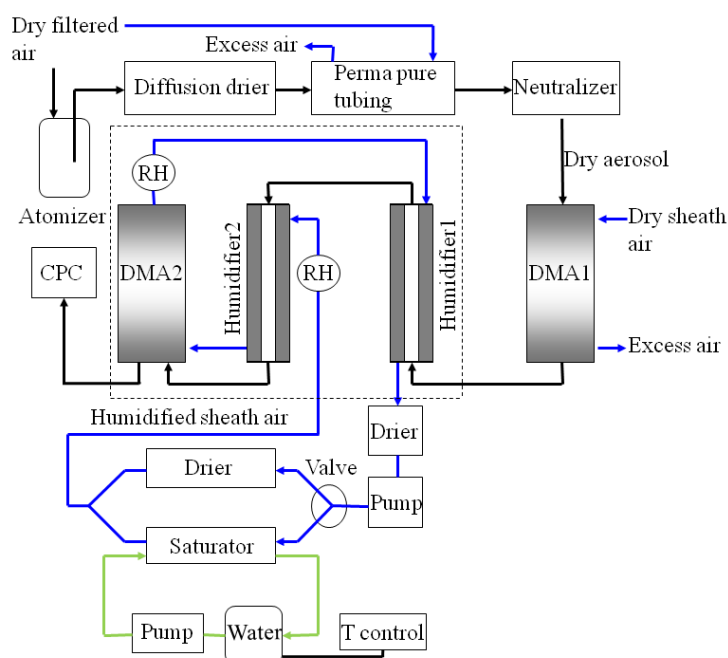
1426 In this section techniques that can be employed to investigate hygroscopic properties of
1427 airborne aerosol particles and can also be deployed for field measurements are reviewed. We
1428 discuss in Section 5.1 humidity-tandem differential mobility analysers which measure mobility
1429 diameter change of aerosol particles upon humidity change. Hygroscopic growth would further
1430 lead to change in aerosol optical properties, which can be measured to infer aerosol
1431 hygroscopicity, as reviewed in Section 5.2. In Section 5.3 we discuss in brief a few techniques
1432 developed to explore hygroscopic properties of black carbon aerosol in specific.



1433 **5.1 Humidity-tandem differential mobility analyser (H-TDMA)**

1434 **5.1.1. Basic H-TDMA**

1435 The tandem differential mobility analyser (TDMA) was pioneered in 1978 and called the
1436 aerosol mobility chromatograph at that time (Liu et al., 1978). The terminology “TDMA” was
1437 first introduced in 1986 in a study (Rader and McMurry, 1986) which showed that size change
1438 as small as 1% could be readily measured. In addition to size change due to humidification
1439 (humidity-TDMA), TDMAs can also be used to measure particle size change due to other
1440 processing such as heating (Bilde et al., 2015a). H-TDMA is probably the most widely used
1441 technique for aerosol hygroscopicity measurement in both laboratory (Gibson et al., 2006;
1442 Herich et al., 2009; Koehler et al., 2009; Wex et al., 2009a; Good et al., 2010b; Wu et al., 2011;
1443 Hu et al., 2014; Lei et al., 2014; Gomez-Hernandez et al., 2016; Jing et al., 2016; Zieger et al.,
1444 2017) and field studies (McMurry and Stolzenburg, 1989; Swietlicki et al., 2008; Ye et al.,
1445 2011; Ye et al., 2013; Wang et al., 2014b; Yeung et al., 2014b; Atkinson et al., 2015; Cheung
1446 et al., 2015; Wu et al., 2016; Sorooshian et al., 2017). There are a number of H-TDMAs
1447 developed and used by individual research groups, and all the instruments follow the same
1448 principle. Recently these instruments have also become commercially available, e.g., from
1449 Brechtel Manufacturing Inc. (Lopez-Yglesias et al., 2014) and MSP Corporation (Sarangi et
1450 al., 2019). Swietlicki et al. (2008) provided a good description of the operation principle, and
1451 discussed potential error sources for H-TDMA measurements; Duplissy et al. (2009) analyzed
1452 the result from an intercomparison of six different H-TDMAs and recommended guidelines for
1453 design, calibration, operation and data analysis for H-TDMAs. Below we describe in brief how
1454 a typical H-TDMA works.



1455

1456 **Figure 21.** Schematic diagram of a typical H-TDMA instrument. Reprint with permission by
1457 Jing et al. (2016). Copyright 2016 Copernicus Publications.

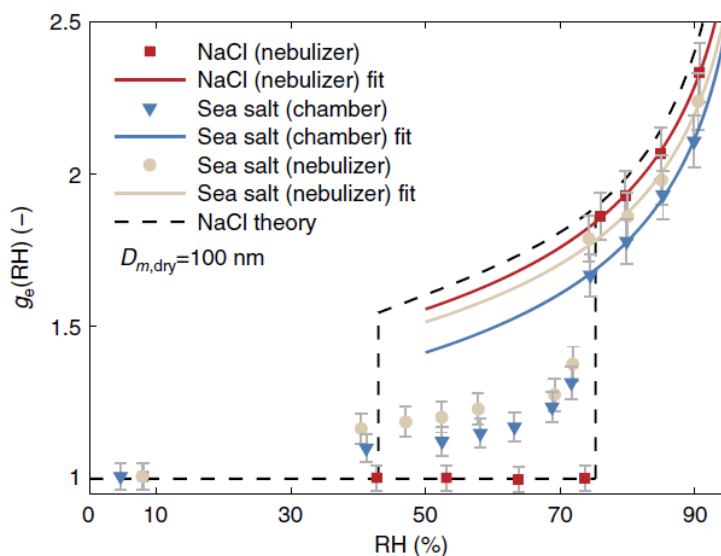
1458

1459 As illustrated in Fig. 21, polydisperse ambient or laboratory-generated aerosol particles
1460 were sampled through an aerosol dryer to reduce the RH to $<15\%$, and the dry aerosol flow
1461 was passed through a neutralizer and then the first DMA (DMA1) to generate quasi-
1462 monodisperse aerosol particles. After that, the aerosol flow was delivered through a
1463 humidification section to be humidified to a given RH, and aerosol particles exiting the
1464 humidification section were monitored using the second DMA (DMA2) coupled with a
1465 condensation particle counter (CPC) to provide number size distributions. The growth factor
1466 (GF) is defined as the ratio of aerosol mobility diameter at a given RH to that at dry condition.
1467 The raw H-TDMA data should be inverted to retrieve the actual growth factor probability
1468 density function (Rader and McMurry, 1986; Gysel et al., 2009; Good et al., 2010a), and
1469 currently the inversion algorithm developed by Gysel et al. (2009) is widely used. One major



1470 uncertainty for H-TDMA measurements stems from the accuracy of RH in the second DMA,
1471 and considerable efforts are needed to minimize the RH and temperature fluctuation (Swietlicki
1472 et al., 2008; Duplissy et al., 2009; Massling et al., 2011; Lopez-Yglesias et al., 2014). The
1473 residence time in the humidification section should exceed 10 s for aerosol particles to reach
1474 the equilibrium under a given RH, while it should not be more than 40 s due to potential
1475 evaporation of semi-volatile species (Chan and Chan, 2005; Duplissy et al., 2009). In addition,
1476 it is important to check the H-TDMA performance via comparing the measured GF with
1477 theoretical values for reference aerosol particles, such as $(\text{NH}_4)_2\text{SO}_4$ and NaCl (Swietlicki et
1478 al., 2008; Duplissy et al., 2009).

1479 In typical laboratory studies (Herich et al., 2009; Koehler et al., 2009; Jing et al., 2016;
1480 Zieger et al., 2017), aerosol size is measured as different RH using the H-TDMA to get the
1481 RH-dependent GF. Humidograms, in which GF are plotted as a function of RH, are shown in
1482 [Fig. 22](#) for NaCl and synthetic sea salt aerosol particles, suggesting that at a given RH, GF of
1483 sea salt aerosol is 8-15% smaller than NaCl aerosol (Zieger et al., 2017). Since both NaCl and
1484 synthetic sea salt aerosol particles are non-spherical under dry conditions, growth factors were
1485 reported after shape factor correction. The difference in GF between NaCl and synthetic sea
1486 salt aerosols was attributed to the presence of hydrates (such as the hydrates of MgCl_2 and
1487 CaCl_2) with lower hygroscopicity (when compared to NaCl) in synthetic sea salt (Zieger et al.,
1488 2017).



1489

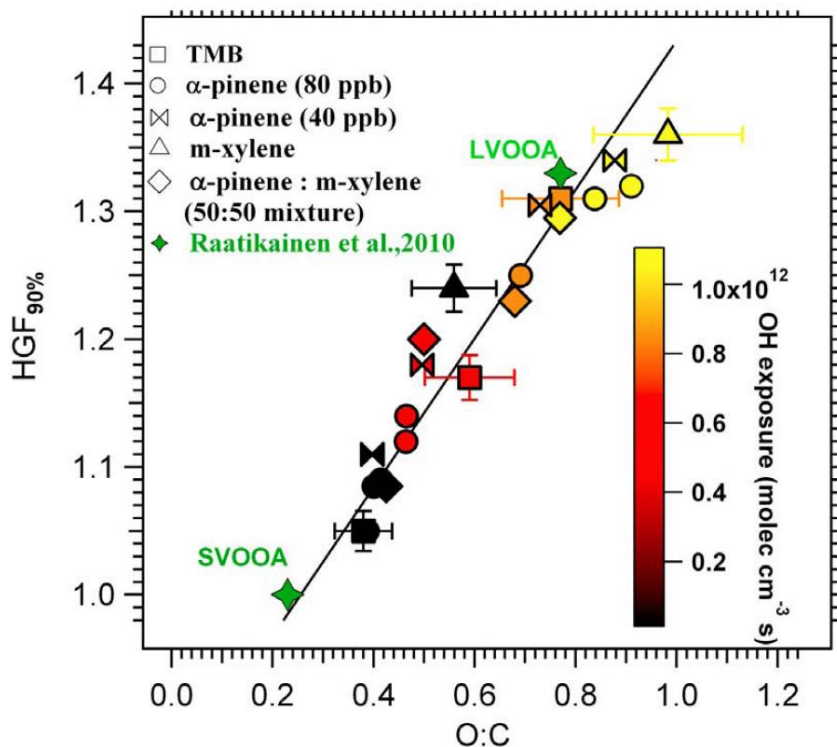
1490 **Figure 22.** Measured hygroscopic growth factors of NaCl and synthetic sea salt aerosol
1491 particles as different RH. NaCl aerosol particles were generated using a nebulizer, and both a
1492 nebulizer and a sea spray chamber were used to generate sea salt aerosol particles. Reprint with
1493 permission by Zieger et al. (2017). Copyright 2017 The Author(s).

1494

1495 H-TDMA has been widely used to investigate hygroscopic growth of secondary organic
1496 aerosol (Prenni et al., 2007; Duplissy et al., 2008; Wex et al., 2009b; Good et al., 2010b;
1497 Massoli et al., 2010; Duplissy et al., 2011; Alfarra et al., 2013; Zhao et al., 2016), which
1498 significantly contributed to submicrometer aerosol particles over the globe (Zhang et al., 2007).
1499 Using an aerosol flow tube, Massoli et al. (2010) generated secondary organic aerosols (SOA)
1500 via OH oxidation of α -pinene, 1,3,5-trimethylbenzenen (TMB), m-xylene and a 50:50 mixture
1501 of α -pinene and m-xylene, and measured their hygroscopic growth at 90% RH using a H-
1502 TDMA. As shown in [Fig. 23](#), measured GF at 90% RH ranged from 1.05 (non-hygroscopic) to
1503 1.35 (moderately hygroscopic) for SOA systems examined, increasing linearly with O:C ratios
1504 determined using an Aerodyne High Resolution Time-of-Flight Mass Spectrometer (Massoli



1505 et al., 2010). In addition, for most SOA systems studied, single hygroscopicity parameters (κ)
1506 derived from H-TDMA measurements were smaller than these derived from CCN activity
1507 measurements (Massoli et al., 2010). Gaps between hygroscopic growth and cloud activation
1508 have also been observed in a number of other studies for SOA (Prenni et al., 2007; Juranyi et
1509 al., 2009; Petters et al., 2009; Wex et al., 2009b; Good et al., 2010b; Whitehead et al., 2014;
1510 Zhao et al., 2016). One major reason for such gaps is that SOA usually contain substantial
1511 amount of slightly soluble materials, which only undergo partial dissolution under water-
1512 subsaturated conditions but can be dissolved to a significantly larger extent under water
1513 supersaturated conditions (when more water is available). Further discussion on reconciliation
1514 between hygroscopic growth and cloud activation can be found elsewhere (Petters et al., 2009;
1515 Wex et al., 2009b). In another study (Li et al., 2014), H-TDMA was used to explore
1516 hygroscopic properties of SOA formed via OH oxidation and direct photolysis of
1517 methoxyphenol (a model compound for biomass burning aerosol) in the aqueous phase. For
1518 SOA generated from aqueous phase OH oxidation, GF at 90% RH was observed to increase
1519 linearly with the O:C ratio, but the slope was around three times smaller than that reported by
1520 Massoli et al. (2010).



1521

1522 **Figure 23.** Growth factors of SOA measured using a H-TDMA at 90% RH as a function of
1523 O:C ratios. Reprint with permission by Massoli et al. (2010). Copyright 2010 American
1524 Geophysical Union.

1525

1526 Since RH scanning is time-consuming, in most ambient applications H-TDMA
1527 measurements are usually carried out at a fixed RH (mostly 90%, and 85% to a less extent) for
1528 one or a few dry particle diameters (Swietlicki et al., 2008; Kreidenweis and Asa-Awuku, 2014;
1529 Cheung et al., 2015). Usually at least one diameter in the center of Aitken mode (~50 nm) and
1530 one size in the center of the accumulation mode (~150 nm) are selected (Swietlicki et al., 2008).
1531 The second DMA is typically scanned over a diameter range to cover a corresponding GF range
1532 between 0.9 and 2.0 (sometimes up to 2.5) at 90% RH (Swietlicki et al., 2008). However, there
1533 have been a few studies which measured GF of size-selected ambient aerosols as a function of

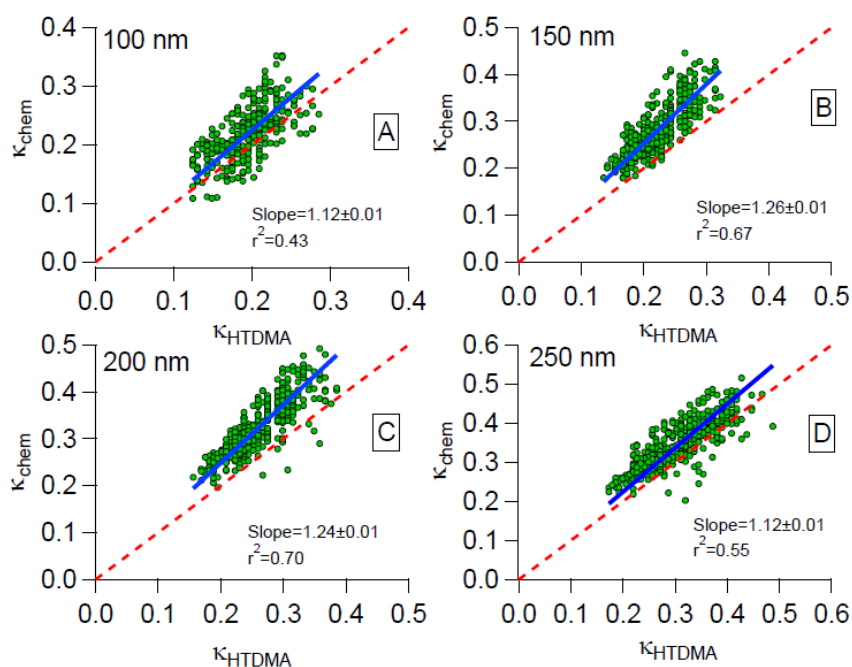


1534 RH (Santarpia et al., 2004; Cheung et al., 2015). For example, Cheung et al. (2015) measured
1535 the GF of ambient aerosol particles (100 and 200 nm) as a function of RH (10-93 %) in Hong
1536 Kong using a H-TDMA, and found that the derived κ values at (or above) 90% RH were
1537 significantly larger than those derived at 40% RH. Each set of such measurements took ~3 h,
1538 limiting its application to periods with large fluctuation in aerosol composition (Cheung et al.,
1539 2015).

1540 To further understand hygroscopic properties of ambient aerosol particles, aerosol
1541 hygroscopicity closure studies have been widely carried out (Swietlicki et al., 1999; Dick et al.,
1542 2000; Gysel et al., 2007; Cerully et al., 2011; Wu et al., 2013; Wu et al., 2016; Schurman et al.,
1543 2017; Hong et al., 2018). In such studies, hygroscopic growth measurements using H-TDMA
1544 are concurrently performed with aerosol chemical composition measurements, and measured
1545 growth factors can then be compared to these calculated based measured chemical composition.
1546 Aerosol chemical compositions were usually measured offline in the early stage (Swietlicki et
1547 al., 1999; Dick et al., 2000) and have been increasingly determined online with high time
1548 resolution using aerosol mass spectrometry (Gysel et al., 2007; Wu et al., 2013) and single
1549 particle mass spectrometry (Wang et al., 2014c; Li et al., 2018a). For example, Wu et al. (2013)
1550 used a H-TDMA to measure aerosol hygroscopic growth at 90% RH and an Aerodyne High
1551 Resolution Time-of-Flight Mass Spectrometer (HR-ToF-AMS) to measure size-resolved
1552 aerosol chemical composition at a middle-level mountain area in central Germany. Single
1553 hygroscopicity parameters, κ_{htdma} , derived from growth factors measured using H-TDMA, were
1554 compared to those derived from aerosol composition (κ_{chem}), assuming ideal mixing. If the
1555 average compositions of submicron particles were used to calculate κ_{chem} , reasonably good
1556 agreement between κ_{htdma} and κ_{chem} was found for 250 nm particles while no correlation was
1557 observed for 100 nm particles (Wu et al., 2013). If size-resolved aerosol compositions were
1558 used to calculate κ_{chem} , as shown in [Fig. 24](#), good closure between κ_{chem} and κ_{htdma} were found



1559 for all the four particle sizes. Fig. 24 also reveals that κ_{chem} were significantly larger than κ_{htdma} ,
1560 indicating that ideal mixing assumption may overestimate aerosol hygroscopic growth (Wu et
1561 al., 2013). Simultaneous H-TDMA and HR-ToF-AMS measurements were also carried out at
1562 a coastal suburban site in Hong Kong (Yeung et al., 2014a). Approximations for growth factors
1563 of organic aerosols, using the fraction of m/z 44, the oxygen-to-carbon ratio and PMF-resolved
1564 organic factors from HR-ToF-AMS measurements, did not yield better closure results, likely
1565 because of the overall dominance of sulfate during the whole measurement period.



1566

1567 **Figure 24.** Comparison between κ_{chem} (calculated using size-resolved aerosol compositions)
1568 and κ_{htdma} (derived from H-TDMA measurements) for aerosol particles with dry diameters of
1569 (a) 100, (b) 150, (c) 200 and (d) 250 nm. Reprint with permission by Wu et al. (2013).

1570 Copyright 2013 Copernicus Publications.

1571



1572 H-TDMA measurements in Shanghai at wintertime showed that aerosol particles (250 nm
1573 in dry diameter) could be classified into two modes according to their hygroscopicity (Wang
1574 et al., 2014b). The first mode had growth factors of ~ 1.05 at 85% RH, mainly containing fresh
1575 elemental carbon and minerals, as revealed by measurements using an Aerosol Time-of-Flight
1576 mass spectrometer. In contrast, the second mode had growth factors of ~ 1.46 at 85% RH and
1577 were enriched with elemental carbon and organic carbon particles internally mixed with
1578 secondary inorganic materials.

1579 **5.1.2 H-TDMAs with extended performance**

1580 While most H-TDMAs only work at around room temperature, Weingartner et al. (2002)
1581 designed a H-TDMA which could measure hygroscopic growth of aerosol particle below 0 °C
1582 (temperature: -20 to 30 °C; RH: 10-90 %). Measured hygroscopic growth factors showed good
1583 agreement with theoretical calculations for $(\text{NH}_4)_2\text{SO}_4$, NaCl and NaNO_3 at both 20 and -10 °C
1584 (Gysel et al., 2002). This instrument was subsequently deployed at a high-alpine site (3580 m
1585 above the seal level) to investigate hygroscopic properties of ambient aerosol particles at -10 °C
1586 (Weingartner et al., 2002), and the average GF at 85% RH were measured to be 1.44, 1.49 and
1587 1.53 for aerosol particles with dry diameters of 50, 100 and 250 nm.

1588 RH in the troposphere frequently exceeds 90%, and it is desirable to investigate
1589 hygroscopic growth of aerosol particles at $>90\%$ RH. Hennig et al. (2005) developed a high
1590 humidity TDMA which could be operated at 98% RH, and the absolute accuracy of RH at 98%
1591 was $\pm 1.2\%$. It was found that within the uncertainties, the measured GF in the RH range of 84-
1592 98% agreed well with theoretical values (Hennig et al., 2005). The Leipzig Aerosol Cloud
1593 Interaction Simulator (LACIS), a laminar flow tube designed to study cloud formation and
1594 growth, could be operated at stable RH ranging from almost 0% up to 99.1% (Stratmann et al.,
1595 2004), and aerosol particles and/or droplets exiting the flow tube were detected using an optical
1596 particle sizer especially developed for this instrument. LACIS was employed to study



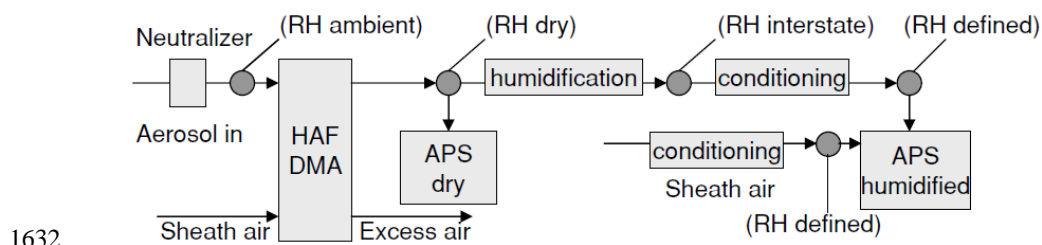
1597 hygroscopic growth of $(\text{NH}_4)_2\text{SO}_4$ and NaCl aerosol particles at 85.8-99.1% RH (Wex et al.,
1598 2005). At 99% RH, measured GF values agreed well with these predicted assuming solution
1599 ideality for NaCl; whereas for $(\text{NH}_4)_2\text{SO}_4$, solution ideality assumption would overestimate GF
1600 values by up to 20% (Wex et al., 2005). In a following study (Niedermeier et al., 2008), LACIS
1601 was used to investigate hygroscopic growth of sea salt aerosol up to 99.1% RH.

1602 Long duration is required by the second DMA to measure size distributions of humidified
1603 aerosol particles, and therefore the H-TDMA technique is usually quite slow. It typically takes
1604 ~30 min for a traditional H-TDMA to determine GF values at a given RH for five different dry
1605 diameters (Cerully et al., 2011; Pinterich et al., 2017b). Instruments with fast duty cycles are
1606 of great interest and have been developed and deployed (Sorooshian et al., 2008; Pinterich et
1607 al., 2017a; Pinterich et al., 2017b). For example, after replacing the second DMA (used in the
1608 traditional H-TDMA) with a water-based fast integrated mobility spectrometer which could
1609 provide 1 Hz size distribution measurements (Pinterich et al., 2017a), the improved instrument,
1610 called the humidity-controlled fast integrated mobility spectrometer (HFIMS), only took ~3
1611 min to measure GF of particles with five different dry diameters at a given RH (Pinterich et al.,
1612 2017b).

1613 Since the upper size limit is <1000 nm for a typical DMA and GF values at 90% RH can
1614 be >2 for atmospheric particles, most H-TDMAs can only be used for particles with dry
1615 diameters smaller than 500 nm (McFiggans et al., 2006; Swietlicki et al., 2008). Several
1616 instruments, which could measure hygroscopic growth of aerosol particles larger than 500 nm
1617 in dry diameter, have been developed (Kreisberg et al., 2001; Hegg et al., 2007; Massling et
1618 al., 2007; Snider and Petters, 2008; Kaaden et al., 2009; Kim et al., 2014). One obvious
1619 approach to overcome the DMA sizing limit is to use optical particle counters for particle sizing,
1620 as adopted by some previous studies (Kreisberg et al., 2001; Hegg et al., 2007; Snider and
1621 Petters, 2008). Another approach is to use Aerodynamic Particle Sizers (APS) for particle



1622 sizing (Massling et al., 2007; Kaaden et al., 2009; Schladitz et al., 2011; Kim and Park, 2012).
1623 For example, a H-DMA-APS was developed to explore hygroscopic growth of large aerosol
1624 particles (Massling et al., 2007; Kaaden et al., 2009). As shown in [Fig. 25](#), the dry aerosol flow
1625 was first delivered through a custom-built high aerosol flow-DMA (HAF-DMA) which could
1626 select particles with dry mobility diameters over 1000 nm, and the dry aerosol flow exiting the
1627 DMA was split into two identical flows; the first flow was directly sampled by the first APS to
1628 measure the aerodynamic size distribution under dry conditions, and the second flow was first
1629 delivered through a humidifier to be humidified to a given RH (e.g., 90%) and then sampled
1630 into the second APS so that the aerodynamic size distribution of the humidified aerosol was
1631 measured.



1632 **Figure 25.** Schematic diagram of a H-DMA-APS apparatus. Reprint with permission by
1633 Kaaden et al. (2009). Copyright 2009 Blackwell Munksgaard.

1635

1636 The utilization of H-TDMAs to measure aerosol hygroscopic growth factors assumes
1637 particle sphericity. Some particles in the atmosphere, such as mineral dust and soot, are known
1638 to be non-spherical, and therefore GF measured using H-TDMA may not correctly reflect the
1639 amount of aerosol liquid water (Weingartner et al., 1997; Rissler et al., 2005; Vlasenko et al.,
1640 2005; Koehler et al., 2009; Tritscher et al., 2011). Very recently an instrument, called
1641 differential mobility analyser-humidified centrifugal particles mass analyser (DMA-HCPMA),
1642 was developed to measure mass change of submicron aerosol particles at different RH (10-
1643 95 %) (Vlasenko et al., 2017). In this set-up, a dry aerosol flow was delivered through a DMA



1644 to produce quasi-monodisperse particles and then through an aerosol humidifier to be
1645 humidified to a given RH; after that, the aerosol flow was delivered through a centrifugal particle
1646 mass analyser (which would classify aerosol particles according to their mass-to-charge ratios)
1647 (Olfert and Collings, 2005; Rissler et al., 2014; Kuwata, 2015) and then a CPC so that aerosol
1648 particle mass could be determined as a function of RH (Vlasenko et al., 2017). The measured
1649 mass growth factors were found to agree well with theoretical values for $(\text{NH}_4)_2\text{SO}_4$ and NaCl,
1650 and this newly-developed DMA-HCPMA set-up was successfully deployed to explore
1651 hygroscopic properties of ambient aerosol particles (Vlasenko et al., 2017). It can be expected
1652 that DMA-HCPMA would significantly improve our knowledge of hygroscopicity of non-
1653 spherical aerosol particles.

1654 **5.2 Optical properties**

1655 Optical properties of aerosol particles depend on their size and refractive indices, both
1656 strongly affected by their hygroscopic properties. Measurements of aerosol optical properties
1657 as a function of RH, indispensable for elucidating the impacts of aerosol particles on visibility
1658 and radiative balance, can be used to infer aerosol hygroscopicity. Several techniques have
1659 been developed and deployed, as discussed in this section.

1660 **5.2.1 Extinction**

1661 Cavity ring-down spectroscopy (CRDS), a highly sensitive method for optical extinction
1662 measurement, has been extensively employed for gas and aerosol detection (Brown, 2003;
1663 Baynard et al., 2006; Baynard et al., 2007; Langridge et al., 2011; Sobanski et al., 2016; Peng
1664 et al., 2018). For a typical CRDS set-up, a laser beam pulse is coupled into a high-finesse
1665 optical cavity (which has one high reflectivity mirror on each end) from one end of the cavity,
1666 and the decay of the intensity of the light transmitted from the other end is monitored. The
1667 change in decay lifetimes of transmitted light intensity can be related to the extinction
1668 coefficient, α_{ext} , using Eq. (3) (Baynard et al., 2007; Langridge et al., 2011):

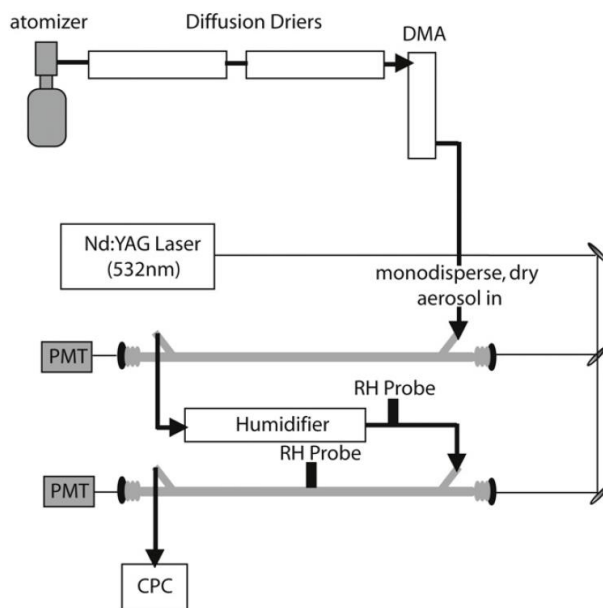


1669
$$\alpha_{ext} = \frac{R_L}{c} \left(\frac{1}{\tau} - \frac{1}{\tau_0} \right) \quad (3)$$

1670 where R_L is the ratio of the distance between the two mirrors to the length of the cavity filled
1671 with aerosol particles, c is the speed of light (m s^{-1}), and τ and τ_0 are the measured decay
1672 lifetimes of light intensity with and without aerosol particles present in the cavity. If aerosol
1673 particles delivered into the cavity are monodisperse, the extinction coefficient of each
1674 individual particles, σ_{ext} , can be calculated using Eq. (4) (Freedman et al., 2009):

1675
$$\sigma_{ext} = \frac{\alpha_{ext}}{N_p} \quad (4)$$

1676 where N_p is the aerosol number concentration (cm^{-3}).



1677
1678 **Figure 26.** Schematic diagram of the apparatus used by Tolbert and co-workers to measure the
1679 dependence of aerosol light extinction on RH. Reprint with permission by Beaver et al. (2008).
1680 Copyright 2008 IOP Publishing Ltd.

1681

1682 A CRD spectrometer was employed by Tolbert and co-workers to investigate the effects
1683 of RH on aerosol optical extinction at 532 nm, and its schematic diagram is depicted in [Fig. 26](#)



1684 (Beaver et al., 2008). The aerosol flow generated using an atomizer was delivered through
1685 diffusion dryers to reduce its RH to <10% and passed through a DMA to produce quasi-
1686 monodisperse aerosol particles. The aerosol flow was then delivered into the first cavity to
1687 measure the aerosol optical extinction at 532 nm under dry conditions; after that, the aerosol
1688 flow entered a humidifier to be humidified to a given RH, and was then delivered into the
1689 second cavity to measure the aerosol optical extinction under the humidified condition. In the
1690 final, the aerosol flow was sampled by a CPC to measure the number concentration. For
1691 $(\text{NH}_4)_2\text{SO}_4$ aerosol particles in the size range of 200-700 nm, the measured optical growth
1692 factors at 80% RH, defined as the ratio of the extinction coefficient at 80% RH to that under
1693 dry conditions, were found to be in good agreement with those calculated from diameter-based
1694 growth factors using the Mie theory (Garland et al., 2007).

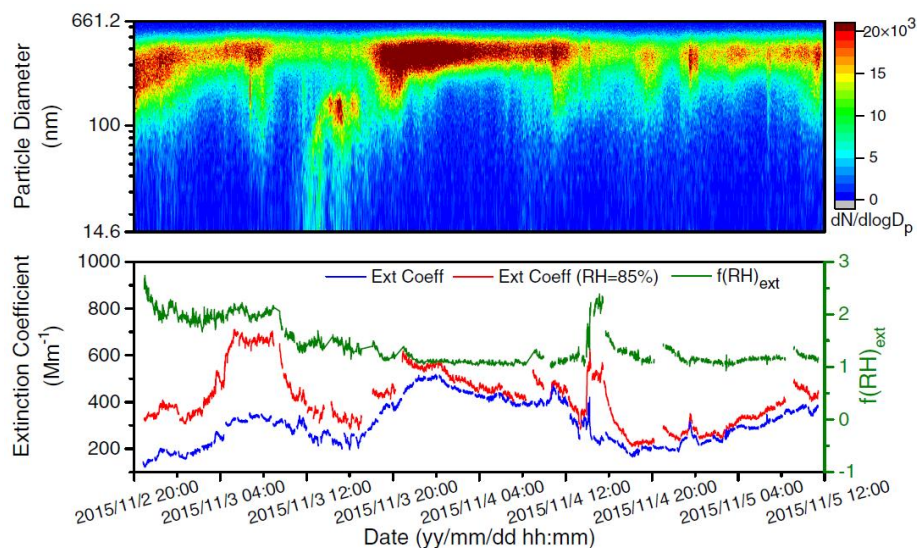
1695 CRDS was used to examine the effect of RH on aerosol optical extinction for phthalic
1696 acid, pyromellitic acid and 4-hydroxybenzoic acid aerosol particles in the size range of 150-
1697 500 nm (Beaver et al., 2008). The optical growth factors were found to be smaller for the three
1698 organic compounds examined, compared to $(\text{NH}_4)_2\text{SO}_4$. For example, for aerosol particles with
1699 a dry diameter of 335 nm, optical growth factors at 80% RH were measured to be 1.3 and 1.1
1700 for phthalic and pyromellitic acid (Beaver et al., 2008), compared to 3.0 for $(\text{NH}_4)_2\text{SO}_4$. Optical
1701 extinction coefficients of 4-hydroxybenzoic acid particles at 80% RH were smaller than those
1702 under dry conditions (Beaver et al., 2008), implying that morphological and structural change
1703 may occur for these particles during humidification. Similarly, optical growth factors of illite
1704 and kaolinite aerosol particles were found to be <1 at 50 and 68% RH (Attwood and Greenslade,
1705 2011), due to structural rearrangement of clay mineral particles after water uptake. Optical
1706 growth factors of internally mixed aerosol particles, which contained $(\text{NH}_4)_2\text{SO}_4$ and organic
1707 materials, were also studied (Garland et al., 2007; Robinson et al., 2013; Robinson et al., 2014).
1708 Another study (Flores et al., 2012) measured optical growth factors (at wavelengths of 355 and



1709 532 nm) at 80 and 90% RH for aerosol particles with different extent of optical absorption
1710 ranging from purely scattering (e.g., $(\text{NH}_4)_2\text{SO}_4$) to highly absorbing (e.g., nigrosine), and
1711 found good agreement between measured optical growth factors and those calculated using the
1712 Mie theory.

1713 CRDS has also been widely deployed to investigate optical extinction of ambient aerosol
1714 particles at different RH (Zhang et al., 2014b; Atkinson et al., 2015; Brock et al., 2016a). For
1715 example, an eight-channel CRD spectrometer was developed by NOAA Earth System
1716 Research Laboratory (Langridge et al., 2011). This instrument could measure aerosol optical
1717 growth factors at three wavelengths (405, 532 and 662 nm) simultaneously, and has been
1718 successfully deployed for aircraft measurements (Langridge et al., 2011).

1719 In addition to CRDS, broadband cavity enhanced spectroscopy (BBCEAS), also called
1720 cavity enhanced differential optical absorption spectroscopy (CE-DOAS), is an alternative
1721 high-finesse cavity based technique with high sensitivity in optical extinction measurements
1722 (Platt et al., 2009; Washenfelder et al., 2013; Washenfelder et al., 2016). Compared to CRDS,
1723 one major advantage of BBCEAS is that optical extinction can be measured as a function of
1724 wavelength. BBCEAS, as described in details elsewhere (Platt et al., 2009; Varma et al., 2013;
1725 Washenfelder et al., 2013; Zhao et al., 2014; Washenfelder et al., 2016; Wang et al., 2017a; Li
1726 et al., 2018b), has also been widely used in gas and aerosol measurements. Zhao et al. (2014)
1727 utilized BBCEAS to measure aerosol optical extinction at 641 nm as a function of RH, and for
1728 200 nm $(\text{NH}_4)_2\text{SO}_4$, the measured optical growth factors agreed well with those calculated
1729 using the Mie theory. The instrument was further deployed to simultaneously measure optical
1730 extinction of ambient submicrometer aerosol at <20% and 85% RH at Hefei Radiation
1731 Observatory. The result is displayed in Fig. 27, suggesting that the optical growth factors at 85%
1732 RH varied from ~1 to >2.5 during the campaign (Zhao et al., 2017).



1733

1734 **Figure 27.** Aerosol properties measured at Hefei Radiation Observatory. Upper panel: aerosol
1735 number size distribution of submicrometer particles; lower panel: extinction coefficient of
1736 submicrometer particles under dry conditions (blue curve, left y-axis) and at 85% RH (red curve,
1737 left y-axis) and optical growth factors at 85% RH (green curve, right y-axis). Reprint with
1738 permission by Zhao et al. (2017). Copyright 2017 Optical Society of America.

1739

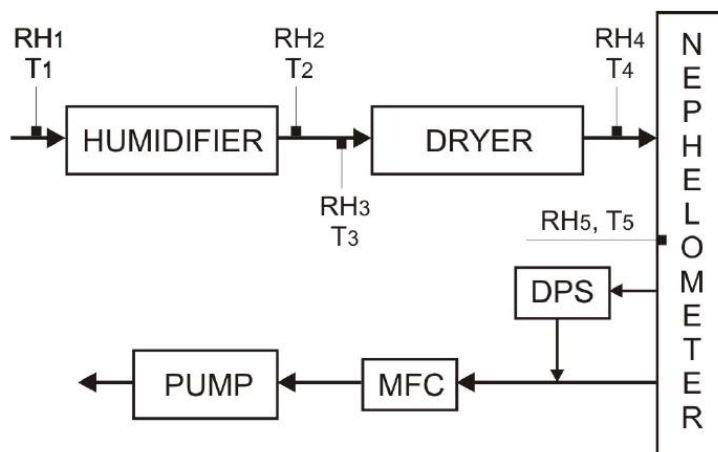
1740 5.2.2 Scattering

1741 Humidified nephelometry, which was first developed as early as in the 1960s (Pilat and
1742 Charlson, 1966; Covert et al., 1972), has been widely used to measure aerosol light scattering
1743 coefficients at different RH (Rood et al., 1985; Carrico et al., 1998; Li-Jones et al., 1998; Day
1744 et al., 2000; Malm et al., 2000a; Malm et al., 2000b; Koloutsou-Vakakis et al., 2001; Fierz-
1745 Schmidhauser et al., 2010a; Zieger et al., 2010; Zieger et al., 2013; Kreidenweis and Asa-
1746 Awuku, 2014; Zhang et al., 2015; Titos et al., 2016). Due to its high time resolution, this
1747 technique is very suitable for online measurement of ambient aerosols. A very recent review
1748 paper (Titos et al., 2016) summarized and discussed theories, history, measurement
1749 uncertainties and ambient applications of this technique in a comprehensive manner. As a result,



1750 herein we only introduce in brief its basic principle, representative instrumental configurations
1751 and exemplary applications.

1752 The scattering enhancement factor, $f(\text{RH})$, defined as the ratio of the aerosol scattering
1753 coefficient at a given RH to that at dry conditions, is typically reported by humidified
1754 nephelometry measurements (Kreidenweis and Asa-Awuku, 2014; Titos et al., 2016). [Fig. 28](#)
1755 shows the schematic diagram of a humidified three-wavelength integrating nephelometer (TSI
1756 3563) at 450, 550 and 700 nm (Fierz-Schmidhauser et al., 2010c). The aerosol flow was first
1757 delivered through an aerosol humidifier which could increase the RH to 95% and then through
1758 an aerosol dryer to reduce the RH to below 40%. After that, the aerosol flow was sampled into
1759 the nephelometer to measure aerosol scattering coefficients at three different wavelengths. The
1760 flow exiting the nephelometer was pulled through a mass flow controller (to control the sample
1761 flow rate) by a pump. The performance of the aerosol dryer could be adjusted to vary the RH
1762 of the flow entering the nephelometer, and thus scattering coefficients could be measured as a
1763 function of RH (40-90 %); in addition, using such a configuration, light scattering properties
1764 of supersaturated aerosol particles, i.e. the hysteresis effect, could be examined (Fierz-
1765 Schmidhauser et al., 2010c). The humidified nephelometer was used to measure light scattering
1766 properties of monodisperse $(\text{NH}_4)_2\text{SO}_4$ and NaCl aerosol particles with dry diameters of 100,
1767 150, 240 and 300 nm, and the measured $f(\text{RH})$ values agreed with these predicted using Mie
1768 theory (Fierz-Schmidhauser et al., 2010c). Some instruments could measure aerosol light
1769 scattering at different RH in a simultaneous manner, via using two or more nephelometers in
1770 parallel (Carrico et al., 1998).



1771

1772 **Figure 28.** Schematic diagram of a humidified three-wavelength integrating nephelometer
1773 (DPS: dew point sensor; MFC: mass flow controller). Reprint with permission by
1774 Schmidhauser et al. (2010c). Copyright 2010 Copernicus Publications.

1775

1776 A number of previous studies have carried out field measurements of $f(\text{RH})$ at various
1777 locations over the globe (Zieger et al., 2013; Kreidenweis and Asa-Awuku, 2014; Titos et al.,
1778 2016). As summarized by Titos et al. (2016), $f(\text{RH})$ values (for 80-85% RH) were larger for
1779 marine sites (ranging from 1.5 to 3.5), when compared with most continental sites; furthermore,
1780 $f(\text{RH})$ values were found to be in the range of 1.1-2.1 for dust particles, and larger $f(\text{RH})$ values
1781 observed for dust may be caused by the co-presence of sea salt aerosol. A field study (Li-Jones
1782 et al., 1998) carried out on Barbados (West Indies) found that $f(\text{RH})$ values (for RH in the range
1783 of 67-83%) were very small (1.0-1.1) for mineral dust transported from North Africa,
1784 indicating that large variation in ambient RH may not lead to significant change in optical
1785 properties of mineral dust aerosol.

1786 Since aerosol light scattering coefficients depend on particle size and refractive index in
1787 a complex manner even for spherical particles, it is not straightforward to link $f(\text{RH})$ with the
1788 aerosol liquid water content (Kreidenweis and Asa-Awuku, 2014). A number of studies (Malm



1789 and Day, 2001; Fierz-Schmidhauser et al., 2010b; Zieger et al., 2010; Chen et al., 2014;
1790 Kreidenweis and Asa-Awuku, 2014; Kuang et al., 2017; Kuang et al., 2018) have discussed
1791 how measured $f(\text{RH})$ values could be used to derive single hygroscopicity parameters (κ)
1792 (Petters and Kreidenweis, 2007) and aerosol liquid water contents. In addition, it should be
1793 emphasized that humidity-dependent aerosol scattering coefficients (as well as aerosol
1794 extinction and absorption coefficients) themselves are important parameters to assess the
1795 impacts of aerosols on visibility and direct radiative forcing.

1796 5.2.3 Absorption

1797 Photoacoustic spectroscopy has been developed and deployed to measure aerosol optical
1798 absorption in a direct manner (Arnott et al., 2003; Lack et al., 2009; Lewis et al., 2009;
1799 Moosmuller et al., 2009; Gyawali et al., 2012; Langridge et al., 2013; Lack et al., 2014). In
1800 brief, the aerosol flow is continuously sampled into a cell which serves as an acoustic resonator
1801 section and illuminated by a modulated laser beam. The laser radiation absorbed by aerosol
1802 particles is transferred to the surrounding air as heat, leading to the generation of acoustic wave
1803 which is amplified in the resonator and detected using a microphone (Moosmuller et al., 2009;
1804 Gyawali et al., 2012). The signal intensity measured by the microphone is proportional to
1805 optical absorption and can be used to derive aerosol optical absorption coefficients after proper
1806 calibration (Moosmuller et al., 2009; Gyawali et al., 2012). In principle, hygroscopic growth
1807 of aerosol particles at elevated RH would lead to increase in particle size and thus enhancement
1808 in aerosol optical absorption due to the lensing effect (Lewis et al., 2009). Nevertheless, several
1809 studies suggested that photoacoustic spectroscopy measurements at high RH are likely to
1810 significantly underestimate the actual aerosol optical absorption (Arnott et al., 2003; Lewis et
1811 al., 2009; Langridge et al., 2013). For example, Langridge et al. (2013) used photoacoustic
1812 spectroscopy at 532 nm to measure optical absorption of several types of aerosol particles with
1813 various hygroscopicity, morphology and refractive indices, and found that the measured



1814 absorption exhibited strong low biases at high RH. The underestimation of optical absorption
1815 is due to that acoustic signals are affected by evaporation of aerosol liquid water when aerosol
1816 particles absorb radiation and get heated. As a result, Langridge et al. (2013) concluded that
1817 photoacoustic spectroscopy was not a suitable technique to measure aerosol optical absorption
1818 at elevated RH. Similarly, other techniques used for direct measurement of aerosol optical
1819 absorption, such as the filter-based method and photothermal interferometry, did not perform
1820 well at elevated RH either (Schmid et al., 2006; Sedlacek and Lee, 2007).

1821 An indirect method has been developed (Khalizov et al., 2009; Xue et al., 2009; Brem et
1822 al., 2012; Chen et al., 2015) to explore the effect of RH on aerosol optical absorption, which
1823 was calculated as the difference between aerosol light extinction and scattering. In the set-up
1824 developed by Brem et al. (2012), aerosol light extinction and scattering at three wavelengths
1825 (467, 530 and 660 nm) were measured at different RH using an optical extinction cell and a
1826 nephelometer. As RH was increased from 38 to 95%, light absorption of nigrosine aerosol was
1827 enhanced by a factor of ~1.24 for all the three wavelengths (Brem et al., 2012). In some other
1828 work (Khalizov et al., 2009; Xue et al., 2009; Chen et al., 2015), CRDS, instead of the optical
1829 extinction cell, was used to measure the aerosol optical extinction.

1830 **5.3 Other aerosol-based techniques**

1831 Black carbon (BC) aerosol is of great concern due to its impacts on human health and
1832 climate (Bond et al., 2013). The hygroscopicity of BC, varying with atmospheric aging
1833 processes, largely determines its dry and wet deposition rates and thus lifetimes (Schwarz et
1834 al., 2010; Wang et al., 2014a) and also affects its optical absorption through lensing effects
1835 (Redemann et al., 2001). Therefore, it is important to understand hygroscopic properties of BC
1836 aerosol in the troposphere; however, techniques discussed in Sections 5.1-5.2 are not specific
1837 to BC-containing particles. Since typical BC mass fractions in submicrometer particles are only



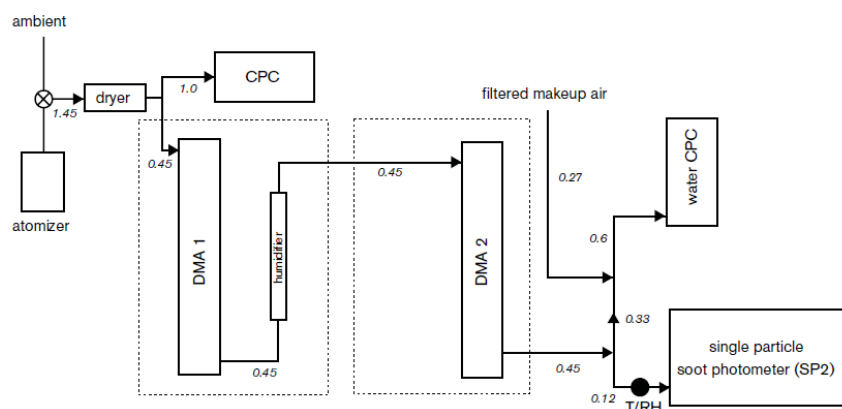
1838 a few percentages, in general these techniques cannot provide specific information on ambient
1839 BC aerosol hygroscopicity.

1840 Single particle soot photometers (SP2), as described in a number of studies (Gao et al.,
1841 2007; Slowik et al., 2007; Schwarz et al., 2008; Moteki and Kondo, 2010), have been widely
1842 employed to measure mass and mixing state of individual BC particles in the troposphere. In
1843 brief, when an aerosol particle which contains a detectable amount of refractory BC enters a
1844 SP2, it is heated by a laser beam (1064 nm) to the incandescence temperature, leading to the
1845 emission of thermal radiation. The intensity of the thermal radiation, proportional to the mass
1846 of refractory BC, is monitored to quantify the amount of BC contained by individual particles.
1847 In addition, measurement of the light scattered by the particle during its initial interaction with
1848 the laser beam can be used to derive the optical diameter. Therefore, a SP2 measures both the
1849 mass of non-refractory BC and the optical diameter of each individual particles. In the last
1850 several year a few SP2-based instruments have been developed to measure hygroscopic
1851 properties of BC aerosol in specific (McMeeking et al., 2011; Liu et al., 2013a; Schwarz et al.,
1852 2015; Ohata et al., 2016), as introduced below.

1853 A SP2 was coupled to a H-TDMA to measure hygroscopic properties of BC aerosol
1854 (McMeeking et al., 2011), and the experimental diagram is displayed in [Fig. 29](#). The aerosol
1855 flow was dried to <20% RH and then passed through the first DMA to produce quasi-
1856 monodisperse aerosol with a specific size; after that, the aerosol flow was humidified to a
1857 specific RH and then passed through the second DMA. The aerosol flow exiting the second
1858 DMA was then split to two flows, sampled by a CPC and a SP2, respectively. The usage of
1859 SP2 enabled identification of BC aerosol particles, and mobility diameter changes of aerosol
1860 particles identified to be BC could be used to calculate hygroscopic growth factors specific to
1861 BC aerosol; alternatively, hygroscopic properties of BC aerosol could be obtained from the
1862 change in optical diameter measured by the SP2 (McMeeking et al., 2011). The H-TDMA-SP2



1863 apparatus was deployed to investigate hygroscopic properties of BC aerosol in June-July 2011
1864 at the Weybourne Atmospheric Observatory near the North Norfolk coastline. During this
1865 campaign two types of BC aerosol with distinctive hygroscopicity were observed (Liu et al.,
1866 2013a). Hygroscopic growth factors at 90% RH were measured to be ~ 1.05 for the first type
1867 BC aerosol and ranged from ~ 1.25 to ~ 1.6 for the second type, depending on the composition
1868 of soluble materials associated with BC particles (Liu et al., 2013a).



1869

1870 **Figure 29.** Schematic diagram of the H-TDMA-SP2 apparatus. Flow rates shown in this figure
1871 are in the unit of L/min. Reprint with permission by McMeeking et al. (2011). Copyright 2011
1872 Copernicus Publications.

1873

1874 Schwarz et al. (2015) developed a humidified-dual SP2 setup (HD-SP2) to measure
1875 hygroscopic properties of BC aerosol. In this set-up, one sample flow was dried, and optical
1876 diameters of each BC-containing particles were measured under dry conditions using the first
1877 SP2; the other sample flow was first humidified to a given RH (e.g., 90%), and optical
1878 diameters of individual BC-containing particles were determined using the second SP2. Optical
1879 diameters of BC particles measured under dry and humidified conditions could then be used to
1880 determine hygroscopic properties specific to BC-containing particles. The HD-SP2 was
1881 deployed on the NASA DC-8 aircraft in the summer of 2013 to investigate hygroscopic



1882 properties of BC aerosol in North American wildfire plumes (Perring et al., 2017). An average
1883 κ value of 0.04 was found for the sampled BC aerosol, and was increased by ~ 0.06 after 40 h
1884 aging in the atmosphere (Perring et al., 2017).

1885 In another study (Ohata et al., 2016), an aerosol particle mass analyser (APM) was coupled
1886 to a humidified SP2 to investigate hygroscopic properties of BC aerosol. The experimental
1887 scheme employed can be summarized as below (Ohata et al., 2016): (i) the sample flow, dried
1888 to $<10\%$ RH, was delivered through an APM to select particles with a given mass-to-charge
1889 ratio (with identical mass if multiple charged particles were excluded in data analysis); (ii) the
1890 aerosol flow exiting the APM was humidified to a given RH and sampled into a SP2 to measure
1891 optical diameters of BC-containing particles under humidified conditions. Since dry diameters
1892 of BC-containing particles could be calculated from the mass of particles selected using the
1893 APM, hygroscopic growth factors of BC aerosol could be consequently determined (Ohata et
1894 al., 2016).

1895 **5.4 Discussion**

1896 All the techniques covered in Section 5 can be (and have been) used in laboratory and field
1897 measurements. Since airborne particles are examined, aerosol water contents can be quantified
1898 for unsaturated and supersaturated samples using these techniques. Because these techniques
1899 rely on measurements of particle diameters to investigate hygroscopic properties, it can be non-
1900 trivial to determine aerosol liquid water content for nonspherical aerosol particles. In addition,
1901 they may not be sensitive enough to study water adsorption. Although in general these
1902 techniques do not measure chemical compositions themselves, a number of offline and online
1903 instruments, including advanced mass spectroscopic tools (e.g., aerosol mass spectrometers
1904 and single particle mass spectrometers), are available to provide chemical information in
1905 parallel, significantly deepening our knowledge of hygroscopic properties of complex aerosols.



1906 **6 Summary and final remarks**

1907 Hygroscopicity is one of the most important physiochemical properties of atmospheric
1908 aerosols, largely determining their environmental and climatic impacts. In addition to
1909 atmospheric science, it is also of great concern in many other scientific and technical fields,
1910 such as surface science, heterogeneous catalysis, geochemistry/astrochemistry, pharmaceutical
1911 and food science, and etc. A myriad of experimental techniques have been developed and
1912 employed to explore hygroscopic properties of aerosol particles for $RH < 100\%$. In this paper
1913 we have reviewed experimental techniques for investigating aerosol hygroscopicity in a
1914 comprehensive manner. Future directions are outlined and discussed below in order to improve
1915 existing techniques and develop new techniques for a better understanding of aerosol
1916 hygroscopicity.

1917 1) The majority of instruments covered in this paper are not applicable to ambient aerosol
1918 particles. Future directions should focus on the development of aerosol hygroscopicity
1919 techniques that are field deployable, robust, and automatic. Especially up to now most ambient
1920 measurements conducted were ground-based, and therefore instruments which have high time
1921 resolution to be deployed on aircrafts (Langridge et al., 2011; Pinterich et al., 2017b) are highly
1922 needed.

1923 2) The maximum RH that many techniques/instruments can currently reach is usually
1924 around 90%, and recent studies have revealed the importance of hygroscopic growth
1925 measurements at RH very close to 100% (Wex et al., 2009b). Therefore, efforts should be made
1926 to improve these instruments so that they can be employed to investigate hygroscopic
1927 properties at very high RH (e.g., up to 99% RH).

1928 3) Temperatures in the troposphere range from ~ 200 K to >300 K, and temperature has
1929 been found to have a profound effect on particle phase state and thus liquid water content.
1930 Nevertheless, most techniques available currently, especially those which investigate



1931 hygroscopic properties of aerosol particles, can only be operated at around room temperature.

1932 Further instrumental development, which would enable hygroscopic growth measurements at
1933 lower temperatures, is warranted.

1934 4) Most techniques are operated under ambient pressure, while many processes involved
1935 aerosol particles are often carried out at pressures substantially lower than atmospheric pressure
1936 (Zhao et al., 2009; Schilling and Winterer, 2014; Rosenberger et al., 2018). As a result, new
1937 techniques that allow direct measurements of hygroscopic properties at lower pressure are
1938 needed for better characterization of aerosol hygroscopicity under conditions with reduced
1939 pressure. Such instruments would also be very valuable for characterizing aerosol particles at
1940 high altitudes where the pressure is significantly lower than the ground level.

1941 5) Aerosol hygroscopicity is a property that depends on chemical compositions and its
1942 measurements can be affected by phase state and viscosity of the particles. Application of
1943 multiple techniques to examine the same type of atmospherically relevant particles will deepen
1944 our understanding of aerosol hygroscopicity. In addition, simultaneous measurements of
1945 chemical composition and other physicochemical properties (e.g., particle phase state and
1946 viscosity) of aerosol particles of different hygroscopicity can be very valuable.

1947 6) As shown in this review paper, many instruments employed to probe aerosol
1948 hygroscopicity are custom built; furthermore, even for the same type of instruments,
1949 operational protocols may vary at different groups. Instrumental comparisons, proven to be a
1950 good approach to validate instrumental performance and identify potential issues, have been
1951 carried out for H-TDMAs (Duplissy et al., 2009; Massling et al., 2011), and similar
1952 intercomparison should be performed for other techniques and instruments. Furthermore,
1953 standardized procedures for calibration, operation, data analysis and quality assurance, if can
1954 be formulated, would help increase data quality for aerosol hygroscopicity measurements.

1955



1956 **Data availability**

1957 This is a review paper, and all the data used come from literature cited.

1958 **Author contribution**

1959 Mingjin Tang and Chak K Chan conceived and coordinated this paper; Mingjin Tang, Chak K

1960 Chan, Yong Jie Li, Hang Su, Qingxin Ma and Zhijun Wu wrote the paper with contribution

1961 from all the other coauthors.

1962 **Competing interests**

1963 The authors declare that they have no conflict of interest.

1964

1965 **Acknowledgement**

1966 This work is financially supported by National Natural Science Foundation of China

1967 (91644106, 91744204, 4167517, 41875142 and 91844301), the Chinese Academy of Sciences

1968 international collaborative project (132744KYSB20160036), State Key Laboratory of Organic

1969 Geochemistry (SKLOG2016-A05) and Guangdong Foundation for Program of Science and

1970 Technology Research (2017B030314057). Mingjin Tang would like to thank the CAS Pioneer

1971 Hundred Talents program for providing a starting grant. This is contribution no. IS-XXXX

1972 from GIGCAS.

1973

1974 **Reference**

- 1975 Adachi, K., Freney, E. J., and Buseck, P. R.: Shapes of internally mixed hygroscopic aerosol
1976 particles after deliquescence, and their effect on light scattering, *Geophys. Res. Lett.*, 38,
1977 L13804, doi: 13810.11029/12011gl047540, 2011.
- 1978 Adams, J. R., and Merz, A. R.: Hygroscopicity of Fertilizer Materials and Mixtures, *Ind. Eng.*
1979 *Chem.*, 21, 305-307, 1929.
- 1980 Ahlneck, C., and Zografi, G.: The molecular basis of moisture effects on the physical and
1981 chemical stability of drugs in the solid state, *Int. J. Pharm.*, 62, 87-95, 1990.
- 1982 Ahn, K.-H., Kim, S.-M., Jung, H.-J., Lee, M.-J., Eom, H.-J., Maskey, S., and Ro, C.-U.:
1983 Combined Use of Optical and Electron Microscopic Techniques for the Measurement of
1984 Hygroscopic Property, Chemical Composition, and Morphology of Individual Aerosol
1985 Particles, *Anal. Chem.*, 82, 7999-8009, 2010.
- 1986 Al-Abadleh, H. A., and Grassian, V. H.: Heterogeneous Reaction of NO₂ on Hexane Soot: A
1987 Knudsen Cell and FT-IR Study, *J. Phys. Chem. A*, 104, 11926-11933, 2000.
- 1988 Al-Abadleh, H. A., Krueger, B. J., Ross, J. L., and Grassian, V. H.: Phase transitions in
1989 calcium nitrate thin films, *Chem. Commun.*, 2796-2797, 2003.
- 1990 Alfara, M. R., Good, N., Wyche, K. P., Hamilton, J. E., Monks, P. S., Lewis, A. C., and
1991 McFiggans, G.: Water uptake is independent of the inferred composition of secondary
1992 aerosols derived from multiple biogenic VOCs, *Atmos. Chem. Phys.*, 13, 11769-11789, 2013.
- 1993 Allan, M., and Mauer, L. J.: Comparison of methods for determining the deliquescence points
1994 of single crystalline ingredients and blends, *Food Chem.*, 195, 29-38, 2016.
- 1995 Amdur, S.: Determination of solute properties by vapor pressure measurements of the solvent
1996 in dilute solutions, *J. Chem. Phys.*, 61, 3445-3449, 1974.
- 1997 Apelblat, A.: The vapor pressures of water over saturated solutions of barium chloride,
1998 magnesium nitrate, calcium nitrate, potassium carbonate, and zinc sulfate at temperatures
1999 from 283 K to 323 K, *J. Chem. Thermodyn.*, 24, 619-626, 1992.
- 2000 Arenas, K. J. L., Schill, S. R., Malla, A., and Hudson, P. K.: Deliquescence Phase Transition
2001 Measurements by Quartz Crystal Microbalance Frequency Shifts, *J. Phys. Chem. A*, 116,
2002 7658-7667, 2012.
- 2003 Arnott, W. P., Moosmuller, H., Sheridan, P. J., Ogren, J. A., Raspet, R., Slaton, W. V., Hand,
2004 J. L., Kreidenweis, S. M., and Collett, J. L.: Photoacoustic and filter-based ambient aerosol
2005 light absorption measurements: Instrument comparisons and the role of relative humidity, *J.*
2006 *Geophys. Res.-Atmos.*, 108, 4034, DOI: 4010.1029/2002JD002165, 2003.
- 2007 Asad, A., Mmereki, B. T., and Donaldson, D. J.: Enhanced uptake of water by oxidatively
2008 processed oleic acid, *Atmos. Chem. Phys.*, 4, 2083-2089, 2004a.
- 2009 Asad, A., Mmereki, B. T., and Donaldson, D. J.: Enhanced uptake of water by oxidatively
2010 processed oleic acid, *Atmos. Chem. Phys.*, 4, 2083-2089, 2004b.
- 2011 Ashkin, A.: Acceleration and trapping of particles by radiation pressure, *Phys. Rev. Lett.*, 24,
2012 156-159, 1970.
- 2013 Ashkin, A., and Dziedzic, J. M.: Optical levitation by radiation pressure, *Appl. Phys. Lett.*,
2014 19, 283-285, 1971.
- 2015 Ashkin, A., and Dziedzic, J. M.: Optical levitation of liquid droplets by radiation pressure,
2016 *Science*, 187, 1073-1075, 1975.
- 2017 Ashkin, A.: History of optical trapping and manipulation of small-neutral particle, atoms, and
2018 molecules, *Ieee Journal of Selected Topics in Quantum Electronics*, 6, 841-856, 2000.
- 2019 Atkins, P. W.: *Physical Chemistry (Sixth Edition)*, Oxford University Press, Oxford, UK,
2020 1998.
- 2021 Atkinson, D. B., Radney, J. G., Lum, J., Kolesar, K. R., Cziczko, D. J., Pekour, M. S., Zhang,
2022 Q., Setyan, A., Zelenyuk, A., and Cappa, C. D.: Aerosol optical hygroscopicity



- 2023 measurements during the 2010 CARES campaign, *Atmos. Chem. Phys.*, 15, 4045-4061,
2024 2015.
- 2025 Attwood, A. R., and Greenslade, M. E.: Optical Properties and Associated Hygroscopicity of
2026 Clay Aerosols, *Aerosol Sci. Technol.*, 45, 1350-1359, 2011.
- 2027 Ault, A. P., Zhao, D. F., Ebben, C. J., Tauber, M. J., Geiger, F. M., Prather, K. A., and
2028 Grassian, V. H.: Raman microspectroscopy and vibrational sum frequency generation
2029 spectroscopy as probes of the bulk and surface compositions of size-resolved sea spray
2030 aerosol particles, *Phys. Chem. Chem. Phys.*, 15, 6206-6214, 2013.
- 2031 Ault, A. P., and Axson, J. L.: Atmospheric Aerosol Chemistry: Spectroscopic and
2032 Microscopic Advances, *Anal. Chem.*, 89, 430-452, 2017.
- 2033 Baynard, T., Garland, R. M., Ravishankara, A. R., Tolbert, M. A., and Lovejoy, E. R.: Key
2034 factors influencing the relative humidity dependence of aerosol light scattering, *Geophys.*
2035 *Res. Lett.*, 33, L06813, doi: 06810.01029/02005gl024898, 2006.
- 2036 Baynard, T., Lovejoy, E. R., Pettersson, A., Brown, S. S., Lack, D., Osthoff, H., Massoli, P.,
2037 Ciciora, S., Dube, W. P., and Ravishankara, A. R.: Design and application of a pulsed cavity
2038 ring-down aerosol extinction spectrometer for field measurements, *Aerosol Sci. Technol.*, 41,
2039 447-462, 2007.
- 2040 Beaver, M. R., Garland, R. M., Hasenkopf, C. A., Baynard, T., Ravishankara, A. R., and
2041 Tolbert, M. A.: A laboratory investigation of the relative humidity dependence of light
2042 extinction by organic compounds from lignin combustion, *Environ. Res. Lett.*, 3, 045003,
2043 2008.
- 2044 Bechtold, M. F., and Newton, R. F.: The vapor pressures of salt solutions, *J. Am. Chem. Soc.*,
2045 62, 1390-1393, 1940.
- 2046 Bedoya-Velasquez, A. E., Navas-Guzman, F., Granados-Munoz, M. J., Titos, G., Roman, R.,
2047 Casquero-Vera, J. A., Ortiz-Amezcuca, P., Benavent-Oltra, J. A., Moreira, G. D., Montilla-
2048 Rosero, E., Hoyos, C. D., Artinano, B., Coz, E., Olmo-Reyes, F. J., Alados-Arboledas, L.,
2049 and Guerrero-Rascado, J. L.: Hygroscopic growth study in the framework of EARLINET
2050 during the SLOPE I campaign: synergy of remote sensing and in situ instrumentation, *Atmos.*
2051 *Chem. Phys.*, 18, 7001-7017, 2018.
- 2052 Bertram, A. K., Martin, S. T., Hanna, S. J., Smith, M. L., Bodsworth, A., Chen, Q., Kuwata,
2053 M., Liu, A., You, Y., and Zorn, S. R.: Predicting the relative humidities of liquid-liquid phase
2054 separation, efflorescence, and deliquescence of mixed particles of ammonium sulfate, organic
2055 material, and water using the organic-to-sulfate mass ratio of the particle and the oxygen-to-
2056 carbon elemental ratio of the organic component, *Atmos. Chem. Phys.*, 11, 10995-11006,
2057 2011.
- 2058 Bertram, T. H., and Thornton, J. A.: Toward a general parameterization of N₂O₅ reactivity
2059 on aqueous particles: the competing effects of particle liquid water, nitrate and chloride,
2060 *Atmos. Chem. Phys.*, 9, 8351-8363, 2009.
- 2061 Beyer, K. D., Schroeder, J. R., and Kissinger, J. A.: Temperature-Dependent Deliquescence
2062 Relative Humidities and Water Activities Using Humidity Controlled Thermogravimetric
2063 Analysis with Application to Malonic Acid, *J. Phys. Chem. A*, 118, 2488-2497, 2014.
- 2064 Bilde, M., Barsanti, K., Booth, M., Cappa, C. D., Donahue, N. M., Emanuelsson, E. U.,
2065 McFiggans, G., Krieger, U. K., Marcolli, C., Topping, D., Ziemann, P., Barley, M., Clegg, S.,
2066 Dennis-Smith, B., Hallquist, M., Hallquist, Å. M., Khlystov, A., Kulmala, M., Mogensen,
2067 D., Percival, C. J., Pope, F., Reid, J. P., Ribeiro da Silva, M. A. V., Rosenoern, T., Salo, K.,
2068 Soonsin, V. P., Yli-Juuti, T., Prisle, N. L., Pagels, J., Rarey, J., Zardini, A. A., and Riipinen,
2069 I.: Saturation Vapor Pressures and Transition Enthalpies of Low-Volatility Organic
2070 Molecules of Atmospheric Relevance: From Dicarboxylic Acids to Complex Mixtures,
2071 *Chem. Rev.*, 115, 4115-4156, 2015a.



- 2072 Bilde, M., Barsanti, K., Booth, M., Cappa, C. D., Donahue, N. M., Emanuelsson, E. U.,
2073 McFiggans, G., Krieger, U. K., Marcolli, C., Topping, D., Ziemann, P., Barley, M., Clegg, S.,
2074 Dennis-Smith, B., Hallquist, M., Hallquist, Å. M., Khlystov, A., Kulmala, M., Mogensen,
2075 D., Percival, C. J., Pope, F., Reid, J. P., Ribeiro da Silva, M. A. V., Rosenoern, T., Salo, K.,
2076 Soonsin, V. P., Yli-Juuti, T., Prisle, N. L., Pagels, J., Rarey, J., Zardini, A. A., and Riipinen,
2077 I.: Saturation Vapor Pressures and Transition Enthalpies of Low-Volatility Organic
2078 Molecules of Atmospheric Relevance: From Dicarboxylic Acids to Complex Mixtures,
2079 Chem. Rev., 115, 4115-4156, 2015b.
- 2080 Bond, T. C., Doherty, S. J., Fahey, D. W., Forster, P. M., Bernsten, T., DeAngelo, B. J.,
2081 Flanner, M. G., Ghan, S., Karcher, B., Koch, D., Kinne, S., Kondo, Y., Quinn, P. K., Sarofim,
2082 M. C., Schultz, M. G., Schulz, M., Venkataraman, C., Zhang, H., Zhang, S., Bellouin, N.,
2083 Guttikunda, S. K., Hopke, P. K., Jacobson, M. Z., Kaiser, J. W., Klimont, Z., Lohmann, U.,
2084 Schwarz, J. P., Shindell, D., Storelvmo, T., Warren, S. G., and Zender, C. S.: Bounding the
2085 role of black carbon in the climate system: A scientific assessment, J. Geophys. Res.-Atmos.,
2086 118, 5380-5552, 2013.
- 2087 Braban, C. F., Abbatt, J. P. D., and Cziczo, D. J.: Deliquescence of ammonium sulfate
2088 particles at sub-eutectic temperatures, Geophys. Res. Lett., 28, 3879-3882, 2001.
- 2089 Brem, B. T., Gonzalez, F. C. M., Meyers, S. R., Bond, T. C., and Rood, M. J.: Laboratory-
2090 Measured Optical Properties of Inorganic and Organic Aerosols at Relative Humidities up to
2091 95%, Aerosol Sci. Technol., 46, 178-190, 2012.
- 2092 Brock, C. A., Wagner, N. L., Anderson, B. E., Attwood, A. R., Beyersdorf, A., Campuzano-
2093 Jost, P., Carlton, A. G., Day, D. A., Diskin, G. S., Gordon, T. D., Jimenez, J. L., Lack, D. A.,
2094 Liao, J., Markovic, M. Z., Middlebrook, A. M., Ng, N. L., Perring, A. E., Richardson, M. S.,
2095 Schwarz, J. P., Washenfelder, R. A., Welti, A., Xu, L., Ziemba, L. D., and Murphy, D. M.:
2096 Aerosol optical properties in the southeastern United States in summer - Part 1: Hygroscopic
2097 growth, Atmos. Chem. Phys., 16, 4987-5007, 2016a.
- 2098 Brock, C. A., Wagner, N. L., Anderson, B. E., Beyersdorf, A., Campuzano-Jost, P., Day, D.
2099 A., Diskin, G. S., Gordon, T. D., Jimenez, J. L., Lack, D. A., Liao, J., Markovic, M. Z.,
2100 Middlebrook, A. M., Perring, A. E., Richardson, M. S., Schwarz, J. P., Welti, A., Ziemba, L.
2101 D., and Murphy, D. M.: Aerosol optical properties in the southeastern United States in
2102 summer - Part 2: Sensitivity of aerosol optical depth to relative humidity and aerosol
2103 parameters, Atmos. Chem. Phys., 16, 5009-5019, 2016b.
- 2104 Brooks, S. D., Wise, M. E., Cushing, M., and Tolbert, M. A.: Deliquescence behavior of
2105 organic/ammonium sulfate aerosol, Geophys. Res. Lett., 29, 1917, doi:
2106 1910.1029/2002gl014733, 2002.
- 2107 Brotton, S. J., and Kaiser, R. I.: In Situ Raman Spectroscopic Study of Gypsum
2108 (CaSO₄*2H₂O) and Epsomite (MgSO₄*7H₂O) Dehydration Utilizing an Ultrasonic
2109 Levitator, J. Phys. Chem. Lett., 4, 669-673, 2013.
- 2110 Brown, J. K. M., and Hovmoller, M. S.: Epidemiology - Aerial dispersal of pathogens on the
2111 global and continental scales and its impact on plant disease, Science, 297, 537-541, 2002.
- 2112 Brown, S. S.: Absorption spectroscopy in high-finesse cavities for atmospheric studies,
2113 Chem. Rev., 103, 5219-5238, 2003.
- 2114 Bruzewicz, D. A., Checco, A., Ocko, B. M., Lewis, E. R., McGraw, R. L., and Schwartz, S.
2115 E.: Reversible uptake of water on NaCl nanoparticles at relative humidity below
2116 deliquescence point observed by noncontact environmental atomic force microscopy, J.
2117 Chem. Phys., 134, 044702, doi: 044710.041063/044701.3524195, 2011.
- 2118 Buajarn, J., Mitchem, L., Ward, A. D., Nahler, N. H., McGloin, D., and Reid, J. P.:
2119 Controlling and characterizing the coagulation of liquid aerosol droplets, J. Chem. Phys., 125,
2120 114506, doi: 114510.111063/114501.2336772, 2006.



- 2121 Buajarn, J., Mitchem, L., and Reid, J. P.: Characterizing the formation of organic layers on
2122 the surface of inorganic/aqueous aerosols by Raman spectroscopy, *J. Phys. Chem. A*, 111,
2123 11852-11859, 2007.
- 2124 Burnham, D. R., and McGloin, D.: Radius measurements of optically trapped aerosols
2125 through Brownian motion, *New Journal of Physics*, 11, 063022, 2009.
- 2126 Butler, J. R., Mitchem, L., Hanford, K. L., Treuel, L., and Reid, J. P.: In situ comparative
2127 measurements of the properties of aerosol droplets of different chemical composition,
2128 *Faraday Discuss.*, 137, 351-366, 2008.
- 2129 Cai, C., and Zhang, Y.: Application of optical tweezers technology in physical chemistry
2130 characterization of aerosol, *Chinese Optics*, 10, 641-655, 2017.
- 2131 Carrico, C. M., Rood, M. J., and Ogren, J. A.: Aerosol light scattering properties at Cape
2132 Grim, Tasmania, during the First Aerosol Characterization Experiment (ACE 1), *J. Geophys.*
2133 *Res.-Atmos.*, 103, 16565-16574, 1998.
- 2134 Carvalho, T. C., Peters, J. I., and Williams, R. O.: Influence of particle size on regional lung
2135 deposition - What evidence is there?, *International Journal of Pharmaceutics*, 406, 1-10,
2136 2011.
- 2137 Cerully, K. M., Raatikainen, T., Lance, S., Tkacik, D., Tiitta, P., Petaja, T., Ehn, M.,
2138 Kulmala, M., Worsnop, D. R., Laaksonen, A., Smith, J. N., and Nenes, A.: Aerosol
2139 hygroscopicity and CCN activation kinetics in a boreal forest environment during the 2007
2140 EUCAARI campaign, *Atmos. Chem. Phys.*, 11, 12369-12386, 2011.
- 2141 Chan, C. K., Kwok, C. S., and Chow, A. H. L.: Study of hygroscopic properties of aqueous
2142 mixtures of disodium fluorescein and sodium chloride using an electrodynamic balance,
2143 *Pharmaceutical Research*, 14, 1171-1175, 1997.
- 2144 Chan, M. N., and Chan, C. K.: Mass transfer effects in hygroscopic measurements of aerosol
2145 particles, *Atmos. Chem. Phys.*, 5, 2703-2712, 2005.
- 2146 Chen, D. B., Haugstad, G., Li, Z. J., and Suryanarayanan, R.: Water Sorption Induced
2147 Transformations in Crystalline Solid Surfaces: Characterization by Atomic Force
2148 Microscopy, *J. Pharm. Sci.*, 99, 4032-4041, 2010.
- 2149 Chen, H., Hu, D. W., Wang, L., Mellouki, A., and Chen, J. M.: Modification in light
2150 absorption cross section of laboratory-generated black carbon-brown carbon particles upon
2151 surface reaction and hydration, *Atmos. Environ.*, 116, 253-261, 2015.
- 2152 Chen, H. H., Nanayakkara, C. E., and Grassian, V. H.: Titanium Dioxide Photocatalysis in
2153 Atmospheric Chemistry, *Chem. Rev.*, 112, 5919-5948, 2012.
- 2154 Chen, J., Zhao, C. S., Ma, N., and Yan, P.: Aerosol hygroscopicity parameter derived from
2155 the light scattering enhancement factor measurements in the North China Plain, *Atmos.*
2156 *Chem. Phys.*, 14, 8105-8118, 2014.
- 2157 Cheng, Y. F., Wiedensohler, A., Eichler, H., Heintzenberg, J., Tesche, M., Ansmann, A.,
2158 Wendisch, M., Su, H., Althausen, D., Herrmann, H., Gnauk, T., Brüggemann, E., Hu, M., and
2159 Zhang, Y. H.: Relative humidity dependence of aerosol optical properties and direct radiative
2160 forcing in the surface boundary layer at Xinken in Pearl River Delta of China: An observation
2161 based numerical study, *Atmos. Environ.*, 42, 6373-6397, 2008.
- 2162 Cheng, Y. F., Su, H., Koop, T., Mikhailov, E., and Poschl, U.: Size dependence of phase
2163 transitions in aerosol nanoparticles, *Nature Comm.*, 6, 5923, DOI: 5910.1038/ncomms6923,
2164 2015.
- 2165 Cheng, Y. F., Zheng, G. J., Wei, C., Mu, Q., Zheng, B., Wang, Z. B., Gao, M., Zhang, Q.,
2166 He, K. B., Carmichael, G., Pöschl, U., and Su, H.: Reactive nitrogen chemistry in aerosol
2167 water as a source of sulfate during haze events in China, *Science Adv.*, 2, e1601530, DOI:
2168 1601510.1601126/sciadv.1601530, 2016.



- 2169 Cheung, H. H. Y., Yeung, M. C., Li, Y. J., Lee, B. P., and Chan, C. K.: Relative Humidity-
2170 Dependent HTDMA Measurements of Ambient Aerosols at the HKUST Supersite in Hong
2171 Kong, China, *Aerosol Sci. Technol.*, 49, 643-654, 2015.
- 2172 Chin, M., Ginoux, P., Kinne, S., Torres, O., Holben, B. N., Duncan, B. N., Martin, R. V.,
2173 Logan, J. A., Higurashi, A., and Nakajima, T.: Tropospheric aerosol optical thickness from
2174 the GOCART model and comparisons with satellite and Sun photometer measurements, *J.*
2175 *Atmos. Sci.*, 59, 461-483, 2002.
- 2176 Choi, M. Y., and Chan, C. K.: Continuous measurements of the water activities of aqueous
2177 droplets of water-soluble organic compounds, *J. Phys. Chem. A*, 106, 4566-4572, 2002a.
- 2178 Choi, M. Y., and Chan, C. K.: The effects of organic species on the hygroscopic behaviors of
2179 inorganic aerosols, *Environ. Sci. Technol.*, 36, 2422-2428, 2002b.
- 2180 Choi, M. Y., Chan, C. K., and Zhang, Y.-H.: Application of Fluorescence Spectroscopy To
2181 Study the State of Water in Aerosols, *J. Phys. Chem. A.*, 108, 1133-1138, 2004.
- 2182 Choi, M. Y., and Chan, C. K.: Investigation of Efflorescence of Inorganic Aerosols Using
2183 Fluorescence Spectroscopy, *J. Phys. Chem. A*, 109, 1042-1048, 2005.
- 2184 Chow, J. C.: Measurement methods to determine compliance with ambient air quality
2185 standards for suspended particles, *J. Air Waste Manage. Assoc.*, 45, 320-382, 1995.
- 2186 Chow, J. C., Doraiswamy, P., Watson, J. G., Antony-Chen, L. W., Ho, S. S. H., and
2187 Sodeman, D. A.: Advances in integrated and continuous measurements for particle mass and
2188 chemical, composition, *J. Air Waste Manage. Assoc.*, 58, 141-163, 2008.
- 2189 Clegg, S. L., Brimblecombe, P., and Wexler, A. S.: Thermodynamic Model of the System
2190 $H^+ - NH_4^+ - Na^+ - SO_4^{2-} - NO_3^- - Cl^- - H_2O$ at 298.15 K, *J. Phys. Chem. A.*, 102, 2155-2171, 1998.
- 2191 Clegg, S. L., and Wexler, A. S.: Densities and Apparent Molar Volumes of Atmospherically
2192 Important Electrolyte Solutions. 1. The Solutes H_2SO_4 , HNO_3 , HCl , Na_2SO_4 , $NaNO_3$,
2193 $NaCl$, $(NH_4)_2SO_4$, NH_4NO_3 , and NH_4Cl from 0 to 50 degrees C, Including Extrapolations
2194 to Very Low Temperature and to the Pure Liquid State, and $NaHSO_4$, $NaOH$, and NH_3 at 25
2195 degrees C, *J. Phys. Chem. A*, 115, 3393-3460, 2011.
- 2196 Courtney, W. J., Shaw, R. W., and Dzubay, T. G.: Precision and accuracy of a β gauge for
2197 aerosol mass determinations, *Environ. Sci. Technol.*, 16, 236-239, 1982.
- 2198 Covert, D. S., Charlson, R. J., and Ahlquist, N. C.: A Study of the Relationship of Chemical
2199 Composition and Humidity to Light Scattering by Aerosols, *J. Appl. Meteorol.*, 11, 968-976,
2200 1972.
- 2201 Cziczo, D. J., Nowak, J. B., Hu, J. H., and Abbatt, J. P. D.: Infrared spectroscopy of model
2202 tropospheric aerosols as a function of relative humidity: Observation of deliquescence and
2203 crystallization, *J. Geophys. Res.-Atmos.*, 102, 18843-18850, 1997.
- 2204 Cziczo, D. J., and Abbatt, J. P. D.: Deliquescence, efflorescence, and supercooling of
2205 ammonium sulfate aerosols at low temperature: Implications for cirrus cloud formation and
2206 aerosol phase in the atmosphere, *J. Geophys. Res.-Atmos.*, 104, 13781-13790, 1999.
- 2207 Cziczo, D. J., and Abbatt, J. P. D.: Infrared observations of the response of $NaCl$, $MgCl_2$,
2208 NH_4HSO_4 , and NH_4NO_3 aerosols to changes in relative humidity from 298 to 238 K, *J.*
2209 *Phys. Chem. A*, 104, 2038-2047, 2000.
- 2210 Dai, Q., Hu, J., and Salmeron, M.: Adsorption of water on $NaCl$ (100) surfaces: Role of
2211 atomic steps, *J. Phys. Chem. B*, 101, 1994-1998, 1997.
- 2212 Darquenne, C., Fleming, J. S., Katz, I., Martin, A. R., Schroeter, J., Usmani, O. S., Venegas,
2213 J., and Schmid, O.: Bridging the Gap Between Science and Clinical Efficacy: Physiology,
2214 Imaging, and Modeling of Aerosols in the Lung, *Journal of Aerosol Medicine and Pulmonary*
2215 *Drug Delivery*, 29, 107-126, 2016.
- 2216 Davidson, N., Tong, H. J., Kalberer, M., Seville, P. C., Ward, A. D., Kuimova, M. K., and
2217 Pope, F. D.: Measurement of the Raman spectra and hygroscopicity of four pharmaceutical



- 2218 aerosols as they travel from pressurised metered dose inhalers (pMDI) to a model lung,
2219 International Journal of Pharmaceutics, 520, 59-69, 2017.
- 2220 Davies, J. F., and Wilson, K. R.: Raman Spectroscopy of Isotopic Water Diffusion in
2221 Ultraviscous, Glassy, and Gel States in Aerosol by Use of Optical Tweezers, Anal. Chem.,
2222 88, 2361-2366, 2016.
- 2223 Davis, E. J.: A history of single aerosol particle levitation, Aerosol Sci. Technol., 26, 212-
2224 254, 1997.
- 2225 Davis, E. J.: Electrodynamic Levitation of Particles, in: Aerosol Measurement: Principles,
2226 Techniques, and Applications, edited by: Kulkarni, P., Baron, P. A., and Willeke, K., John
2227 Wiley & Sons, Inc., Hoboken, New Jersey, 2011.
- 2228 Davis, R. D., Lance, S., Gordon, J. A., and Tolbert, M. A.: Long Working-Distance Optical
2229 Trap for in Situ Analysis of Contact-Induced Phase Transformations, Anal. Chem., 87, 6186-
2230 6194, 2015a.
- 2231 Davis, R. D., Lance, S., Gordon, J. A., Ushijima, S. B., and Tolbert, M. A.: Contact
2232 efflorescence as a pathway for crystallization of atmospherically relevant particles, Proc.
2233 Natl. Acad. Sci. U. S. A., 112, 15815-15820, 2015b.
- 2234 Day, D. E., Malm, W. C., and Kreidenweis, S. M.: Aerosol light scattering measurements as a
2235 function of relative humidity, J. Air Waste Manage. Assoc., 50, 710-716, 2000.
- 2236 Dazzi, A., Prater, C. B., Hu, Q. C., Chase, D. B., Rabolt, J. F., and Marcott, C.: AFM-IR:
2237 Combining Atomic Force Microscopy and Infrared Spectroscopy for Nanoscale Chemical
2238 Characterization, Appl. Spectrosc., 66, 1365-1384, 2012.
- 2239 Dazzi, A., and Prater, C. B.: AFM-IR: Technology and Applications in Nanoscale Infrared
2240 Spectroscopy and Chemical Imaging, Chem. Rev., 117, 5146-5173, 2017.
- 2241 de Smit, E., Swart, I., Creemer, J. F., Hoveling, G. H., Gilles, M. K., Tylliszczak, T.,
2242 Kooyman, P. J., Zandbergen, H. W., Morin, C., Weckhuysen, B. M., and de Groot, F. M. F.:
2243 Nanoscale chemical imaging of a working catalyst by scanning transmission X-ray
2244 microscopy, Nature, 456, 222-239, 2008.
- 2245 DeMott, P. J., Möhler, O., Stetzer, O., Vali, G., Levin, Z., Petters, M. D., Murakami, M.,
2246 Leisner, T., Bundke, U., Klein, H., Kanji, Z. A., Cotton, R., Jones, H., Benz, S., Brinkmann,
2247 M., Rzesanke, D., Saathoff, H., Nicolet, M., Saito, A., Nillius, B., Bingemer, H., Abbatt, J.,
2248 Ardon, K., Ganor, E., Georgakopoulos, D. G., and Saunders, C.: Resurgence in Ice Nuclei
2249 Measurement Research, Bull. Amer. Meteorol. Soc., 92, 1623-1635, 2011.
- 2250 DeMott, P. J., Möhler, O., Cziczo, D. J., Hiranuma, N., Petters, M. D., Petters, S. S., Belosi,
2251 F., Bingemer, H. G., Brooks, S. D., Budke, C., Burkert-Kohn, M., Collier, K. N., Danielczok,
2252 A., Eppers, O., Felgitsch, L., Garimella, S., Grothe, H., Herenz, P., Hill, T. C. J., Höhler, K.,
2253 Kanji, Z. A., Kiselev, A., Koop, T., Kristensen, T. B., Krüger, K., Kulkarni, G., Levin, E. J.
2254 T., Murray, B. J., Nicosia, A., O'Sullivan, D., Peckhaus, A., Polen, M. J., Price, H. C.,
2255 Reicher, N., Rothenberg, D. A., Rudich, Y., Santachiara, G., Schiebel, T., Schrod, J.,
2256 Seifried, T. M., Stratmann, F., Sullivan, R. C., Suski, K. J., Szakáll, M., Taylor, H. P.,
2257 Ullrich, R., Vergara-Temprado, J., Wagner, R., Whale, T. F., Weber, D., Welti, A., Wilson,
2258 T. W., Wolf, M. J., and Zenker, J.: The Fifth International Workshop on Ice Nucleation phase
2259 2 (FIN-02): laboratory intercomparison of ice nucleation measurements, Atmos. Meas. Tech.,
2260 11, 6231-6257, 2018.
- 2261 Demou, E., Visram, H., Donaldson, D. J., and Makar, P. A.: Uptake of water by organic
2262 films: the dependence on the film oxidation state, Atmos. Environ., 37, 3529-3537, 2003.
- 2263 Dennis-Smith, B. J., Hanford, K. L., Kwamena, N. O. A., Miles, R. E. H., and Reid, J. P.:
2264 Phase, Morphology, and Hygroscopicity of Mixed Oleic Acid/Sodium Chloride/Water
2265 Aerosol Particles before and after Ozonolysis, J. Phys. Chem. A, 116, 6159-6168, 2012.



- 2266 Després, V. R., Huffman, J. A., Burrows, S. M., Hoose, C., Safatov, A. S., Buryak, G.,
2267 Fröhlich-Nowoisky, J., Elbert, W., Andreae, M. O., Pöschl, U., and Jaenicke, R.: Primary
2268 biological aerosol particles in the atmosphere: a review, *Tellus B*, 64, 15598, 2012.
2269 Dick, W. D., Saxena, P., and McMurry, P. H.: Estimation of water uptake by organic
2270 compounds in submicron aerosols measured during the Southeastern Aerosol and Visibility
2271 Study, *J. Geophys. Res.-Atmos.*, 105, 1471-1479, 2000.
2272 Diehl, K., Quick, C., Matthias-Maser, S., Mitra, S. K., and Jaenicke, R.: The ice nucleating
2273 ability of pollen - Part I: Laboratory studies in deposition and condensation freezing modes,
2274 *Atmos. Res.*, 58, 75-87, 2001.
2275 Diehl, K., Ettner-Mahl, M., Hannemann, A., and Mitra, S. K.: Homogeneous freezing of
2276 single sulfuric and nitric acid solution drops levitated in an acoustic trap, *Atmos. Res.*, 94,
2277 356-361, 2009.
2278 Diehl, K., Debertshäuser, M., Eppers, O., Schmithüsen, H., Mitra, S. K., and Borrmann, S.:
2279 Particle surface area dependence of mineral dust in immersion freezing mode: investigations
2280 with freely suspended drops in an acoustic levitator and a vertical wind tunnel, *Atmos. Chem.*
2281 *Phys.*, 14, 12343-12355, 2014.
2282 Duplissy, J., Gysel, M., Alfarra, M. R., Dommen, J., Metzger, A., Prevot, A. S. H.,
2283 Weingartner, E., Laaksonen, A., Raatikainen, T., Good, N., Turner, S. F., McFiggans, G., and
2284 Baltensperger, U.: Cloud forming potential of secondary organic aerosol under near
2285 atmospheric conditions, *Geophys. Res. Lett.*, 35, L03818, DOI:
2286 03810.01029/02007GL031075, 2008.
2287 Duplissy, J., Gysel, M., Sjogren, S., Meyer, N., Good, N., Kammermann, L., Michaud, V.,
2288 Weigel, R., Martins dos Santos, S., Gruening, C., Villani, P., Laj, P., Sellegri, K., Metzger,
2289 A., McFiggans, G. B., Wehrle, G., Richter, R., Dommen, J., Ristovski, Z., Baltensperger, U.,
2290 and Weingartner, E.: Intercomparison study of six HTDMAs: results and recommendations,
2291 *Atmos. Meas. Tech.*, 2, 363-378, 2009.
2292 Duplissy, J., DeCarlo, P. F., Dommen, J., Alfarra, M. R., Metzger, A., Barmpadimos, I.,
2293 Prevot, A. S. H., Weingartner, E., Tritscher, T., Gysel, M., Aiken, A. C., Jimenez, J. L.,
2294 Canagaratna, M. R., Worsnop, D. R., Collins, D. R., Tomlinson, J., and Baltensperger, U.:
2295 Relating hygroscopicity and composition of organic aerosol particulate matter, *Atmos. Chem.*
2296 *Phys.*, 11, 1155-1165, 2011.
2297 Dybwad, G. L.: A sensitive new method for the determination of adhesive bonding between a
2298 particle and a substrate, *J. Appl. Phys.*, 58, 2789-2790, 1985.
2299 Ebert, M., Inerle-Hof, M., and Weinbruch, S.: Environmental scanning electron microscopy
2300 as a new technique to determine the hygroscopic behaviour of individual aerosol particles,
2301 *Atmos. Environ.*, 36, 5909-5916, 2002.
2302 Eichler, H., Cheng, Y. F., Birmili, W., Nowak, A., Wiedensohler, A., Brüggemann, E.,
2303 Gnauk, T., Herrmann, H., Althausen, D., Ansmann, A., Engelmann, R., Tesche, M.,
2304 Wendisch, M., Zhang, Y. H., Hu, M., Liu, S., and Zeng, L. M.: Hygroscopic properties and
2305 extinction of aerosol particles at ambient relative humidity in South-Eastern China, *Atmos.*
2306 *Environ.*, 42, 6321-6334, 2008.
2307 Eliason, T. L., Aloisio, S., Donaldson, D. J., Cziczo, D. J., and Vaida, V.: Processing of
2308 unsaturated organic acid films and aerosols by ozone, *Atmos. Environ.*, 37, 2207-2219, 2003.
2309 Eom, H.-J., Gupta, D., Li, X., Jung, H.-J., Kim, H., and Ro, C.-U.: Influence of Collecting
2310 Substrates on the Characterization of Hygroscopic Properties of Inorganic Aerosol Particles,
2311 *Anal. Chem.*, 86, 2648-2656, 2014.
2312 Ettner, M., Mitra, S. K., and Borrmann, S.: Heterogeneous freezing of single sulfuric acid
2313 solution droplets: laboratory experiments utilizing an acoustic levitator, *Atmos. Chem. Phys.*,
2314 4, 1925-1932, 2004.



- 2315 Ewing, G. E.: Ambient thin film water on insulator surfaces, *Chem. Rev.*, 106, 1511-1526,
2316 2006.
- 2317 Fallman, E., and Axner, O.: Design for fully steerable dual-trap optical tweezers, *Appl.*
2318 *Optics*, 36, 2107-2113, 1997.
- 2319 Fan, S. M., Horowitz, L. W., Levy, H., and Moxim, W. J.: Impact of air pollution on wet
2320 deposition of mineral dust aerosols, *Geophys. Res. Lett.*, 31, 4, L02104,
2321 10.1029/2003gl018501, 2004.
- 2322 Farmer, D. K., Cappa, C. D., and Kreidenweis, S. M.: Atmospheric Processes and Their
2323 Controlling Influence on Cloud Condensation Nuclei Activity, *Chem. Rev.*, 115, 4199-4217,
2324 2015.
- 2325 Feingold, G., and Morley, B.: Aerosol hygroscopic properties as measured by lidar and
2326 comparison with in situ measurements, *J. Geophys. Res.-Atmos.*, 108, 4327, DOI:
2327 4310.1029/2002JD002842, 2003.
- 2328 Fernandez, A. J., Molero, F., Becerril-Valle, M., Coz, E., Salvador, P., Artinano, B., and
2329 Pujadas, M.: Application of remote sensing techniques to study aerosol water vapour uptake
2330 in a real atmosphere, *Atmos. Res.*, 202, 112-127, 2018.
- 2331 Ferrare, R. A., Melfi, S. H., Whiteman, D. N., Evans, K. D., Poellot, M., and Kaufman, Y. J.:
2332 Raman lidar measurements of aerosol extinction and backscattering - 2. Derivation of aerosol
2333 real refractive index, single-scattering albedo, and humidification factor using Raman lidar
2334 and aircraft size distribution measurements, *J. Geophys. Res.-Atmos.*, 103, 19673-19689,
2335 1998.
- 2336 Feth, M. P., Jurascheck, J., Spitzenberg, M., Dillenz, J., Bertele, G., and Stark, H.: New
2337 Technology for the Investigation of Water Vapor Sorption-Induced Crystallographic Form
2338 Transformations of Chemical Compounds: A Water Vapor Sorption Gravimetry-Dispersive
2339 Raman Spectroscopy Coupling, *J. Pharm. Sci.*, 100, 1080-1092, 2011.
- 2340 Fierz-Schmidhauser, R., Zieger, P., Gysel, M., Kammermann, L., DeCarlo, P. F.,
2341 Baltensperger, U., and Weingartner, E.: Measured and predicted aerosol light scattering
2342 enhancement factors at the high alpine site Jungfraujoch, *Atmos. Chem. Phys.*, 10, 2319-
2343 2333, 2010a.
- 2344 Fierz-Schmidhauser, R., Zieger, P., Vaishya, A., Monahan, C., Bialek, J., O'Dowd, C. D.,
2345 Jennings, S. G., Baltensperger, U., and Weingartner, E.: Light scattering enhancement factors
2346 in the marine boundary layer (Mace Head, Ireland), *J. Geophys. Res.-Atmos.*, 115, D20204,
2347 DOI: 20210.21029/22009JD013755, 2010b.
- 2348 Fierz-Schmidhauser, R., Zieger, P., Wehrle, G., Jefferson, A., Ogren, J. A., Baltensperger, U.,
2349 and Weingartner, E.: Measurement of relative humidity dependent light scattering of
2350 aerosols, *Atmos. Meas. Tech.*, 3, 39-50, 2010c.
- 2351 Finlayson-Pitts, B. J., and Pitts, J. N.: *Chemistry of the Upper and Lower Atmosphere:*
2352 *Theory, Experiments, and Applications*, Academic Press, San Diego, 2000.
- 2353 Fisher, M. C., Henk, D. A., Briggs, C. J., Brownstein, J. S., Madoff, L. C., McCraw, S. L.,
2354 and Gurr, S. J.: Emerging fungal threats to animal, plant and ecosystem health, *Nature*, 484,
2355 186-194, 2012.
- 2356 Flores, J. M., Bar-Or, R. Z., Bluvshstein, N., Abo-Riziq, A., Kostinski, A., Borrmann, S.,
2357 Koren, I., Koren, I., and Rudich, Y.: Absorbing aerosols at high relative humidity: linking
2358 hygroscopic growth to optical properties, *Atmos. Chem. Phys.*, 12, 5511-5521, 2012.
- 2359 Fröhlich-Nowoisky, J., Kampf, C. J., Weber, B., Huffman, J. A., Pöhlker, C., Andreae, M.
2360 O., Lang-Yona, N., Burrows, S. M., Gunthe, S. S., Elbert, W., Su, H., Hoor, P., Thines, E.,
2361 Hoffmann, T., Després, V. R., and Pöschl, U.: Bioaerosols in the Earth system: Climate,
2362 health, and ecosystem interactions, *Atmos. Res.*, 182, 346-376, 2016.



- 2363 Freedman, M. A., Hasenkopf, C. A., Beaver, M. R., and Tolbert, M. A.: Optical Properties of
2364 Internally Mixed Aerosol Particles Composed of Dicarboxylic Acids and Ammonium
2365 Sulfate, *J. Phys. Chem. A*, 113, 13584-13592, 2009.
- 2366 Freedman, M. A., Baustian, K. J., Wise, M. E., and Tolbert, M. A.: Characterizing the
2367 Morphology of Organic Aerosols at Ambient Temperature and Pressure, *Anal. Chem.*, 82,
2368 7965-7972, 2010.
- 2369 Freedman, M. A.: Phase separation in organic aerosol, *Chem. Soc. Rev.*, 46, 7694-7705,
2370 2017.
- 2371 Freney, E. J., Martin, S. T., and Buseck, P. R.: Deliquescence and Efflorescence of Potassium
2372 Salts Relevant to Biomass-Burning Aerosol Particles, *Aerosol Sci. Technol.*, 43, 799-807,
2373 2009.
- 2374 Friedbacher, G., Grasserbauer, M., Meslmani, Y., Klaus, N., and Hignatsberger, M. J.:
2375 Investigation of Environmental Aerosol by Atomic Force Microscopy, *Anal. Chem.*, 67,
2376 1749-1754, 1995.
- 2377 Gao, R. S., Schwarz, J. P., Kelly, K. K., Fahey, D. W., Watts, L. A., Thompson, T. L.,
2378 Spackman, J. R., Slowik, J. G., Cross, E. S., Han, J. H., Davidovits, P., Onasch, T. B., and
2379 Worsnop, D. R.: A novel method for estimating light-scattering properties of soot aerosols
2380 using a modified single-particle soot photometer, *Aerosol Sci. Technol.*, 41, 125-135, 2007.
- 2381 Gao, X. Y., Zhang, Y. H., and Liu, Y.: Temperature-dependent hygroscopic behaviors of
2382 atmospherically relevant water-soluble carboxylic acid salts studied by ATR-FTIR
2383 spectroscopy, *Atmos. Environ.*, 191, 312-319, 2018.
- 2384 Garland, R. M., Ravishankara, A. R., Lovejoy, E. R., Tolbert, M. A., and Baynard, T.:
2385 Parameterization for the relative humidity dependence of light extinction: Organic-
2386 ammonium sulfate aerosol, *J. Geophys. Res.-Atmos.*, 112, D19303, DOI:
2387 19310.11029/12006JD008179, 2007.
- 2388 Gen, M., and Chan, C. K.: Electrospray surface-enhanced Raman spectroscopy (ES-SERS)
2389 for probing surface chemical compositions of atmospherically relevant particles, *Atmos.*
2390 *Chem. Phys.*, 17, 14025-14037, 2017.
- 2391 Ghorai, S., and Tivanski, A. V.: Hygroscopic Behavior of Individual Submicrometer Particles
2392 Studied by X-ray Spectromicroscopy, *Anal. Chem.*, 82, 9289-9298, 2010.
- 2393 Ghorai, S., Laskin, A., and Tivanski, A. V.: Spectroscopic Evidence of Keto-Enol
2394 Tautomerism in Deliquesced Malonic Acid Particles, *J. Phys. Chem. A*, 115, 4373-4380,
2395 2011.
- 2396 Ghorai, S., Wang, B., Tivanski, A., and Laskin, A.: Hygroscopic Properties of Internally
2397 Mixed Particles Composed of NaCl and Water-Soluble Organic Acids, *Environ. Sci.*
2398 *Technol.*, 48, 2234-2241, 2014.
- 2399 Gibson, E. R., Hudson, P. K., and Grassian, V. H.: Physicochemical properties of nitrate
2400 aerosols: Implications for the atmosphere, *J. Phys. Chem. A*, 110, 11785-11799, 2006.
- 2401 Golabiazar, R., and Sadeghi, R.: Vapor Pressure Osmometry Determination of the Osmotic
2402 and Activity Coefficients of Dilute Aqueous Solutions of Symmetrical Tetraalkyl
2403 Ammonium Halides at 308.15 K, *J. Chem. Eng. Data*, 59, 76-81, 2014.
- 2404 Gomery, K., Humphrey, E. C., and Herring, R.: Examining Protein Crystallization Using
2405 Scanning Electron Microscopy, *Microscopy and Microanalysis*, 19, 145-149, 2013.
- 2406 Gomez-Hernandez, M., McKeown, M., Secrest, J., Marrero-Ortiz, W., Lavi, A., Rudich, Y.,
2407 Collins, D. R., and Zhang, R. Y.: Hygroscopic Characteristics of Alkylammonium Carboxylate
2408 Aerosols, *Environ. Sci. Technol.*, 50, 2292-2300, 2016.
- 2409 Gong, Z., Pan, Y.-L., Videen, G., and Wang, C.: Optical trapping and manipulation of single
2410 particles in air: Principles, technical details, and applications, *Journal of Quantitative*
2411 *Spectroscopy and Radiative Transfer*, 214, 94-119, 2018.



- 2412 Good, N., Coe, H., and McFiggans, G.: Instrumentational operation and analytical
2413 methodology for the reconciliation of aerosol water uptake under sub- and supersaturated
2414 conditions, *Atmos. Meas. Tech.*, 3, 1241-1254, 2010a.
- 2415 Good, N., Topping, D. O., Duplissy, J., Gysel, M., Meyer, N. K., Metzger, A., Turner, S. F.,
2416 Baltensperger, U., Ristovski, Z., Weingartner, E., Coe, H., and McFiggans, G.: Widening the
2417 gap between measurement and modelling of secondary organic aerosol properties?, *Atmos.*
2418 *Chem. Phys.*, 10, 2577-2593, 2010b.
- 2419 Goodman, A. L., Underwood, G. M., and Grassian, V. H.: A Laboratory Study of the
2420 Heterogeneous Reaction of Nitric Acid on Calcium Carbonate Particles, *J. Geophys. Res.-*
2421 *Atmos.*, 105, 29053-29064, 2000.
- 2422 Goodman, A. L., Bernard, E. T., and Grassian, V. H.: Spectroscopic Study of Nitric Acid and
2423 Water Adsorption on Oxide Particles: Enhanced Nitric Acid Uptake Kinetics in the Presence
2424 of Adsorbed Water, *J. Phys. Chem. A*, 105, 6443-6457, 2001.
- 2425 Gorkowski, K., Beydoun, H., Aboff, M., Walker, J. S., Reid, J. P., and Sullivan, R. C.:
2426 Advanced aerosol optical tweezers chamber design to facilitate phase-separation and
2427 equilibration timescale experiments on complex droplets, *Aerosol Sci. Technol.*, 50, 1327-
2428 1341, 2016.
- 2429 Gough, R. V., Chevrier, V. F., Baustian, K. J., Wise, M. E., and Tolbert, M. A.: Laboratory
2430 studies of perchlorate phase transitions: Support for metastable aqueous perchlorate solutions
2431 on Mars, *Earth Planet. Sci. Lett.*, 312, 371-377, 2011.
- 2432 Gough, R. V., Chevrier, V. F., and Tolbert, M. A.: Formation of liquid water at low
2433 temperatures via the deliquescence of calcium chloride: Implications for Antarctica and Mars,
2434 *Planet. Space Sci.*, 131, 79-87, 2016.
- 2435 Griffiths, P. T., Borlace, J. S., Gallimore, P. J., Kalberer, M., Herzog, M., and Pope, F. D.:
2436 Hygroscopic growth and cloud activation of pollen: a laboratory and modelling study, *Atmos.*
2437 *Sci. Lett.*, 13, 289-295, 2012.
- 2438 Gu, W. J., Li, Y. J., Tang, M. J., Jia, X. H., Ding, X., Bi, X. H., and Wang, X. M.: Water
2439 uptake and hygroscopicity of perchlorates and implications for the existence of liquid water
2440 in some hyperarid environments, *RSC Adv.*, 7, 46866-46873, 2017a.
- 2441 Gu, W. J., Li, Y. J., Zhu, J. X., Jia, X. H., Lin, Q. H., Zhang, G. H., Ding, X., Song, W., Bi,
2442 X. H., Wang, X. M., and Tang, M. J.: Investigation of water adsorption and hygroscopicity of
2443 atmospherically relevant particles using a commercial vapor sorption analyzer, *Atmos. Meas.*
2444 *Tech.*, 10, 3821-3832, 2017b.
- 2445 Guo, L. Y., Gu, W. J., Peng, C., Wang, W. G., Li, Y. J., Zong, T. M., Tang, Y. J., Wu, Z. J.,
2446 Lin, Q. H., Ge, M. F., Zhang, G. H., Hu, M., Bi, X. H., Wang, X. M., and Tang, M. J.: A
2447 comprehensive study of hygroscopic properties of calcium- and magnesium-containing salts:
2448 implication for hygroscopicity of mineral dust and sea salt aerosols, *Atmos. Chem. Phys.*, 19,
2449 2115-2133, 2019.
- 2450 Gupta, D., Eom, H. J., Cho, H. R., and Ro, C. U.: Hygroscopic behavior of NaCl-MgCl₂
2451 mixture particles as nascent sea-spray aerosol surrogates and observation of efflorescence
2452 during humidification, *Atmos. Chem. Phys.*, 15, 11273-11290, 2015.
- 2453 Gustafsson, R. J., Orlov, A., Badger, C. L., Griffiths, P. T., Cox, R. A., and Lambert, R. M.:
2454 A comprehensive evaluation of water uptake on atmospherically relevant mineral surfaces:
2455 DRIFT spectroscopy, thermogravimetric analysis and aerosol growth measurements, *Atmos.*
2456 *Chem. Phys.*, 5, 3415-3421, 2005.
- 2457 Gyawali, M., Arnott, W. P., Zaveri, R. A., Song, C., Moosmuller, H., Liu, L., Mishchenko,
2458 M. I., Chen, L. W. A., Green, M. C., Watson, J. G., and Chow, J. C.: Photoacoustic optical
2459 properties at UV, VIS, and near IR wavelengths for laboratory generated and winter time
2460 ambient urban aerosols, *Atmos. Chem. Phys.*, 12, 2587-2601, 2012.



- 2461 Gysel, M., Weingartner, E., and Baltensperger, U.: Hygroscopicity of Aerosol Particles at
2462 Low Temperatures. 2. Theoretical and Experimental Hygroscopic Properties of Laboratory
2463 Generated Aerosols, *Environ. Sci. Technol.*, 36, 63-68, 2002.
- 2464 Gysel, M., Crosier, J., Topping, D. O., Whitehead, J. D., Bower, K. N., Cubison, M. J.,
2465 Williams, P. I., Flynn, M. J., McFiggans, G. B., and Coe, H.: Closure study between chemical
2466 composition and hygroscopic growth of aerosol particles during TORCH2, *Atmos. Chem.*
2467 *Phys.*, 7, 6131-6144, 2007.
- 2468 Gysel, M., McFiggans, G. B., and Coe, H.: Inversion of tandem differential mobility analyser
2469 (TDMA) measurements, *J. Aerosol. Sci.*, 40, 134-151, 2009.
- 2470 Hänel, G.: The Properties of Atmospheric Aerosol Particles as Functions of the Relative
2471 Humidity at Thermodynamic Equilibrium with the Surrounding Moist Air, in: *Advances in*
2472 *Geophysics*, edited by: Landsberg, H. E., and Mieghem, J. V., Elsevier, 73-188, 1976.
- 2473 Haarig, M., Ansmann, A., Gasteiger, J., Kandler, K., Althausen, D., Baars, H., Radenz, M.,
2474 and Farrell, D. A.: Dry versus wet marine particle optical properties: RH dependence of
2475 depolarization ratio, backscatter, and extinction from multiwavelength lidar measurements
2476 during SALTRACE, *Atmos. Chem. Phys.*, 17, 14199-14217, 2017.
- 2477 Haddrell, A. E., Davies, J. F., Yabushita, A., and Reid, J. P.: Accounting for Changes in
2478 Particle Charge, Dry Mass and Composition Occurring During Studies of Single Levitated
2479 Particles, *J. Phys. Chem. A*, 116, 9941-9953, 2012.
- 2480 Haddrell, A. E., Hargreaves, G., Davies, J. F., and Reid, J. P.: Control over hygroscopic
2481 growth of saline aqueous aerosol using Pluronic polymer additives, *International Journal of*
2482 *Pharmaceutics*, 443, 183-192, 2013.
- 2483 Haddrell, A. E., Davies, J. F., Miles, R. E. H., Reid, J. P., Dailey, L. A., and Murnane, D.:
2484 Dynamics of aerosol size during inhalation: Hygroscopic growth of commercial nebulizer
2485 formulations, *International Journal of Pharmaceutics*, 463, 50-61, 2014.
- 2486 Haddrell, A. E., Miles, R. E. H., Bzdek, B. R., Reid, J. P., Hopkins, R. J., and Walker, J. S.:
2487 Coalescence Sampling and Analysis of Aerosols using Aerosol Optical Tweezers, *Anal.*
2488 *Chem.*, 89, 2345-2352, 2017.
- 2489 Han, J. H., Hung, H. M., and Martin, S. T.: Size effect of hematite and corundum inclusions
2490 on the efflorescence relative humidities of aqueous ammonium nitrate particles, *J. Geophys.*
2491 *Res.-Atmos.*, 107, 4086, DOI: 4010.1029/2001JD001054, 2002.
- 2492 Hand, J. L., and Malm, W. C.: Review of aerosol mass scattering efficiencies from ground-
2493 based measurements since 1990, *J. Geophys. Res.-Atmos.*, 112, D16203, DOI:
2494 16210.11029/12007JD008484, 2007.
- 2495 Hanford, K. L., Mitchem, L., Reid, J. P., Clegg, S. L., Topping, D. O., and McFiggans, G. B.:
2496 Comparative thermodynamic studies of aqueous glutaric acid, ammonium sulfate and sodium
2497 chloride aerosol at high humidity, *J. Phys. Chem. A*, 112, 9413-9422, 2008.
- 2498 Hargreaves, G., Kwamena, N. O. A., Zhang, Y. H., Butler, J. R., Rushworth, S., Clegg, S. L.,
2499 and Reid, J. P.: Measurements of the Equilibrium Size of Supersaturated Aqueous Sodium
2500 Chloride Droplets at Low Relative Humidity Using Aerosol Optical Tweezers and an
2501 Electrodynamic Balance, *J. Phys. Chem. A*, 114, 1806-1815, 2010a.
- 2502 Hargreaves, G., Kwamena, N. O. A., Zhang, Y. H., Butler, J. R., Rushworth, S., Clegg, S. L.,
2503 and Reid, J. P.: Measurements of the Equilibrium Size of Supersaturated Aqueous Sodium
2504 Chloride Droplets at Low Relative Humidity Using Aerosol Optical Tweezers and an
2505 Electrodynamic Balance, *J. Phys. Chem. A*, 114, 1806-1815, 2010b.
- 2506 Hatch, C. D., Gierlus, K. M., Schuttlefield, J. D., and Grassian, V. H.: Water adsorption and
2507 cloud condensation nuclei activity of calcite and calcite coated with model humic and fulvic
2508 acids, *Atmos. Environ.*, 42, 5672-5684, 2008.



- 2509 Hatch, C. D., Wiese, J. S., Crane, C. C., Harris, K. J., Kloss, H. G., and Baltrusaitis, J.: Water
2510 Adsorption on Clay Minerals As a Function of Relative Humidity: Application of BET and
2511 Freundlich Adsorption Models, *Langmuir*, 28, 1790-1803, 2011.
- 2512 He, K. J., Cheng, H., Zhu, Y. Y., Wang, L. Y., and Zhang, Y. H.: Measurement of electric
2513 properties of the single supersaturated aerosol droplet, *Chin. Sci. Bull.*, 53, 1773-1776, 2008.
- 2514 He, Y. B., Tilocca, A., Dulub, O., Selloni, A., and Diebold, U.: Local ordering and electronic
2515 signatures of submonolayer water on anatase TiO₂(101), *Nature Materials*, 8, 585-589, 2009.
- 2516 Hefter, G., May, P. M., Marshall, S. L., Cornish, J., and Kron, I.: Improved apparatus and
2517 procedures for isopiestic studies at elevated temperatures, *Rev. Sci. Instrum.*, 68, 2558-2567,
2518 1997.
- 2519 Hegg, D. A., Covert, D. S., Jonsson, H., and Covert, P. A.: An instrument for measuring size-
2520 resolved aerosol hygroscopicity at both sub- and super-micron sizes, *Aerosol Sci. Technol.*,
2521 41, 873-883, 2007.
- 2522 Hennig, T., Massling, A., Brechtel, F. J., and Wiedensohler, A.: A Tandem DMA for highly
2523 temperature-stabilized hygroscopic particle growth measurements between 90% and 98%
2524 relative humidity, *J. Aerosol Sci.*, 36, 1210-1223, 2005.
- 2525 Hepburn, J. R. I.: 69. The vapour pressure of water over aqueous solutions of the chlorides of
2526 the alkaline-earth metals. Part I. Experimental, with a critical discussion of vapour-pressure
2527 data, *J. Chem. Soc.*, 550-566, 1932.
- 2528 Herich, H., Tritscher, T., Wiacek, A., Gysel, M., Weingartner, E., Lohmann, U.,
2529 Baltensperger, U., and Cziczo, D. J.: Water uptake of clay and desert dust aerosol particles at
2530 sub- and supersaturated water vapor conditions, *Phys. Chem. Chem. Phys.*, 11, 7804-7809,
2531 2009.
- 2532 Hickey, A. J., and Martonen, T. B.: Behavior of hygroscopic pharmaceutical aerosols and the
2533 influence of hydrophobic additives, *Pharmaceutical Research*, 10, 1-7, 1993.
- 2534 Hiranuma, N., Brooks, S. D., Auvermann, B. W., and Littleton, R.: Using environmental
2535 scanning electron microscopy to determine the hygroscopic properties of agricultural
2536 aerosols, *Atmos. Environ.*, 42, 1983-1994, 2008.
- 2537 Hiranuma, N., Augustin-Bauditz, S., Bingemer, H., Budke, C., Curtius, J., Danielczok, A.,
2538 Diehl, K., Dreischmeier, K., Ebert, M., Frank, F., Hoffmann, N., Kandler, K., Kiselev, A.,
2539 Koop, T., Leisner, T., Möhler, O., Nillius, B., Peckhaus, A., Rose, D., Weinbruch, S., Wex,
2540 H., Boose, Y., DeMott, P. J., Hader, J. D., Hill, T. C. J., Kanji, Z. A., Kulkarni, G., Levin, E.
2541 J. T., McCluskey, C. S., Murakami, M., Murray, B. J., Niedermeier, D., Petters, M. D.,
2542 O'Sullivan, D., Saito, A., Schill, G. P., Tajiri, T., Tolbert, M. A., Welti, A., Whale, T. F.,
2543 Wright, T. P., and Yamashita, K.: A comprehensive laboratory study on the immersion
2544 freezing behavior of illite NX particles: a comparison of 17 ice nucleation measurement
2545 techniques, *Atmos. Chem. Phys.*, 15, 2489-2518, 2015.
- 2546 Hitznerberger, R., Berner, A., Dusek, U., and Alabashi, R.: Humidity-Dependent Growth of
2547 Size-Segregated Aerosol Samples, *Aerosol Sci. Technol.*, 27, 116-130, 1997.
- 2548 Hoffman, R. C., Laskin, A., and Finlayson-Pitts, B. J.: Sodium nitrate particles: physical and
2549 chemical properties during hydration and dehydration, and implications for aged sea salt
2550 aerosols, *J. Aerosol. Sci.*, 35, 869-887, 2004.
- 2551 Hofmann, W.: Modelling inhaled particle deposition in the human lung-A review, *J. Aerosol.
2552 Sci.*, 42, 693-724, 2011.
- 2553 Hong, J., Xu, H. B., Tan, H. B., Yin, C. Q., Hao, L. Q., Li, F., Cai, M. F., Deng, X. J., Wang,
2554 N., Su, H., Cheng, Y. F., Wang, L., Petaja, T., and Kerminen, V. M.: Mixing state and
2555 particle hygroscopicity of organic-dominated aerosols over the Pearl River Delta region in
2556 China, *Atmos. Chem. Phys.*, 18, 14079-14094, 2018.
- 2557 Hoese, C., and Moehler, O.: Heterogeneous ice nucleation on atmospheric aerosols: a review
2558 of results from laboratory experiments, *Atmos. Chem. Phys.*, 12, 9817-9854, 2012.



- 2559 Hopkins, R. J., Mitchem, L., Ward, A. D., and Reid, J. P.: Control and characterisation of a
2560 single aerosol droplet in a single-beam gradient-force optical trap, *Physical Chemistry*
2561 *Chemical Physics*, 6, 4924-4927, 2004.
- 2562 Hosny, N. A., Fitzgerald, C., Vysniauskas, A., Athanasiadis, A., Berkemeier, T., Uygur, N.,
2563 Poschl, U., Shiraiwa, M., Kalberer, M., Pope, F. D., and Kuimova, M. K.: Direct imaging of
2564 changes in aerosol particle viscosity upon hydration and chemical aging, *Chemical Science*,
2565 7, 1357-1367, 2016.
- 2566 Hu, D. W., Li, C. L., Chen, H., Chen, J. M., Ye, X. N., Li, L., Yang, X., Wang, X. M.,
2567 Mellouki, A., and Hu, Z. Y.: Hygroscopicity and optical properties of alkylammonium sulfates,
2568 *J. Environ. Sci.*, 26, 37-43, 2014.
- 2569 Hung, H. M., Katrib, Y., and Martin, S. T.: Products and mechanisms of the reaction of oleic
2570 acid with ozone and nitrate radical, *J. Phys. Chem. A*, 109, 4517-4530, 2005.
- 2571 Hung, H. M., Wang, K. C., and Chen, J. P.: Adsorption of nitrogen and water vapor by
2572 insoluble particles and the implication on cloud condensation nuclei activity, *J. Aerosol. Sci.*,
2573 86, 24-31, 2015.
- 2574 Ibrahim, S., Romanias, M. N., Alleman, L. Y., Zeineddine, M. N., Angeli, G. K., Trikalitis, P.
2575 N., and Thevenet, F.: Water Interaction with Mineral Dust Aerosol: Particle Size and
2576 Hygroscopic Properties of Dust, *ACS Earth and Space Chem.*, 2, 376-386, 2018.
- 2577 Inerle-Hof, M., Weinbruch, S., Ebert, M., and Thomassen, Y.: The hygroscopic behaviour of
2578 individual aerosol particles in nickel refineries as investigated by environmental scanning
2579 electron microscopy, *Journal of Environmental Monitoring*, 9, 301-306, 2007.
- 2580 IPCC: *Climate Change 2013: The Physical Science Basis*, Cambridge University Press,
2581 Cambridge, UK, 2013.
- 2582 Jakli, G., and Vanhook, W. A.: Osmotic coefficients of aqueous solutions of NaBr, NaI, KF,
2583 and CaCl₂ between 0 and 90 °C, *J. Chem. Eng. Data*, 17, 348-355, 1972.
- 2584 Jia, X. H., Gu, W. J., Li, Y. J., Cheng, P., Tang, Y. J., Guo, L. Y., Wang, X. M., and Tang,
2585 M. J.: Phase transitions and hygroscopic growth of Mg(ClO₄)₂, NaClO₄, and NaClO₄·H₂O:
2586 implications for the stability of aqueous water in hyperarid environments on Mars and on
2587 Earth, *ACS Earth Space Chem.*, 2, 159-167, 2018.
- 2588 Jickells, T. D., An, Z. S., Andersen, K. K., Baker, A. R., Bergametti, G., Brooks, N., Cao, J.
2589 J., Boyd, P. W., Duce, R. A., Hunter, K. A., Kawahata, H., Kubilay, N., laRoche, J., Liss, P.
2590 S., Mahowald, N., Prospero, J. M., Ridgwell, A. J., Tegen, I., and Torres, R.: Global Iron
2591 Connections between Desert Dust, Ocean Biogeochemistry, and Climate, *Science*, 308, 67-
2592 71, 2005.
- 2593 Jing, B., Tong, S., Liu, Q., Li, K., Wang, W., Zhang, Y., and Ge, M.: Hygroscopic behavior
2594 of multicomponent organic aerosols and their internal mixtures with ammonium sulfate,
2595 *Atmos. Chem. Phys.*, 16, 4101-4118, 2016.
- 2596 Jones, S. H., King, M. D., and Ward, A. D.: Atmospherically relevant core-shell aerosol
2597 studied using optical trapping and Mie scattering, *Chem. Commun.*, 51, 4914-4917, 2015.
- 2598 Joshi, N., Romanias, M. N., Riffault, V., and Thevenet, F.: Investigating water adsorption
2599 onto natural mineral dust particles: Linking DRIFTS experiments and BET theory, *Aeolian*
2600 *Res.*, 27, 35-45, 2017.
- 2601 Joyner, L. G., Weinberger, E. B., and Montgomery, C. W.: Surface Area Measurements of
2602 Activated Carbons, Silica Gel and other Adsorbents, *J. Am. Chem. Soc.*, 67, 2182-2188,
2603 1945.
- 2604 Jubb, A. M., Hua, W., and Allen, H. C.: Environmental Chemistry at Vapor/Water Interfaces:
2605 Insights from Vibrational Sum Frequency Generation Spectroscopy, *Annu. Rev. Phys.*
2606 *Chem.*, 63, 107-130, 2012.
- 2607 Juranyi, Z., Gysel, M., Duplissy, J., Weingartner, E., Tritscher, T., Dommen, J., Henning, S.,
2608 Ziese, M., Kiselev, A., Stratmann, F., George, I., and Baltensperger, U.: Influence of gas-to-



- 2609 particle partitioning on the hygroscopic and droplet activation behaviour of alpha-pinene
2610 secondary organic aerosol, *Physical Chemistry Chemical Physics*, 11, 8091-8097, 2009.
- 2611 Königsberger, E., Königsberger, L.-C., Hefter, G., and May, P. M.: Zdanovskii's Rule and
2612 Isopiestic Measurements Applied to Synthetic Bayer Liquors, *J. Solution Chem.*, 36, 1619-
2613 1634, 2007.
- 2614 Kaaden, N., Massling, A., Schladitz, A., Müller, T., Kandler, K., Schütz, L., Weinzierl, B.,
2615 Petzold, A., Tesche, M., Leinert, S., Deutscher, C., Ebert, M., Weinbruch, S., and
2616 Wiedensohler, A.: State of mixing, shape factor, number size distribution, and hygroscopic
2617 growth of the Saharan anthropogenic and mineral dust aerosol at Tinfou, Morocco, *Tellus B*,
2618 61, 51-63, 2009.
- 2619 Kanji, Z. A., Ladino, L. A., Wex, H., Boose, Y., Burkert-Kohn, M., Cziczo, D. J., and
2620 Krämer, M.: Overview of Ice Nucleating Particles, in: *Ice Formation and Evolution in Clouds
2621 and Precipitation: Measurement and modeling Challenges*, edited by: McFarquhar, G. M.,
2622 Baumgardner, D., and Heymsfield, A. J., American Meteorological Society, 1.1-1.33, 2017.
- 2623 Karagulian, F., and Rossi, M. J.: The heterogeneous chemical kinetics of NO₃ on atmospheric
2624 mineral dust surrogates, *Phys. Chem. Chem. Phys.*, 7, 3150-3162, 2005.
- 2625 Karagulian, F., Santschi, C., and Rossi, M. J.: The heterogeneous chemical kinetics of N₂O₅
2626 on CaCO₃ and other atmospheric mineral dust surrogates, *Atmos. Chem. Phys.*, 6, 1373-
2627 1388, 2006.
- 2628 Kavouras, A., and Krammer, G.: Ultrasonic levitation for the examination of gas/solid
2629 reactions, *Rev. Sci. Instrum.*, 74, 4468-4473, 2003a.
- 2630 Kavouras, A., and Krammer, G.: Ultrasonic levitation for the examination of gas/solid
2631 reactions, *Rev. Sci. Instrum.*, 74, 4468-4473, 2003b.
- 2632 Kelly, J. T., and Wexler, A. S.: Thermodynamics of carbonates and hydrates related to
2633 heterogeneous reactions involving mineral aerosol, *J. Geophys. Res.-Atmos*, 110, D11201,
2634 doi: 11210.11029/12004jd005583, 2005.
- 2635 Kelly, S. T., Nigge, P., Prakash, S., Laskin, A., Wang, B. B., Tylliszczak, T., Leone, S. R.,
2636 and Gilles, M. K.: An environmental sample chamber for reliable scanning transmission x-
2637 ray microscopy measurements under water vapor, *Rev. Sci. Instrum.*, 84, 073708, 2013.
- 2638 Ketteler, G., Yamamoto, S., Bluhm, H., Andersson, K., Starr, D. E., Ogletree, D. F.,
2639 Ogasawara, H., Nilsson, A., and Salmeron, M.: The Nature of Water Nucleation Sites on
2640 TiO₂(110) Surfaces Revealed by Ambient Pressure X-ray Photoelectron Spectroscopy, *J.*
2641 *Phys. Chem. C*, 111, 8278-8282, 2007.
- 2642 Khalizov, A. F., Xue, H., Wang, L., Zheng, J., and Zhang, R.: Enhanced Light Absorption
2643 and Scattering by Carbon Soot Aerosol Internally Mixed with Sulfuric Acid, *J. Phys. Chem.*
2644 *A*, 113, 1066-1074, 2009.
- 2645 Kim, D., Chin, M., Yu, H., Diehl, T., Tan, Q., Kahn, R. A., Tsigaridis, K., Bauer, S. E.,
2646 Takemura, T., Pozzoli, L., Bellouin, N., Schulz, M., Peyridieu, S., Chédin, A., and Koffi, B.:
2647 Sources, sinks, and transatlantic transport of North African dust aerosol: A multimodel
2648 analysis and comparison with remote sensing data, *J. Geophys. Res.-Atmos*, 119, 6259-6277,
2649 2014.
- 2650 Kim, J. S., and Park, K.: Atmospheric Aging of Asian Dust Particles During Long Range
2651 Transport, *Aerosol Sci. Technol.*, 46, 913-924, 2012.
- 2652 Knopf, D. A., Alpert, P. A., and Wang, B.: The Role of Organic Aerosol in Atmospheric Ice
2653 Nucleation: A Review, *ACS Earth and Space Chem.*, 2, 168-202, 2018.
- 2654 Knox, K. J., Reid, J. P., Hanford, K. L., Hudson, A. J., and Mitchem, L.: Direct
2655 measurements of the axial displacement and evolving size of optically trapped aerosol
2656 droplets, *Journal of Optics a-Pure and Applied Optics*, 9, S180-S188, 2007.
- 2657 Knox, K. J., and Reid, J. P.: Ultrasensitive Absorption Spectroscopy of Optically-Trapped
2658 Aerosol Droplets, *J. Phys. Chem. A*, 112, 10439-10441, 2008.



- 2659 Koehler, K. A., Kreidenweis, S. M., DeMott, P. J., Petters, M. D., Prenni, A. J., and Carrico,
2660 C. M.: Hygroscopicity and cloud droplet activation of mineral dust aerosol, *Geophys. Res.*
2661 *Letts.*, 36, L08805, doi: 08810.01029/02009gl037348, 2009.
- 2662 Koloutsou-Vakakis, S., Carrico, C. M., Kus, P., Rood, M. J., Li, Z., Shrestha, R., Ogren, J.
2663 A., Chow, J. C., and Watson, J. G.: Aerosol properties at a midlatitude Northern Hemisphere
2664 continental site, *J. Geophys. Res.-Atmos.*, 106, 3019-3032, 2001.
- 2665 Koop, T., Bookhold, J., Shiraiwa, M., and Poschl, U.: Glass transition and phase state of
2666 organic compounds: dependency on molecular properties and implications for secondary
2667 organic aerosols in the atmosphere, *Phys. Chem. Chem. Phys.*, 13, 19238-19255, 2011.
- 2668 Kreidenweis, S. M., and Asa-Awuku, A.: 5.13 - Aerosol Hygroscopicity: Particle Water
2669 Content and Its Role in Atmospheric Processes, in: *Treatise on Geochemistry (Second*
2670 *Edition)*, edited by: Turekian, K. K., Elsevier, Oxford, 331-361, 2014.
- 2671 Kreisberg, N. M., Stolzenburg, M. R., Hering, S. V., Dick, W. D., and McMurry, P. H.: A
2672 new method for measuring the dependence of particle size distributions on relative humidity,
2673 with application to the Southeastern Aerosol and Visibility Study, *J. Geophys. Res.-Atmos.*,
2674 106, 14935-14949, 2001.
- 2675 Krieger, U. K., Marcolli, C., and Reid, J. P.: Exploring the complexity of aerosol particle
2676 properties and processes using single particle techniques, *Chem. Soc. Rev.*, 41, 6631-6662,
2677 2012.
- 2678 Krueger, B. J., Grassian, V. H., Laskin, A., and Cowin, J. P.: The Transformation of Solid
2679 Atmospheric Particles into Liquid Droplets through Heterogeneous Chemistry: Laboratory
2680 Insights into the Processing of Calcium Containing Mineral Dust Aerosol in the Troposphere,
2681 *Geophys. Res. Letts.*, 30, 1148, doi: 1110.1029/2002gl016563, 2003.
- 2682 Krueger, B. J., Grassian, V. H., Cowin, J. P., and Laskin, A.: Heterogeneous chemistry of
2683 individual mineral dust particles from different dust source regions: the importance of particle
2684 mineralogy, *Atmos. Environ.*, 38, 6253-6261, 2004.
- 2685 Krueger, B. J., Ross, J. L., and Grassian, V. H.: Formation of microcrystals, micropuddles,
2686 and other spatial inhomogenities in surface reactions under ambient conditions: An atomic
2687 force microscopy study of water and nitric acid adsorption on MgO(100) and CaCO₃(1014),
2688 *Langmuir*, 21, 8793-8801, 2005.
- 2689 Kuang, Y., Zhao, C., Tao, J., Bian, Y., Ma, N., and Zhao, G.: A novel method for deriving
2690 the aerosol hygroscopicity parameter based only on measurements from a humidified
2691 nephelometer system, *Atmos. Chem. Phys.*, 17, 6651-6662, 2017.
- 2692 Kuang, Y., Zhao, C. S., Zhao, G., Tao, J. C., Xu, W., Ma, N., and Bian, Y. X.: A novel
2693 method for calculating ambient aerosol liquid water content based on measurements of a
2694 humidified nephelometer system, *Atmos. Meas. Tech.*, 11, 2967-2982, 2018.
- 2695 Kulkarni, P., Baron, P. A., and Willeke, K.: *Aerosol Measurement: Principles, Techniques,*
2696 *and Applications (Third edition)*, ed., John Wiley & Sons, Inc., Hoboken, New Jersey, 2011.
- 2697 Kumar, R., Saunders, R. W., Mahajan, A. S., Plane, J. M. C., and Murray, B. J.: Physical
2698 properties of iodate solutions and the deliquescence of crystalline I₂O₅ and HIO₃, *Atmos.*
2699 *Chem. Phys.*, 10, 12251-12260, 2010.
- 2700 Kuwata, M.: Particle Classification by the Tandem Differential Mobility Analyzer-Particle
2701 Mass Analyzer System, *Aerosol Sci. Technol.*, 49, 508-520, 2015.
- 2702 Kuzmiakova, A., Dillner, A. M., and Takahama, S.: An automated baseline correction
2703 protocol for infrared spectra of atmospheric aerosols collected on polytetrafluoroethylene
2704 (Teflon) filters, *Atmos. Meas. Tech.*, 9, 2615-2631, 2016.
- 2705 Lack, D. A., Quinn, P. K., Massoli, P., Bates, T. S., Coffman, D., Covert, D. S., Sierau, B.,
2706 Tucker, S., Baynard, T., Lovejoy, E., Murphy, D. M., and Ravishankara, A. R.: Relative
2707 humidity dependence of light absorption by mineral dust after long-range atmospheric
2708 transport from the Sahara, *Geophys. Res. Letts.*, 36, 10.1029/2009gl041002, 2009.



- 2709 Lack, D. A., Moosmuller, H., McMeeking, G. R., Chakrabarty, R. K., and Baumgardner, D.:
2710 Characterizing elemental, equivalent black, and refractory black carbon aerosol particles: a
2711 review of techniques, their limitations and uncertainties, *Anal. Bioanal. Chem.*, 406, 99-122,
2712 2014.
- 2713 Ladino, L. A., Stetzer, O., and Lohmann, U.: Contact freezing: a review of experimental
2714 studies, *Atmos. Chem. Phys.*, 13, 9745-9769, 2013.
- 2715 Lance, S., Medina, J., Smith, J. N., and Nenes, A.: Mapping the operation of the DMT
2716 Continuous Flow CCN counter, *Aerosol Sci. Technol.*, 40, 242-254, 2006.
- 2717 Langridge, J. M., Richardson, M. S., Lack, D., Law, D., and Murphy, D. M.: Aircraft
2718 Instrument for Comprehensive Characterization of Aerosol Optical Properties, Part I:
2719 Wavelength-Dependent Optical Extinction and Its Relative Humidity Dependence Measured
2720 Using Cavity Ringdown Spectroscopy, *Aerosol Sci. Technol.*, 45, 1305-1318, 2011.
- 2721 Langridge, J. M., Richardson, M. S., Lack, D. A., Brock, C. A., and Murphy, D. M.:
2722 Limitations of the Photoacoustic Technique for Aerosol Absorption Measurement at High
2723 Relative Humidity, *Aerosol Sci. Technol.*, 47, 1163-1173, 2013.
- 2724 Laskin, A., Iedema, M. J., Ichkovich, A., Graber, E. R., Taraniuk, I., and Rudich, Y.: Direct
2725 Observation of Completely Processed Calcium Carbonate Dust Particles, *Faraday Discuss.*,
2726 130, 453-468, 2005.
- 2727 Laskina, O., Morris, H. S., Grandquist, J. R., Estillore, A. D., Stone, E. A., Grassian, V. H.,
2728 and Tivanski, A. V.: Substrate-Deposited Sea Spray Aerosol Particles: Influence of
2729 Analytical Method, Substrate, and Storage Conditions on Particle Size, Phase, and
2730 Morphology, *Environ. Sci. Technol.*, 49, 13447-13453, 2015a.
- 2731 Laskina, O., Morris, H. S., Grandquist, J. R., Estillore, A. D., Stone, E. A., Grassian, V. H.,
2732 and Tivanski, A. V.: Substrate-Deposited Sea Spray Aerosol Particles: Influence of
2733 Analytical Method, Substrate, and Storage Conditions on Particle Size, Phase, and
2734 Morphology, *Environ. Sci. Technol.*, 49, 13447-13453, 2015b.
- 2735 Lathem, T. L., and Nenes, A.: Water Vapor Depletion in the DMT Continuous-Flow CCN
2736 Chamber: Effects on Supersaturation and Droplet Growth, *Aerosol Sci. Technol.*, 45, 604-
2737 615, 2011.
- 2738 Lau, N. T., Chan, C. K., Chan, L. I., and Fang, M.: A microscopic study of the effects of
2739 particle size and composition of atmospheric aerosols on the corrosion of mild steel,
2740 *Corrosion Science*, 50, 2927-2933, 2008.
- 2741 Lee, A. K. Y., and Chan, C. K.: Heterogeneous Reactions of Linoleic Acid and Linolenic
2742 Acid Particles with Ozone: Reaction Pathways and Changes in Particle Mass,
2743 Hygroscopicity, and Morphology, *J. Phys. Chem. A*, 111, 6285-6295, 2007.
- 2744 Lee, A. K. Y., Ling, T. Y., and Chan, C. K.: Understanding hygroscopic growth and phase
2745 transformation of aerosols using single particle Raman spectroscopy in an electrodynamic
2746 balance, *Faraday Discuss.*, 137, 245-263, 2008.
- 2747 Lee, C. T., and Hsu, W. C.: A novel method to measure aerosol water mass, *J. Aerosol. Sci.*,
2748 29, 827-837, 1998.
- 2749 Lee, C. T., and Hsu, W. C.: The measurement of liquid water mass associated with collected
2750 hygroscopic particles, *J. Aerosol. Sci.*, 31, 189-197, 2000.
- 2751 Lee, C. T., and Chang, S. Y.: A GC-TCD method for measuring the liquid water mass of
2752 collected aerosols, *Atmos. Environ.*, 36, 1883-1894, 2002.
- 2753 Lehmpuhl, D. W., Ramirez-Aguilar, K. A., Michel, A. E., Rowlen, K. L., and Birks, J. W.:
2754 Physical and chemical characterization of atmospheric aerosols by atomic force microscopy,
2755 *Anal. Chem.*, 71, 379-383, 1999.
- 2756 Lehmuskero, A., Johansson, P., Rubinsztein-Dunlop, H., Tong, L. M., and Kall, M.: Laser
2757 Trapping of Colloidal Metal Nanoparticles, *ACS Nano*, 9, 3453-3469, 2015.



- 2758 Lei, T., Zuend, A., Wang, W. G., Zhang, Y. H., and Ge, M. F.: Hygroscopicity of organic
2759 compounds from biomass burning and their influence on the water uptake of mixed organic
2760 ammonium sulfate aerosols, *Atmos. Chem. Phys.*, 14, 11165-11183, 2014.
- 2761 Leng, C. B., Pang, S. F., Zhang, Y., Cai, C., Liu, Y., and Zhang, Y. H.: Vacuum FTIR
2762 Observation on the Dynamic Hygroscopicity of Aerosols under Pulsed Relative Humidity,
2763 *Environ. Sci. Technol.*, 49, 9107-9115, 2015.
- 2764 Lewis, K. A., Arnott, W. P., Moosmuller, H., Chakrabarty, R. K., Carrico, C. M.,
2765 Kreidenweis, S. M., Day, D. E., Malm, W. C., Laskin, A., Jimenez, J. L., Ulbrich, I. M.,
2766 Huffman, J. A., Onasch, T. B., Trimborn, A., Liu, L., and Mishchenko, M. I.: Reduction in
2767 biomass burning aerosol light absorption upon humidification: roles of inorganically-induced
2768 hygroscopicity, particle collapse, and photoacoustic heat and mass transfer, *Atmos. Chem.*
2769 *Phys.*, 9, 8949-8966, 2009.
- 2770 Li-Jones, X., Maring, H. B., and Prospero, J. M.: Effect of relative humidity on light
2771 scattering by mineral dust aerosol as measured in the marine boundary layer over the tropical
2772 Atlantic Ocean, *J. Geophys. Res.-Atmos.*, 103, 31113-31121, 1998.
- 2773 Li, H. J., Zhu, T., Zhao, D. F., Zhang, Z. F., and Chen, Z. M.: Kinetics and mechanisms of
2774 heterogeneous reaction of NO₂ on CaCO₃ surfaces under dry and wet conditions, *Atmos.*
2775 *Chem. Phys.*, 10, 463-474, 2010.
- 2776 Li, K. N., Ye, X. N., Pang, H. W., Lu, X. H., Chen, H., Wang, X. F., Yang, X., Chen, J. M.,
2777 and Chen, Y. J.: Temporal variations in the hygroscopicity and mixing state of black carbon
2778 aerosols in a polluted megacity area, *Atmos. Chem. Phys.*, 18, 15201-15218, 2018a.
- 2779 Li, W., Shao, L., Zhang, D., Ro, C.-U., Hu, M., Bi, X., Geng, H., Matsuki, A., Niu, H., and
2780 Chen, J.: A Review of Single Aerosol Particle Studies in the Atmosphere of East Asia:
2781 Morphology, Mixing State, Source, and Heterogeneous Reactions, *J. Clean. Prod.*, 112, 1330-
2782 1349, 2015.
- 2783 Li, X. H., Wang, F., Lu, P. D., Dong, J. L., Wang, L. Y., and Zhang, Y. H.: Confocal Raman
2784 observation of the efflorescence/deliquescence processes of individual NaNO₃ particles on
2785 quartz, *J. Phys. Chem. B*, 110, 24993-24998, 2006.
- 2786 Li, Y. J., Huang, D. D., Cheung, H. Y., Lee, A. K. Y., and Chan, C. K.: Aqueous-phase
2787 photochemical oxidation and direct photolysis of vanillin – a model compound of methoxy
2788 phenols from biomass burning, *Atmos. Chem. Phys.*, 14, 2871-2885, 2014.
- 2789 Li, Z., Gu, X., Wang, L., Li, D., Xie, Y., Li, K., Dubovik, O., Schuster, G., Goloub, P.,
2790 Zhang, Y., Li, L., Ma, Y., and Xu, H.: Aerosol physical and chemical properties retrieved
2791 from ground-based remote sensing measurements during heavy haze days in Beijing winter,
2792 *Atmos. Chem. Phys.*, 13, 10171-10183, 2013.
- 2793 Li, Z. Y., Hu, R. Z., Xie, P. H., Wang, H. C., Lu, K. D., and Wang, D.: Intercomparison of in
2794 situ CRDS and CEAS for measurements of atmospheric N₂O₅ in Beijing, China, *Sci. Total*
2795 *Environ.*, 613, 131-139, 2018b.
- 2796 Ling, T. Y., and Chan, C. K.: Formation and transformation of metastable double salts from
2797 the crystallization of mixed ammonium nitrate and ammonium sulfate particles, *Environ. Sci.*
2798 *Technol.*, 41, 8077-8083, 2007.
- 2799 Ling, T. Y., and Chan, C. K.: Partial crystallization and deliquescence of particles containing
2800 ammonium sulfate and dicarboxylic acids, *J. Geophys. Res.-Atmos.*, 113, D14205, DOI:
2801 14210.11029/12008JD009779, 2008.
- 2802 Liu, B. Y. H., Pui, D. Y. H., Whitby, K. T., Kittelson, D. B., Kousaka, Y., and McKenzie, R.
2803 L.: The aerosol mobility chromatograph: A new detector for sulfuric acid aerosols, *Atmos.*
2804 *Environ.*, 12, 99-104, 1978.
- 2805 Liu, C., Ma, Q. X., He, H., He, G. Z., Ma, J. Z., Liu, Y. C., and Wu, Y.: Structure-activity
2806 relationship of surface hydroxyl groups during NO₂ adsorption and transformation on TiO₂
2807 nanoparticles, *Environ. Sci.: Nano*, 4, 2388-2394, 2017.



- 2808 Liu, D., Allan, J., Whitehead, J., Young, D., Flynn, M., Coe, H., McFiggans, G., Fleming, Z.
2809 L., and Bandy, B.: Ambient black carbon particle hygroscopic properties controlled by
2810 mixing state and composition, *Atmos. Chem. Phys.*, 13, 2015-2029, 2013a.
- 2811 Liu, D. F., Ma, G., Xu, M., and Allen, H. C.: Adsorption of Ethylene Glycol Vapor on α -
2812 $\text{Al}_2\text{O}_3(0001)$ and Amorphous SiO_2 Surfaces: Observation of Molecular Orientation and
2813 Surface Hydroxyl Groups as Sorption Sites, *Environ. Sci. Technol.*, 39, 206-212, 2005.
- 2814 Liu, P. F., Li, Y. J., Wang, Y., Gilles, M. K., Zaveri, R. A., Bertram, A. K., and Martin, S. T.:
2815 Lability of secondary organic particulate matter, *Proc. Natl. Acad. Sci. U. S. A.*, 113, 12643-
2816 12648, 2016.
- 2817 Liu, X. G., Zhang, Y. H., Cheng, Y. F., Hu, M., and Han, T. T.: Aerosol hygroscopicity and
2818 its impact on atmospheric visibility and radiative forcing in Guangzhou during the 2006
2819 PRIDE-PRD campaign, *Atmos. Environ.*, 60, 59-67, 2012.
- 2820 Liu, X. G., Gu, J. W., Li, Y. P., Cheng, Y. F., Qu, Y., Han, T. T., Wang, J. L., Tian, H. Z.,
2821 Chen, J., and Zhang, Y. H.: Increase of aerosol scattering by hygroscopic growth:
2822 Observation, modeling, and implications on visibility, *Atmos. Res.*, 132, 91-101, 2013b.
- 2823 Liu, Y., Yang, Z., Desyaterik, Y., Gassman, P. L., Wang, H., and Laskin, A.: Hygroscopic
2824 behavior of substrate-deposited particles studied by micro-FT-IR spectroscopy and
2825 complementary methods of particle analysis, *Anal. Chem.*, 80, 633-642, 2008a.
- 2826 Liu, Y., Yang, Z., Desyaterik, Y., Gassman, P. L., Wang, H., and Laskin, A.: Hygroscopic
2827 behavior of substrate-deposited particles studied by micro-FT-IR spectroscopy and
2828 complementary methods of particle analysis, *Anal. Chem.*, 80, 633-642, 2008b.
- 2829 Liu, Y., and Laskin, A.: Hygroscopic Properties of $\text{CH}_3\text{SO}_3\text{Na}$, $\text{CH}_3\text{SO}_3\text{NH}_4$,
2830 $(\text{CH}_3\text{SO}_3)_2\text{Mg}$, and $(\text{CH}_3\text{SO}_3)_2\text{Ca}$ Particles Studied by micro-FTIR Spectroscopy, *J.*
2831 *Phys. Chem. A*, 113, 1531-1538, 2009.
- 2832 Liu, Y., Ma, Q., and He, H.: Comparative study of the effect of water on the heterogeneous
2833 reactions of carbonyl sulfide on the surface of $\alpha\text{-Al}_2\text{O}_3$ and
2834 MgO , *Atmos. Chem. Phys.*, 9, 6273-6286, 2009.
- 2835 Liu, Y. J., Zhu, T., Zhao, D. F., and Zhang, Z. F.: Investigation of the hygroscopic properties
2836 of $\text{Ca}(\text{NO}_3)_2$ and internally mixed $\text{Ca}(\text{NO}_3)_2/\text{CaCO}_3$ particles by micro-Raman spectrometry,
2837 *Atmos. Chem. Phys.*, 8, 7205-7215, 2008c.
- 2838 Lohmann, U., and Feichter, J.: Global indirect aerosol effects: a review, *Atmos. Chem. Phys.*,
2839 5, 715-737, 2005.
- 2840 Lohmann, U., Lüönd, F., and Mahrt, F.: *An Introduction to Clouds: From the Microscale to*
2841 *Climate*, Cambridge University Press, Cambridge, 2016.
- 2842 Lopez-Yglesias, X. F., Yeung, M. C., Dey, S. E., Brechtel, F. J., and Chan, C. K.:
2843 Performance Evaluation of the Brechtel Mfg. Humidified Tandem Differential Mobility
2844 Analyzer (BMI HTDMA) for Studying Hygroscopic Properties of Aerosol Particles, *Aerosol*
2845 *Sci. Technol.*, 48, 969-980, 2014.
- 2846 Lu, J. W., Rickards, A. M. J., Walker, J. S., Knox, K. J., Miles, R. E. H., Reid, J. P., and
2847 Signorell, R.: Timescales of water transport in viscous aerosol: measurements on sub-micron
2848 particles and dependence on conditioning history, *Phys. Chem. Chem. Phys.*, 16, 9819-9830,
2849 2014.
- 2850 Lv, M., Liu, D., Li, Z. Q., Mao, J. T., Sun, Y. L., Wang, Z. Z., Wang, Y. J., and Xie, C. B.:
2851 Hygroscopic growth of atmospheric aerosol particles based on lidar, radiosonde, and in situ
2852 measurements: Case studies from the Xinzhou field campaign, *J. Quant. Spectrosc. Radiat.*
2853 *Transf.*, 188, 60-70, 2017.
- 2854 Ma, G., Liu, D. F., and Allen, H. C.: Piperidine adsorption on hydrated alpha-alumina (0001)
2855 surface studied by vibrational sum frequency generation spectroscopy, *Langmuir*, 20, 11620-
2856 11629, 2004.



- 2857 Ma, Q., and He, H.: Synergistic effect in the humidifying process of atmospheric relevant
2858 calcium nitrate, calcite and oxalic acid mixtures, *Atmos. Environ.*, 50, 97-102, 2012.
- 2859 Ma, Q., He, H., Liu, Y., Liu, C., and Grassian, V. H.: Heterogeneous and multiphase
2860 formation pathways of gypsum in the atmosphere, *Phys. Chem. Chem. Phys.*, 15, 19196-
2861 19204, 2013a.
- 2862 Ma, Q. X., He, H., and Liu, Y. C.: In Situ DRIFTS Study of Hygroscopic Behavior of
2863 Mineral Aerosol, *J. Environ. Sci.*, 22, 555-560, 2010a.
- 2864 Ma, Q. X., Liu, Y. C., and He, H.: The Utilization of Physisorption Analyzer for Studying the
2865 Hygroscopic Properties of Atmospheric Relevant Particles, *J. Phys. Chem. A*, 114, 4232-
2866 4237, 2010b.
- 2867 Ma, Q. X., Liu, Y. C., Liu, C., and He, H.: Heterogeneous Reaction of Acetic Acid on MgO,
2868 α -Al₂O₃, and CaCO₃ and the Effect on the Hygroscopic Behavior of These Particles, *Phys.*
2869 *Chem. Chem. Phys.*, 14, 8403-8409, 2012a.
- 2870 Ma, Q. X., Liu, Y. C., Liu, C., Ma, J. Z., and He, H.: A case study of Asian dust storm
2871 particles: Chemical composition, reactivity to SO₂ and hygroscopic properties, *J. Environ.*
2872 *Sci.*, 24, 62-71, 2012b.
- 2873 Ma, Q. X., Ma, J. Z., Liu, C., Lai, C. Y., and He, H.: Laboratory Study on the Hygroscopic
2874 Behavior of External and Internal C-2-C-4 Dicarboxylic Acid-NaCl Mixtures, *Environ. Sci.*
2875 *Technol.*, 47, 10381-10388, 2013b.
- 2876 Maffia, M. C., and Meirelles, A. J. A.: Water activity and pH in aqueous polycarboxylic acid
2877 systems, *J. Chem. Eng. Data*, 46, 582-587, 2001.
- 2878 Magome, N., Kohira, M. I., Hayata, E., Mukai, S., and Yoshikawa, K.: Optical trapping of a
2879 growing water droplet in air, *J. Phys. Chem. B*, 107, 3988-3990, 2003.
- 2880 Mahowald, N.: Aerosol Indirect Effect on Biogeochemical Cycles and Climate, *Science*, 334,
2881 794-796, 2011.
- 2882 Mahowald, N., Ward, D. S., Kloster, S., Flanner, M. G., Heald, C. L., Heavens, N. G., Hess,
2883 P. G., Lamarque, J.-F., and Chuang, P. Y.: Aerosol Impacts on Climate and Biogeochemistry,
2884 *Annu. Rev. Environ. Resour.*, 36, 45-74, 2011.
- 2885 Malm, W. C., Day, D. E., and Kreidenweis, S. M.: Light scattering characteristics of aerosols
2886 at ambient and as a function of relative humidity: Part II - A comparison of measured
2887 scattering and aerosol concentrations using statistical models, *J. Air Waste Manage. Assoc.*,
2888 50, 701-709, 2000a.
- 2889 Malm, W. C., Day, D. E., and Kreidenweis, S. M.: Light scattering characteristics of aerosols
2890 as a function of relative humidity: Part I - A comparison of measured scattering and aerosol
2891 concentrations using the theoretical models, *J. Air Waste Manage. Assoc.*, 50, 686-700,
2892 2000b.
- 2893 Malm, W. C., and Day, D. E.: Estimates of aerosol species scattering characteristics as a
2894 function of relative humidity, *Atmos. Environ.*, 35, 2845-2860, 2001.
- 2895 Marcolli, C., Luo, B. P., and Peter, T.: Mixing of the organic aerosol fractions: Liquids as the
2896 thermodynamically stable phases, *J. Phys. Chem. A*, 108, 2216-2224, 2004.
- 2897 Maria, S. F., Russell, L. M., Turpin, B. J., and Porcja, R. J.: FTIR measurements of functional
2898 groups and organic mass in aerosol samples over the Caribbean, *Atmos. Environ.*, 36, 5185-
2899 5196, 2002.
- 2900 Martin-Torres, F. J., Zorzano, M. P., Valentin-Serrano, P., Harri, A. M., Genzer, M.,
2901 Kempinen, O., Rivera-Valentin, E. G., Jun, I., Wray, J., Madsen, M. B., Goetz, W.,
2902 McEwen, A. S., Hardgrove, C., Renno, N., Chevrier, V. F., Mischna, M., Navarro-Gonzalez,
2903 R., Martinez-Frias, J., Conrad, P., McConnochie, T., Cockell, C. S., Berger, G., Vasavada, A.
2904 R., Sumner, D., and Vaniman, D.: Transient liquid water and water activity at Gale crater on
2905 Mars, *Nature Geoscience*, 8, 357-361, 2015.



- 2906 Martin, S. T.: Phase transitions of aqueous atmospheric particles, *Chem. Rev.*, 100, 3403-
2907 3453, 2000.
- 2908 Mason, N. J., Drage, E. A., Webb, S. M., Dawes, A., McPheat, R., and Hayes, G.: The
2909 spectroscopy and chemical dynamics of microparticles explored using an ultrasonic trap,
2910 *Faraday Discuss.*, 137, 367-376, 2008.
- 2911 Massling, A., Leinert, S., Wiedensohler, A., and Covert, D.: Hygroscopic growth of sub-
2912 micrometer and one-micrometer aerosol particles measured during ACE-Asia, *Atmos. Chem.*
2913 *Phys.*, 7, 3249-3259, 2007.
- 2914 Massling, A., Niedermeier, N., Hennig, T., Fors, E. O., Swietlicki, E., Ehn, M., Hämeri, K.,
2915 Villani, P., Laj, P., Good, N., McFiggans, G., and Wiedensohler, A.: Results and
2916 recommendations from an intercomparison of six Hygroscopicity-TDMA systems, *Atmos.*
2917 *Meas. Tech.*, 4, 485-497, 2011.
- 2918 Massoli, P., Lambe, A. T., Ahern, A. T., Williams, L. R., Ehn, M., Mikkilä, J., Canagaratna,
2919 M. R., Brune, W. H., Onasch, T. B., Jayne, J. T., Petaja, T., Kulmala, M., Laaksonen, A.,
2920 Kolb, C. E., Davidovits, P., and Worsnop, D. R.: Relationship between aerosol oxidation
2921 level and hygroscopic properties of laboratory generated secondary organic aerosol (SOA)
2922 particles, *Geophys. Res. Lett.*, 37, L24801, DOI: 24810.21029/22010GL045258, 2010.
- 2923 Matsuki, A., Iwasaka, Y., Shi, G. Y., Zhang, D. Z., Trochkin, D., Yamada, M., Kim, Y. S.,
2924 Chen, B., Nagatani, T., Miyazawa, T., Nagatani, M., and Nakata, H.: Morphological and
2925 chemical modification of mineral dust: Observational insight into the heterogeneous uptake
2926 of acidic gases, *Geophys. Res. Lett.*, 32, L22806, doi: 22810.21029/22005gl024176, 2005.
- 2927 Matsumura, T., and Hayashi, M.: Hygroscopic growth of an (NH₄)₂SO₄ aqueous solution
2928 droplet measured using an environmental scanning electron microscope (ESEM), *Aerosol*
2929 *Sci. Technol.*, 41, 770-774, 2007.
- 2930 Mauer, L. J., and Taylor, L. S.: Water-Solids Interactions: Deliquescence, *Annu. Rev. Food*
2931 *Sci. Technol.*, 1, 41-63, 2010a.
- 2932 Mauer, L. J., and Taylor, L. S.: Deliquescence of pharmaceutical systems, *Pharm. Dev.*
2933 *Technol.*, 15, 582-594, 2010b.
- 2934 McFiggans, G., Artaxo, P., Baltensperger, U., Coe, H., Facchini, M. C., Feingold, G., Fuzzi,
2935 S., Gysel, M., Laaksonen, A., Lohmann, U., Mentel, T. F., Murphy, D. M., O'Dowd, C. D.,
2936 Snider, J. R., and Weingartner, E.: The effect of physical and chemical aerosol properties on
2937 warm cloud droplet activation, *Atmos. Chem. Phys.*, 6, 2593-2649, 2006.
- 2938 McGloin, D.: Optical tweezers: 20 years on, *Philosophical Transactions of the Royal Society*
2939 *a-Mathematical Physical and Engineering Sciences*, 364, 3521-3537, 2006.
- 2940 McInnes, L. M., Quinn, P. K., Covert, D. S., and Anderson, T. L.: Gravimetric analysis, ionic
2941 composition, and associated water mass of the marine aerosol, *Atmos. Environ.*, 30, 869-884,
2942 1996.
- 2943 McMeeking, G. R., Good, N., Petters, M. D., McFiggans, G., and Coe, H.: Influences on the
2944 fraction of hydrophobic and hydrophilic black carbon in the atmosphere, *Atmos. Chem.*
2945 *Phys.*, 11, 5099-5112, 2011.
- 2946 McMurry, P. H., and Stolzenburg, M. R.: On the sensitivity of particle size to relative
2947 humidity for Los Angeles aerosols, *Atmos. Environ.*, 23, 497-507, 1989.
- 2948 McMurry, P. H.: A review of atmospheric aerosol measurements, *Atmos. Environ.*, 34, 1959-
2949 1999, 2000.
- 2950 Mikhailov, E., Vlasenko, S., Martin, S. T., Koop, T., and Poschl, U.: Amorphous and
2951 crystalline aerosol particles interacting with water vapor: conceptual framework and
2952 experimental evidence for restructuring, phase transitions and kinetic limitations, *Atmos.*
2953 *Chem. Phys.*, 9, 9491-9522, 2009.



- 2954 Mikhailov, E., Vlasenko, S., Rose, D., and Pöschl, U.: Mass-based hygroscopicity parameter
2955 interaction model and measurement of atmospheric aerosol water uptake, *Atmos. Chem.*
2956 *Phys.*, 13, 717-740, 2013.
- 2957 Mikhailov, E. F., Merkulov, V. V., Vlasenko, S. S., Ryshkevich, T. I., and Pöschl, U. J.:
2958 Filter-based differential hygroscopicity analyzer of aerosol particles, *Izvestiya, Atmospheric*
2959 *and Oceanic Physics*, 47, 747-759, 2011.
- 2960 Mikhailov, E. F., Mironov, G. N., Pöhlker, C., Chi, X., Krüger, M. L., Shiraiwa, M., Förster,
2961 J. D., Pöschl, U., Vlasenko, S. S., Ryshkevich, T. I., Weigand, M., Kilcoyne, A. L. D., and
2962 Andreae, M. O.: Chemical composition, microstructure, and hygroscopic properties of
2963 aerosol particles at the Zotino Tall Tower Observatory (ZOTTO), Siberia, during a summer
2964 campaign, *Atmos. Chem. Phys.*, 15, 8847-8869, 2015.
- 2965 Miranda, P. B., Xu, L., Shen, Y. R., and Salmeron, M.: Icelike water monolayer adsorbed on
2966 mica at room temperature, *Phys. Rev. Lett.*, 81, 5876-5879, 1998.
- 2967 Mitchem, L., Buajarearn, J., Hopkins, R. J., Ward, A. D., Gilham, R. J. J., Johnston, R. L., and
2968 Reid, J. P.: Spectroscopy of growing and evaporating water droplets: Exploring the variation
2969 in equilibrium droplet size with relative humidity, *J. Phys. Chem. A*, 110, 8116-8125, 2006a.
- 2970 Mitchem, L., Buajarearn, J., Ward, A. D., and Reid, J. P.: A strategy for characterizing the
2971 mixing state of immiscible aerosol components and the formation of multiphase aerosol
2972 particles through coagulation, *J. Phys. Chem. B*, 110, 13700-13703, 2006b.
- 2973 Mitchem, L., and Reid, J. P.: Optical manipulation and characterisation of aerosol particles
2974 using a single-beam gradient force optical trap, *Chem. Soc. Rev.*, 37, 756-769, 2008.
- 2975 Montgomery, J. F., Rogak, S. N., Green, S. I., You, Y., and Bertram, A. K.: Structural
2976 Change of Aerosol Particle Aggregates with Exposure to Elevated Relative Humidity,
2977 *Environ. Sci. Technol.*, 49, 12054-12061, 2015.
- 2978 Moosmuller, H., Chakrabarty, R. K., and Arnott, W. P.: Aerosol light absorption and its
2979 measurement: A review, *J. Quant. Spectrosc. Radiat. Transf.*, 110, 844-878, 2009.
- 2980 Morris, H. S., Grassian, V. H., and Tivanski, A. V.: Humidity-dependent surface tension
2981 measurements of individual inorganic and organic submicrometre liquid particles, *Chem.*
2982 *Sci.*, 6, 3242-3247, 2015.
- 2983 Morris, H. S., Estillore, A. D., Laskina, O., Grassian, V. H., and Tivanski, A. V.: Quantifying
2984 the Hygroscopic Growth of Individual Submicrometer Particles with Atomic Force
2985 Microscopy, *Anal. Chem.*, 88, 3647-3654, 2016.
- 2986 Moteki, N., and Kondo, Y.: Dependence of Laser-Induced Incandescence on Physical
2987 Properties of Black Carbon Aerosols: Measurements and Theoretical Interpretation, *Aerosol*
2988 *Sci. Technol.*, 44, 663-675, 2010.
- 2989 Mu, Q., Shiraiwa, M., Octaviani, M., Ma, N., Ding, A. J., Su, H., Lammel, G., Poeschl, U.,
2990 and Cheng, Y. F.: Temperature effect on phase state and reactivity controls atmospheric
2991 multiphase chemistry and transport of PAHs, *Science Advances*, 4, 10.1126/sciadv.aap7314,
2992 2018.
- 2993 Murray, B. J., O'Sullivan, D., Atkinson, J. D., and Webb, M. E.: Ice nucleation by particles
2994 immersed in supercooled cloud droplets, *Chem. Soc. Rev.*, 41, 6519-6554, 2012.
- 2995 Najera, J. J., Percival, C. J., and Horn, A. B.: Infrared spectroscopic studies of the
2996 heterogeneous reaction of ozone with dry maleic and fumaric acid aerosol particles, *Physical*
2997 *Chemistry Chemical Physics*, 11, 9093-9103, 2009.
- 2998 Navea, J. G., Chen, H. H., Huang, M., Carmichael, G. R., and Grassian, V. H.: A comparative
2999 evaluation of water uptake on several mineral dust sources, *Environ. Chem.*, 7, 162-170,
3000 2010.
- 3001 Navea, J. G., Richmond, E., Stortini, T., and Greenspan, J.: Water Adsorption Isotherms on
3002 Fly Ash from Several Sources, *Langmuir*, 33, 10161-10171, 2017.



- 3003 Nenes, A., Chuang, P. Y., Flagan, R. C., and Seinfeld, J. H.: A theoretical analysis of cloud
3004 condensation nucleus (CCN) instruments, *J. Geophys. Res.-Atmos.*, 106, 3449-3474, 2001.
- 3005 Newman, A. W., Reutzel-Edens, S. M., and Zograf, G.: Characterization of the
3006 "Hygroscopic" properties of active pharmaceutical ingredients, *J. Pharm. Sci.*, 97, 1047-1059,
3007 2008.
- 3008 Niedermeier, D., Wex, H., Voigtlander, J., Stratmann, F., Brüggemann, E., Kiselev, A.,
3009 Henk, H., and Heintzenberg, J.: LACIS-measurements and parameterization of sea-salt
3010 particle hygroscopic growth and activation, *Atmos. Chem. Phys.*, 8, 579-590, 2008.
- 3011 Ohata, S., Schwarz, J. P., Moteki, N., Koike, M., Takami, A., and Kondo, Y.: Hygroscopicity
3012 of materials internally mixed with black carbon measured in Tokyo, *J. Geophys. Res.-*
3013 *Atmos.*, 121, 362-381, 2016.
- 3014 Olfert, J. S., and Collings, N.: New method for particle mass classification - the Couette
3015 centrifugal particle mass analyzer, *J. Aerosol. Sci.*, 36, 1338-1352, 2005.
- 3016 Onasch, T. B., Siefert, R. L., Brooks, S. D., Prenni, A. J., Murray, B., Wilson, M. A., and
3017 Tolbert, M. A.: Infrared spectroscopic study of the deliquescence and efflorescence of
3018 ammonium sulfate aerosol as a function of temperature, *J. Geophys. Res.-Atmos.*, 104,
3019 21317-21326, 1999.
- 3020 Pöhlker, C., Saturno, J., Krüger, M. L., Förster, J.-D., Weigand, M., Wiedemann, K. T.,
3021 Bechtel, M., Artaxo, P., and Andreae, M. O.: Efflorescence upon humidification? X-ray
3022 microspectroscopic in situ observation of changes in aerosol microstructure and phase state
3023 upon hydration, *Geophys. Res. Lett.*, 41, 3681-3689, 2014.
- 3024 Pöschl, U.: Atmospheric Aerosols: Composition, Transformation, Climate and Health
3025 Effects, *Angew. Chem.-Int. Edit.*, 44, 7520-7540, 2005.
- 3026 Pöschl, U., and Shiraiwa, M.: Multiphase Chemistry at the Atmosphere–Biosphere Interface
3027 Influencing Climate and Public Health in the Anthropocene, *Chem. Rev.*, 115, 4440-4475,
3028 2015.
- 3029 Pahlow, M., Feingold, G., Jefferson, A., Andrews, E., Ogren, J. A., Wang, J., Lee, Y. N.,
3030 Ferrare, R. A., and Turner, D. D.: Comparison between lidar and nephelometer measurements
3031 of aerosol hygroscopicity at the Southern Great Plains Atmospheric Radiation Measurement
3032 site, *J. Geophys. Res.-Atmos.*, 111, D05S15, DOI: 10.1029/2004JD005646, 2006.
- 3033 Pant, A., Fok, A., Parsons, M. T., Mak, J., and Bertram, A. K.: Deliquescence and
3034 crystallization of ammonium sulfate-glutaric acid and sodium chloride-glutaric acid particles,
3035 *Geophys. Res. Lett.*, 31, L12111, 10.1029/2004gl020025, 2004.
- 3036 Pant, A., Parsons, M. T., and Bertram, A. K.: Crystallization of aqueous ammonium sulfate
3037 particles internally mixed with soot and kaolinite: Crystallization relative humidities and
3038 nucleation rates, *J. Phys. Chem. A*, 110, 8701-8709, 2006.
- 3039 Parsons, M. T., Knopf, D. A., and Bertram, A. K.: Deliquescence and Crystallization of
3040 Ammonium Sulfate Particles Internally Mixed with Water-Soluble Organic Compounds, *J.*
3041 *Phys. Chem. A*, 108, 11600-11608, 2004a.
- 3042 Parsons, M. T., Mak, J., Lipetz, S. R., and Bertram, A. K.: Deliquescence of malonic,
3043 succinic, glutaric, and adipic acid particles, *J. Geophys. Res.-Atmos.*, 109, D06212, doi:
3044 10.1029/2003jd004075, 2004b.
- 3045 Parsons, M. T., Riffell, J. L., and Bertram, A. K.: Crystallization of aqueous inorganic-
3046 malonic acid particles: Nucleation rates, dependence on size, and dependence on the
3047 ammonium-to-sulfate, *J. Phys. Chem. A*, 110, 8108-8115, 2006.
- 3048 Patashnick, H., and Rupprecht, E. G.: Continuous PM-10 measurement using the tapered
3049 element oscillating microbalance, *J. Air Waste Manage. Assoc.*, 41, 1079-1083, 1991.
- 3050 Patterson, J. P., Collins, D. B., Michaud, J. M., Axson, J. L., Sultana, C. M., Moser, T.,
3051 Dommer, A. C., Conner, J., Grassian, V. H., Stokes, M. D., Deane, G. B., Evans, J. E.,
3052 Burkart, M. D., Prather, K. A., and Gianneschi, N. C.: Sea Spray Aerosol Structure and



- 3053 Composition Using Cryogenic Transmission Electron Microscopy, *ACS Central Science*, 2,
3054 40-47, 2016.
- 3055 Peng, C., and Chan, C. K.: The water cycles of water-soluble organic salts of atmospheric
3056 importance, *Atmos. Environ.*, 35, 1183-1192, 2001a.
- 3057 Peng, C., Chan, M. N., and Chan, C. K.: The hygroscopic properties of dicarboxylic and
3058 multifunctional acids: Measurements and UNIFAC predictions, *Environ. Sci. Technol.*, 35,
3059 4495-4501, 2001.
- 3060 Peng, C., Wang, W. G., Li, K., Li, J. L., Zhou, L., Wang, L. S., and Ge, M. F.: The Optical
3061 Properties of Limonene Secondary Organic Aerosols: The Role of NO₃, OH, and O₃ in the
3062 Oxidation Processes, *J. Geophys. Res.-Atmos.*, 123, 3292-3303, 2018.
- 3063 Peng, C. G., Chow, A. H. L., and Chan, C. K.: Study of the hygroscopic properties of
3064 selected pharmaceutical aerosols using single particle levitation, *Pharmaceutical Research*,
3065 17, 1104-1109, 2000.
- 3066 Peng, C. G., and Chan, C. K.: The water cycles of water-soluble organic salts of atmospheric
3067 importance, *Atmos. Environ.*, 35, 1183-1192, 2001b.
- 3068 Perring, A. E., Schwarz, J. P., Markovic, M. Z., Fahey, D. W., Jimenez, J. L., Campuzano-
3069 Jost, P., Palm, B. D., Wisthaler, A., Mikoviny, T., Diskin, G., Sachse, G., Ziemba, L.,
3070 Anderson, B., Shingler, T., Crosbie, E., Sorooshian, A., Yokelson, R., and Gao, R. S.: In situ
3071 measurements of water uptake by black carbon-containing aerosol in wildfire plumes, *J.*
3072 *Geophys. Res.-Atmos.*, 122, 1086-1097, 2017.
- 3073 Petters, M. D., and Kreidenweis, S. M.: A single parameter representation of hygroscopic
3074 growth and cloud condensation nucleus activity, *Atmos. Chem. Phys.*, 7, 1961-1971, 2007.
- 3075 Petters, M. D., Prenni, A. J., Kreidenweis, S. M., and DeMott, P. J.: On measuring the critical
3076 diameter of cloud condensation nuclei using mobility selected aerosol, *Aerosol Sci. Technol.*,
3077 41, 907-913, 2007.
- 3078 Petters, M. D., Wex, H., Carrico, C. M., Hallbauer, E., Massling, A., McMeeking, G. R.,
3079 Poulain, L., Wu, Z., Kreidenweis, S. M., and Stratmann, F.: Towards closing the gap between
3080 hygroscopic growth and activation for secondary organic aerosol - Part 2: Theoretical
3081 approaches, *Atmos. Chem. Phys.*, 9, 3999-4009, 2009.
- 3082 Piens, D. S., Kelly, S. T., Harder, T. H., Petters, M. D., O'Brien, R. E., Wang, B. B., Teske,
3083 K., Dowell, P., Laskin, A., and Gilles, M. K.: Measuring Mass-Based Hygroscopicity of
3084 Atmospheric Particles through in Situ Imaging, *Environ. Sci. Technol.*, 50, 5172-5180, 2016.
- 3085 Pilat, M. J., and Charlson, R. J.: Theoretical and optical studies of humidity effects on the
3086 size distribution of a hygroscopic aerosol, *J. Rech. Atmos.*, 1, 165-170, 1966.
- 3087 Pinterich, T., Spielman, S. R., Hering, S., and Wang, J.: A water-based fast integrated
3088 mobility spectrometer (WFIMS) with enhanced dynamic size range, *Aerosol Sci. Technol.*,
3089 51, 1212-1222, 2017a.
- 3090 Pinterich, T., Spielman, S. R., Wang, Y., Hering, S. V., and Wang, J.: A humidity-controlled
3091 fast integrated mobility spectrometer (HFIMS) for rapid measurements of particle
3092 hygroscopic growth, *Atmos. Meas. Tech.*, 10, 4915-4925, 2017b.
- 3093 Pitzer, K. S.: *Activity Coefficients in Electrolyte Solutions*, CRC Press, Boca Raton, Florida,
3094 USA, 1991.
- 3095 Platt, U., Meinen, J., Pöhler, D., and Leisner, T.: Broadband Cavity Enhanced Differential
3096 Optical Absorption Spectroscopy (CE-DOAS) – applicability and corrections, *Atmos.*
3097 *Meas. Tech.*, 2, 713-723, 2009.
- 3098 Pomorska, A., Shchukin, D., Hammond, R., Cooper, M. A., Grundmeier, G., and
3099 Johannsmann, D.: Positive Frequency Shifts Observed Upon Adsorbing Micron-Sized Solid
3100 Objects to a Quartz Crystal Microbalance from the Liquid Phase, *Anal. Chem.*, 82, 2237-
3101 2242, 2010.



- 3102 Pope, F. D.: Pollen grains are efficient cloud condensation nuclei, *Environ. Res. Lett.*, 5,
3103 044015, 2010.
- 3104 Pope, F. D., Dennis-Smith, B. J., Griffiths, P. T., Clegg, S. L., and Cox, R. A.: Studies of
3105 Single Aerosol Particles Containing Malonic Acid, Glutaric Acid, and Their Mixtures with
3106 Sodium Chloride. I. Hygroscopic Growth, *J. Phys. Chem. A*, 114, 5335-5341, 2010a.
- 3107 Pope, F. D., Gallimore, P. J., Fuller, S. J., Cox, R. A., and Kalberer, M.: Ozonolysis of
3108 Maleic Acid Aerosols: Effect upon Aerosol Hygroscopicity, Phase and Mass, *Environ. Sci.*
3109 *Technol.*, 44, 6656-6660, 2010b.
- 3110 Popovicheva, O., Persiantseva, N. M., Shonija, N. K., DeMott, P., Koehler, K., Petters, M.,
3111 Kreidenweis, S., Tishkova, V., Demirdjian, B., and Suzanne, J.: Water interaction with
3112 hydrophobic and hydrophilic soot particles, *Phys. Chem. Chem. Phys.*, 10, 2332-2344, 2008a.
- 3113 Popovicheva, O. B., Persiantseva, N. M., Tishkova, V., Shonija, N. K., and Zubareva, N. A.:
3114 Quantification of water uptake by soot particles, *Environ. Res. Lett.*, 3, 025009, 2008b.
- 3115 Popovicheva, O. B., Trukhin, M. E., Persiantseva, N. M., and Shonija, N. K.: Water
3116 adsorption on aircraft-combustor soot under young plume conditions, *Atmos. Environ.*, 35,
3117 1673-1676, 2001.
- 3118 Posfai, M., Xu, H. F., Anderson, J. R., and Buseck, P. R.: Wet and dry sizes of atmospheric
3119 aerosol particles: An AFM-TEM study, *Geophys. Res. Lett.*, 25, 1907-1910, 1998.
- 3120 Posfai, M., and Buseck, P. R.: Nature and Climate Effects of Individual Tropospheric
3121 Aerosol Particles, *Annu. Rev. Earth Planet. Sci.*, 38, 17-43, 2010.
- 3122 Power, R. M., Simpson, S. H., Reid, J. P., and Hudson, A. J.: The transition from liquid to
3123 solid-like behaviour in ultrahigh viscosity aerosol particles, *Chem. Sci.*, 4, 2597-2604, 2013.
- 3124 Prather, K. A., Hatch, C. D., and Grassian, V. H.: Analysis of Atmospheric Aerosols, *Ann.*
3125 *Rev. Phys. Chem.*, 1, 485-514, 2008.
- 3126 Prenni, A. J., Petters, M. D., Kreidenweis, S. M., DeMott, P. J., and Ziemann, P. J.: Cloud
3127 droplet activation of secondary organic aerosol, *J. Geophys. Res.-Atmos.*, 112, D10223, DOI:
3128 10210.11029/12006JD007963, 2007.
- 3129 Pruppacher, H. R., and Klett, J. D.: *Microphysics of Clouds and Precipitation*, 2nd ed.,
3130 Kluwer Academic Publishers, Dordrecht, Netherlands 1997.
- 3131 Quinn, P. K., Bates, T. S., Baynard, T., Clarke, A. D., Onasch, T. B., Wang, W., Rood, M. J.,
3132 Andrews, E., Allan, J., Carrico, C. M., Coffman, D., and Worsnop, D.: Impact of particulate
3133 organic matter on the relative humidity dependence of light scattering: A simplified
3134 parameterization, *Geophys. Res. Lett.*, 32, L22809, DOI: 22810.21029/22005GL024322,
3135 2005.
- 3136 Quinn, P. K., Collins, D. B., Grassian, V. H., Prather, K. A., and Bates, T. S.: Chemistry and
3137 Related Properties of Freshly Emitted Sea Spray Aerosol, *Chem. Rev.*, 115, 4383-4399,
3138 2015.
- 3139 Rader, D. J., and McMurry, P. H.: Application of the tandem differential mobility analyzer to
3140 studies of droplet growth or evaporation, *J. Aerosol. Sci.*, 17, 771-787, 1986.
- 3141 Rard, J. A., and Miller, D. G.: Isopiestic determination of the osmotic and activity
3142 coefficients of aqueous magnesium chloride solutions at 25 °C, *J. Chem. Eng. Data*, 26, 38-
3143 43, 1981.
- 3144 Rard, J. A., and Clegg, S. L.: Critical Evaluation of the Thermodynamic Properties of
3145 Aqueous Calcium Chloride. 1. Osmotic and Activity Coefficients of 0–10.77 mol·kg⁻¹
3146 Aqueous Calcium Chloride Solutions at 298.15 K and Correlation with Extended Pitzer Ion-
3147 Interaction Models, *J. Chem. Eng. Data*, 42, 819-849, 1997.
- 3148 Redemann, J., Russell, P. B., and Hamill, P.: Dependence of aerosol light absorption and
3149 single-scattering albedo on ambient relative humidity for sulfate aerosols with black carbon
3150 cores, *J. Geophys. Res.-Atmos.*, 106, 27485-27495, 2001.



- 3151 Reid, J. P., and Sayer, R. M.: Heterogeneous atmospheric aerosol chemistry: laboratory
3152 studies of chemistry on water droplets, *Chem. Soc. Rev.*, 32, 70-79, 2003.
- 3153 Reid, J. P., Meresman, H., Mitchem, L., and Symes, R.: Spectroscopic studies of the size and
3154 composition of single aerosol droplets, *Int. Rev. Phys. Chem.*, 26, 139-192, 2007.
- 3155 Reid, J. P., Bertram, A. K., Topping, D. O., Laskin, A., Martin, S. T., Petters, M. D., Pope, F.
3156 D., and Rovelli, G.: The viscosity of atmospherically relevant organic particles, *Nature*
3157 *Comm.*, 9, 956, DOI: 910.1038/s41467-41018-03027-z, 2018.
- 3158 Renbaum-Wolff, L., Grayson, J. W., Bateman, A. P., Kuwata, M., Sellier, M., Murray, B. J.,
3159 Shilling, J. E., Martin, S. T., and Bertram, A. K.: Viscosity of alpha-pinene secondary organic
3160 material and implications for particle growth and reactivity, *Proc. Natl. Acad. Sci. U. S. A.*,
3161 110, 8014-8019, 2013.
- 3162 Reutter, P., Su, H., Trentmann, J., Simmel, M., Rose, D., Gunthe, S. S., Wernli, H., Andreae,
3163 M. O., and Poschl, U.: Aerosol- and updraft-limited regimes of cloud droplet formation:
3164 influence of particle number, size and hygroscopicity on the activation of cloud condensation
3165 nuclei (CCN), *Atmos. Chem. Phys.*, 9, 7067-7080, 2009.
- 3166 Rissler, J., Pagels, J., Swietlicki, E., Wierzbicka, A., Strand, M., Lillieblad, L., Sanati, M.,
3167 and Bohgard, M.: Hygroscopic behavior of aerosol particles emitted from biomass fired grate
3168 boilers, *Aerosol Sci. Technol.*, 39, 919-930, 2005.
- 3169 Rissler, J., Nordin, E. Z., Eriksson, A. C., Nilsson, P. T., Frosch, M., Sporre, M. K.,
3170 Wierzbicka, A., Svenningsson, B., Londahl, J., Messing, M. E., Sjogren, S., Hemmingsen, J.
3171 G., Loft, S., Pagels, J. H., and Swietlicki, E.: Effective Density and Mixing State of Aerosol
3172 Particles in a Near-Traffic Urban Environment, *Environ. Sci. Technol.*, 48, 6300-6308, 2014.
- 3173 Rkiouak, L., Tang, M. J., Camp, J. C. J., McGregor, J., Watson, I. M., Cox, R. A., Kalberer,
3174 M., Ward, A. D., and Pope, F. D.: Optical trapping and Raman Spectroscopy of solid aerosol
3175 particles, *Phys. Chem. Chem. Phys.*, 16, 11426-11434, 2014.
- 3176 Roberts, G. C., and Nenes, A.: A continuous-flow streamwise thermal-gradient CCN
3177 chamber for atmospheric measurements, *Aerosol Sci. Technol.*, 39, 206-221, 2005.
- 3178 Robinson, C. B., Schill, G. P., Zarzana, K. J., and Tolbert, M. A.: Impact of Organic Coating
3179 on Optical Growth of Ammonium Sulfate Particles, *Environ. Sci. Technol.*, 47, 13339-13346,
3180 2013.
- 3181 Robinson, C. B., Schill, G. P., and Tolbert, M. A.: Optical growth of highly viscous
3182 organic/sulfate particles, *J. Atmos. Chem.*, 71, 145-156, 2014.
- 3183 Robinson, R. J., and Yu, C. P.: Theoretical analysis of hygroscopic growth rate of
3184 mainstream and sidestream cigarette smoke particles in the human respiratory tract, *Aerosol*
3185 *Sci. Technol.*, 28, 21-32, 1998.
- 3186 Rodahl, M., and Kasemo, B.: On the measurement of thin liquid overlayers with the quartz-
3187 crystal microbalance, *Sensors and Actuators*, 54, 448-456, 1996.
- 3188 Rogaski, C. A., Golden, D. M., and Williams, L. R.: Reactive uptake and hydration
3189 experiments on amorphous carbon treated with NO₂, SO₂, O₃, HNO₃, and H₂SO₄,
3190 *Geophys. Res. Lett.*, 24, 381-384, 1997.
- 3191 Rogers, C. F., Watson, J. G., Day, D., and Oraltay, R. G.: Real-time liquid water mass
3192 measurement for airborne particulates, *Aerosol Sci. Technol.*, 29, 557-562, 1998.
- 3193 Rood, M. J., Larson, T. V., Covert, D. S., and Ahlquist, N. C.: Measurement of laboratory
3194 and ambient aerosols with temperature and humidity controlled nephelometry, *Atmos.*
3195 *Environ.*, 19, 1181-1190, 1985.
- 3196 Rosenberger, T., Münzer, A., Kiesler, D., Wiggers, H., and Krus, F. E.: Ejector-based
3197 sampling from low-pressure aerosol reactors, *J. Aerosol. Sci.*, 123, 105-115, 2018.
- 3198 Rubasinghege, G., and Grassian, V. H.: Role(s) of Adsorbed Water in the Surface Chemistry
3199 of Environmental Interfaces, *Chem. Commun.*, 49, 3071-3094, 2013.



- 3200 Russell, L. M., Bahadur, R., and Ziemann, P. J.: Identifying organic aerosol sources by
3201 comparing functional group composition in chamber and atmospheric particles, Proc. Natl.
3202 Acad. Sci. U.S.A., 108, 3516-3521, 2011.
- 3203 Sadeghi, R., and Shahebrahimi, Y.: Vapor–Liquid Equilibria of Aqueous Polymer Solutions
3204 from Vapor-Pressure Osmometry and Isopiestic Measurements, J. Chem. Eng. Dara, 56, 789-
3205 799, 2011.
- 3206 Salcedo, D.: Equilibrium Phase Diagrams of Aqueous Mixtures of Malonic Acid and
3207 Sulfate/Ammonium Salts, J. Phys. Chem. A, 110, 12158-12165, 2006.
- 3208 Salmeron, M., and Schlogl, R.: Ambient pressure photoelectron spectroscopy: A new tool for
3209 surface science and nanotechnology, Surface Science Reports, 63, 169-199, 2008.
- 3210 Santarpia, J. L., Li, R., and Collins, D. R.: Direct measurement of the hydration state of
3211 ambient aerosol populations, J. Geophys. Res.-Atmos, 109, doi:10.1029/2004JD004653,
3212 2004.
- 3213 Sarangi, B., Ramachandran, S., Rajesh, T. A., and Dhaker, V. K.: Black carbon linked
3214 aerosol hygroscopic growth: Size and mixing state are crucial, Atmos. Environ., 200, 110-
3215 118, 2019.
- 3216 Sauerbrey, G.: VERWENDUNG VON SCHWINGQUARZEN ZUR WAGUNG DUNNER
3217 SCHICHTEN UND ZUR MIKROWAGUNG, Zeitschrift Fur Physik, 155, 206-222, 1959.
- 3218 Schenk, J., Panne, U., and Albrecht, M.: Interaction of Levitated Ionic Liquid Droplets with
3219 Water, J. Phys. Chem. B, 116, 14171-14177, 2012.
- 3220 Schilling, C., and Winterer, M.: Preserving Particle Characteristics at Increasing Production
3221 Rate of ZnO Nanoparticles by Chemical Vapor Synthesis, Chemical Vapor Deposition, 20,
3222 138-145, 2014.
- 3223 Schindelholz, E., Risteen, B. E., and Kelly, R. G.: Effect of Relative Humidity on Corrosion
3224 of Steel under Sea Salt Aerosol Proxies: II. MgCl₂, Artificial Seawater, Journal of the
3225 Electrochemical Society, 161, C460-C470, 2014a.
- 3226 Schindelholz, E., Risteen, B. E., and Kelly, R. G.: Effect of Relative Humidity on Corrosion
3227 of Steel under Sea Salt Aerosol Proxies: I. NaCl, Journal of the Electrochemical Society, 161,
3228 C450-C459, 2014b.
- 3229 Schindelholz, E., Tsui, L. K., and Kelly, R. G.: Hygroscopic Particle Behavior Studied by
3230 Interdigitated Array Microelectrode Impedance Sensors, J. Phys. Chem. A, 118, 167-177,
3231 2014c.
- 3232 Schladitz, A., Müller, Thomas, Nowak, A., Kandler, K., Lieke, K., Massling, A., and
3233 Wiedensohler, A.: In situ aerosol characterization at Cape Verde. Part I: particle number size
3234 distributions, hygroscopic growth and state of mixing of the marine and Saharan dust aerosol,
3235 Tellus B, 63, 531-548, 2011.
- 3236 Schmid, O., Artaxo, P., Arnott, W. P., Chand, D., Gatti, L. V., Frank, G. P., Hoffer, A.,
3237 Schnaiter, M., and Andreae, M. O.: Spectral light absorption by ambient aerosols influenced
3238 by biomass burning in the Amazon Basin. I: Comparison and field calibration of absorption
3239 measurement techniques, Atmos. Chem. Phys., 6, 3443-3462, 2006.
- 3240 Schroeder, J. R., and Beyer, K. D.: Deliquescence Relative Humidities of Organic and
3241 Inorganic Salts Important in the Atmosphere, J. Phys. Chem. A, 120, 9948-9957, 2016.
- 3242 Schurman, M. I., Kim, J. Y., Cheung, H. H. Y., and Chan, C. K.: Atmospheric particle
3243 composition-hygroscopic growth measurements using an in-series hybrid tandem differential
3244 mobility analyzer and aerosol mass spectrometer, Aerosol Sci. Technol., 51, 694-703, 2017.
- 3245 Schuster, G. L., Lin, B., and Dubovik, O.: Remote sensing of aerosol water uptake, Geophys.
3246 Res. Lett., 36, L03814, DOI: 03810.01029/02008GL036576, 2009.
- 3247 Schuttlefield, J., Al-Hosney, H., Zachariah, A., and Grassian, V. H.: Attenuated Total
3248 Reflection Fourier Transform Infrared Spectroscopy to Investigate Water Uptake and Phase
3249 Transitions in Atmospherically Relevant Particles, Appl. Spectrosc., 61, 283-292, 2007a.



- 3250 Schuttlefield, J. D., Cox, D., and Grassian, V. H.: An investigation of water uptake on clays
3251 minerals using ATR-FTIR spectroscopy coupled with quartz crystal microbalance
3252 measurements, *J. Geophys. Res.-Atmos.*, 112, D21303, doi: 21310.21029/22007JD008973,
3253 2007b.
- 3254 Schwarz, J. P., Gao, R. S., Spackman, J. R., Watts, L. A., Thomson, D. S., Fahey, D. W.,
3255 Ryerson, T. B., Peischl, J., Holloway, J. S., Trainer, M., Frost, G. J., Baynard, T., Lack, D.
3256 A., de Gouw, J. A., Warneke, C., and Del Negro, L. A.: Measurement of the mixing state,
3257 mass, and optical size of individual black carbon particles in urban and biomass burning
3258 emissions, *Geophys. Res. Lett.*, 35, L13810, DOI: 13810.11029/12008GL033968, 2008.
- 3259 Schwarz, J. P., Spackman, J. R., Gao, R. S., Watts, L. A., Stier, P., Schulz, M., Davis, S. M.,
3260 Wofsy, S. C., and Fahey, D. W.: Global-scale black carbon profiles observed in the remote
3261 atmosphere and compared to models, *Geophys. Res. Lett.*, 37, L18812, DOI:
3262 18810.11029/12010GL044372, 2010.
- 3263 Schwarz, J. P., Perring, A. E., Markovic, M. Z., Gao, R. S., Ohata, S., Langridge, J., Law, D.,
3264 McLaughlin, R., and Fahey, D. W.: Technique and theoretical approach for quantifying the
3265 hygroscopicity of black-carbon-containing aerosol using a single particle soot photometer, *J.*
3266 *Aerosol. Sci.*, 81, 110-126, 2015.
- 3267 Sedlacek, A., and Lee, J.: Photothermal interferometric aerosol absorption spectrometry,
3268 *Aerosol Sci. Technol.*, 41, 1089-1101, 2007.
- 3269 Seinfeld, J. H., and Pandis, S. N.: *Atmospheric Chemistry and Physics: From Air Pollution to*
3270 *Climate Change (Third edition)*, Wiley Interscience, New York, 2016.
- 3271 Seisel, S., Lian, Y., Keil, T., Trukhin, M. E., and Zellner, R.: Kinetics of the interaction of
3272 water vapour with mineral dust and soot surfaces at T=298 K, *Phys. Chem. Chem. Phys.*, 6,
3273 1926-1932, 2004.
- 3274 Seisel, S., Pashkova, A., Lian, Y., and Zellner, R.: Water uptake on mineral dust and soot: A
3275 fundamental view of the hydrophilicity of atmospheric particles?, *Faraday Discuss.*, 130,
3276 437-451, 2005.
- 3277 Semeniuk, T. A., Wise, M. E., Martin, S. T., Russell, L. M., and Buseck, P. R.: Hygroscopic
3278 behavior of aerosol particles from biomass fires using environmental transmission electron
3279 microscopy, *J. Atmos. Chem.*, 56, 259-273, 2007a.
- 3280 Semeniuk, T. A., Wise, M. E., Martin, S. T., Russell, L. M., and Buseck, P. R.: Water uptake
3281 characteristics of individual atmospheric particles having coatings, *Atmos. Environ.*, 41,
3282 6225-6235, 2007b.
- 3283 Shi, Z., Zhang, D., Hayashi, M., Ogata, H., Ji, H., and Fujie, W.: Influences of sulfate and
3284 nitrate on the hygroscopic behaviour of coarse dust particles, *Atmos. Environ.*, 42, 822-827,
3285 2008.
- 3286 Shiraiwa, M., Ammann, M., Koop, T., and Pöschl, U.: Gas uptake and chemical aging of
3287 semisolid organic aerosol particles, *Proc. Natl. Acad. Sci. U. S. A.*, 108, 11003-11008, 2011.
- 3288 Shiraiwa, M., Li, Y., Tsimpidi, A. P., Karydis, V. A., Berkemeier, T., Pandis, S. N.,
3289 Lelieveld, J., Koop, T., and Pöschl, U.: Global distribution of particle phase state in
3290 atmospheric secondary organic aerosols, *Nature Communications*, 8, 15002,
3291 10.1038/ncomms15002, 2017a.
- 3292 Shiraiwa, M., Ueda, K., Pozzer, A., Lammel, G., Kampf, C. J., Fushimi, A., Enami, S.,
3293 Arangio, A. M., Frohlich-Nowoisky, J., Fujitani, Y., Furuyama, A., Lakey, P. S. J., Lelieveld,
3294 J., Lucas, K., Morino, Y., Pöschl, U., Takaharna, S., Takami, A., Tong, H. J., Weber, B.,
3295 Yoshino, A., and Sato, K.: Aerosol Health Effects from Molecular to Global Scales, *Environ.*
3296 *Sci. Technol.*, 51, 13545-13567, 2017b.
- 3297 Slowik, J. G., Cross, E. S., Han, J. H., Davidovits, P., Onasch, T. B., Jayne, J. T., Williams,
3298 L. R., Canagaratna, M. R., Worsnop, D. R., Chakrabarty, R. K., Moosmuller, H., Arnott, W.
3299 P., Schwarz, J. P., Gao, R. S., Fahey, D. W., Kok, G. L., and Petzold, A.: An inter-



- 3300 comparison of instruments measuring black carbon content of soot particles, *Aerosol Sci.*
3301 *Technol.*, 41, 295-314, 2007.
- 3302 Snider, J. R., and Petters, M. D.: Optical particle counter measurement of marine aerosol
3303 hygroscopic growth, *Atmos. Chem. Phys.*, 8, 1949-1962, 2008.
- 3304 Sobanski, N., Schuladen, J., Schuster, G., Lelieveld, J., and Crowley, J. N.: A five-channel
3305 cavity ring-down spectrometer for the detection of NO₂, NO₃, N₂O₅, total peroxy nitrates
3306 and total alkyl nitrates, *Atmos. Meas. Tech.*, 9, 5103-5118, 2016.
- 3307 Solomon, P. A., and Sioutas, C.: Continuous and semicontinuous monitoring techniques for
3308 particulate matter mass and chemical components: A synthesis of findings from EPA's
3309 particulate matter supersites program and related studies, *J. Air Waste Manage. Assoc.*, 58,
3310 164-195, 2008.
- 3311 Song, M. J., Liu, P. F., Martin, S. T., and Bertram, A. K.: Liquid-liquid phase separation in
3312 particles containing secondary organic material free of inorganic salts, *Atmos. Chem. Phys.*,
3313 17, 11261-11271, 2017.
- 3314 Song, M. J., Ham, S., Andrews, R. J., You, Y., and Bertram, A. K.: Liquid-liquid phase
3315 separation in organic particles containing one and two organic species: importance of the
3316 average O: C, *Atmos. Chem. Phys.*, 18, 12075-12084, 2018.
- 3317 Song, X. W., and Boily, J. F.: Water Vapor Adsorption on Goethite, *Environ. Sci. Technol.*,
3318 47, 7171-7177, 2013.
- 3319 Song, Y. C., Haddrell, A. E., Bzdek, B. R., Reid, J. P., Bannan, T., Topping, D. O., Percival,
3320 C., and Cai, C.: Measurements and Predictions of Binary Component Aerosol Particle
3321 Viscosity, *J. Phys. Chem. A*, 120, 8123-8137, 2016.
- 3322 Sorooshian, A., Hersey, S., Brechtel, F. J., Corless, A., Flagan, R. C., and Seinfeld, J. H.:
3323 Rapid, size-resolved aerosol hygroscopic growth measurements: Differential aerosol sizing
3324 and hygroscopicity spectrometer probe (DASH-SP), *Aerosol Sci. Technol.*, 42, 445-464,
3325 2008.
- 3326 Sorooshian, A., Shingler, T., Crosbie, E., Barth, M. C., Homeyer, C. R., Campuzano-Jost, P.,
3327 Day, D. A., Jimenez, J. L., Thornhill, K. L., Ziemba, L. D., Blake, D. R., and Fried, A.:
3328 Contrasting aerosol refractive index and hygroscopicity in the inflow and outflow of deep
3329 convective storms: Analysis of airborne data from DC3, *J. Geophys. Res.-Atmos.*, 122, 4565-
3330 4577, 2017.
- 3331 Spedding, F. H., Weber, H. O., Saeger, V. W., Petheram, H. H., Rard, J. A., and
3332 Habenschuss, A.: Isopiestic determination of the activity coefficients of some aqueous rare
3333 earth electrolyte solutions at 25 °C. 1. The rare earth chlorides, *J. Chem. Eng. Data*, 21, 341-
3334 360, 1976.
- 3335 Speer, R. E., Barnes, H. M., and Brown, R.: An instrument for measuring the liquid water
3336 content of aerosols, *Aerosol Sci. Technol.*, 27, 50-61, 1997.
- 3337 Spesyvtseva, S. E. S., and Dholakia, K.: Trapping in a Material World, *ACS Photonics*, 3,
3338 719-736, 2016.
- 3339 Steimer, S. S., Krieger, U. K., Te, Y. F., Lienhard, D. M., Huisman, A. J., Luo, B. P.,
3340 Ammann, M., and Peter, T.: Electrodynamic balance measurements of thermodynamic,
3341 kinetic, and optical aerosol properties inaccessible to bulk methods, *Atmos. Meas. Tech.*, 8,
3342 2397-2408, 2015.
- 3343 Stokes, R. H., and Robinson, R. A.: Ionic Hydration and Activity in Electrolyte Solutions, *J.*
3344 *Am. Chem. Soc.*, 70, 1870-1878, 1948.
- 3345 Stratmann, F., Kiselev, A., Wurzler, S., Wendisch, M., Heintzenberg, J., Charlson, R. J.,
3346 Diehl, K., Wex, H., and Schmidt, S.: Laboratory Studies and Numerical Simulations of Cloud
3347 Droplet Formation under Realistic Supersaturation Conditions, *J. Atmos. Ocean. Technol.*,
3348 21, 876-887, 2004.



- 3349 Su, H., Rose, D., Cheng, Y. F., Gunthe, S. S., Massling, A., Stock, M., Wiedensohler, A.,
3350 Andreae, M. O., and Poschl, U.: Hygroscopicity distribution concept for measurement data
3351 analysis and modeling of aerosol particle mixing state with regard to hygroscopic growth and
3352 CCN activation, *Atmos. Chem. Phys.*, 10, 7489-7503, 2010.
- 3353 Swietlicki, E., Zhou, J. C., Berg, O. H., Martinsson, B. G., Frank, G., Cederfelt, S. I., Dusek,
3354 U., Berner, A., Birmili, W., Wiedensohler, A., Yuskiewicz, B., and Bower, K. N.: A closure
3355 study of sub-micrometer aerosol particle hygroscopic behaviour, *Atmos. Res.*, 50, 205-240,
3356 1999.
- 3357 Swietlicki, E., Hansson, H. C., Hameri, K., Svenningsson, B., Massling, A., McFiggans, G.,
3358 McMurry, P. H., Petaja, T., Tunved, P., Gysel, M., Topping, D., Weingartner, E.,
3359 Baltensperger, U., Rissler, J., Wiedensohler, A., and Kulmala, M.: Hygroscopic properties of
3360 submicrometer atmospheric aerosol particles measured with H-TDMA instruments in various
3361 environments - a review, *Tellus Ser. B-Chem. Phys. Meteorol.*, 60, 432-469, 2008.
- 3362 Tabazadeh, A., and Toon, O. B.: The role of ammoniated aerosols in cirrus cloud nucleation,
3363 *Geophys. Res. Lett.*, 25, 1379-1382, 1998.
- 3364 Takahama, S., Johnson, A., and Russell, L. M.: Quantification of Carboxylic and Carbonyl
3365 Functional Groups in Organic Aerosol Infrared Absorbance Spectra, *Aerosol Sci. Technol.*,
3366 47, 310-325, 2013.
- 3367 Takahama, S., Ruggieri, G., and Dillner, A. M.: Analysis of functional groups in atmospheric
3368 aerosols by infrared spectroscopy: sparse methods for statistical selection of relevant
3369 absorption bands, *Atmos. Meas. Tech.*, 9, 3429-3454, 2016.
- 3370 Takahama, S., Dillner, A. M., Weakley, A. T., Reggante, M., Burki, C., Lbadaoui-Darvas,
3371 M., Debus, B., Kuzmiakova, A., and Wexler, A. S.: Atmospheric particulate matter
3372 characterization by Fourier transform infrared spectroscopy: a review of statistical calibration
3373 strategies for carbonaceous aerosol quantification in US measurement networks, *Atmos.*
3374 *Meas. Tech.*, 12, 525-567, 2019.
- 3375 Tan, F., Tong, S. R., Jing, B., Hou, S., Liu, Q., Li, K., Zhang, Y., and Ge, M. F.:
3376 Heterogeneous reactions of NO₂ with CaCO₃-(NH₄)₂SO₄ mixtures at different relative
3377 humidities, *Atmos. Chem. Phys.*, 16, 8081-8093, 2016.
- 3378 Tang, I. N., and Munkelwitz, H. R.: Water activities, densities, and refractive indices of
3379 aqueous sulfates and sodium nitrate droplets of atmospheric importance, *J. Geophys. Res.-*
3380 *Atmos.*, 99, 18801-18808, 1994.
- 3381 Tang, I. N., Fung, K. H., Imre, D. G., and Munkelwitz, H. R.: Phase transformation and
3382 metastability of hygroscopic microparticles, *Aerosol Sci. Technol.*, 23, 443-453, 1995.
- 3383 Tang, I. N.: Thermodynamic and optical properties of mixed-salt aerosols of atmospheric
3384 importance, *J. Geophys. Res.-Atmos.*, 102, 1883-1893, 1997.
- 3385 Tang, I. N., and Fung, K. H.: Hydration and Raman scattering studies of levitated
3386 microparticles: Ba(NO₃)₂, Sr(NO₃)₂, and Ca(NO₃)₂, *J. Chem. Phys.*, 106, 1653-1660, 1997.
- 3387 Tang, I. N., Tridico, A. C., and Fung, K. H.: Thermodynamic and optical properties of sea
3388 salt aerosols, *J. Geophys. Res.-Atmos.*, 102, 23269-23275, 1997.
- 3389 Tang, M. J., Camp, J. C. J., Rkiouak, L., McGregor, J., Watson, I. M., Cox, R. A., Kalberer,
3390 M., Ward, A. D., and Pope, F. D.: Heterogeneous Interaction of SiO₂ with N₂O₅: Aerosol
3391 Flow Tube and Single Particle Optical Levitation-Raman Spectroscopy Studies, *J. Phys.*
3392 *Chem. A*, 118, 8817-8827, 2014.
- 3393 Tang, M. J., Cziczko, D. J., and Grassian, V. H.: Interactions of Water with Mineral Dust
3394 Aerosol: Water Adsorption, Hygroscopicity, Cloud Condensation and Ice Nucleation, *Chem.*
3395 *Rev.*, 116, 4205-4259, 2016a.
- 3396 Tang, M. J., Larish, W., Fang, Y., Gankanda, A., and Grassian, V. H.: Heterogeneous
3397 Reactions of Acetic Acid with Oxide Surfaces: Effects of Mineralogy and Relative Humidity,
3398 *J. Phys. Chem. A*, 120, 5609-5616, 2016b.



- 3399 Tang, M. J., Huang, X., Lu, K. D., Ge, M. F., Li, Y. J., Cheng, P., Zhu, T., Ding, A. J.,
3400 Zhang, Y. H., Gligorovski, S., Song, W., Ding, X., Bi, X. H., and Wang, X. M.:
3401 Heterogeneous reactions of mineral dust aerosol: implications for tropospheric oxidation
3402 capacity, *Atmos. Chem. Phys.*, 17, 11727-11777, 2017.
- 3403 Tang, M. J., Chen, J., and Wu, Z. J.: Ice nucleating particles in the troposphere: Progresses,
3404 challenges and opportunities, *Atmos. Environ.*, 192, 206-208, 2018.
- 3405 Tang, M. J., Gu, W. J., Ma, Q. X., Li, Y. J., Zhong, C., Li, S., Yin, X., Huang, R. J., He, H.,
3406 and Wang, X. M.: Water adsorption and hygroscopic growth of six anemophilous pollen
3407 species: the effect of temperature, *Atmos. Chem. Phys.*, 19, 2247-2258, 2019.
- 3408 Thomas, E., Rudich, Y., Trakhtenberg, S., and Ussyshkin, R.: Water adsorption by
3409 hydrophobic organic surfaces: Experimental evidence and implications to the atmospheric
3410 properties of organic aerosols, *J. Geophys. Res.-Atmos.*, 104, 16053-16059, 1999.
- 3411 Thomas, S., Cole, M., Villa-Lopez, F. H., and Gardner, J. W.: High frequency surface
3412 acoustic wave resonator-based sensor for particulate matter detection, *Sens. Actuators, A*,
3413 244, 138-145, 2016.
- 3414 Titos, G., Cazorla, A., Zieger, P., Andrews, E., Lyamani, H., Granados-Munoz, M. J., Olmo,
3415 F. J., and Alados-Arboledas, L.: Effect of hygroscopic growth on the aerosol light-scattering
3416 coefficient: A review of measurements, techniques and error sources, *Atmos. Environ.*, 141,
3417 494-507, 2016.
- 3418 Tobo, Y., Zhang, D., Matsuki, A., and Iwasaka, Y.: Asian Dust Particles Converted into
3419 Aqueous Droplets under Remote Marine Atmospheric Conditions, *Proc. Natl. Acad. Sci. U.*
3420 *S. A.*, 107, 17905-17910, 2010.
- 3421 Tobo, Y., DeMott, P. J., Raddatz, M., Niedermeier, D., Hartmann, S., Kreidenweis, S. M.,
3422 Stratmann, F., and Wex, H.: Impacts of chemical reactivity on ice nucleation of kaolinite
3423 particles: A case study of levoglucosan and sulfuric acid, *Geophys. Res. Lett.*, 39, L19803,
3424 doi: 19810.11029/12012gl053007, 2012.
- 3425 Tong, H. H. Y., Chow, A. S. F., Chan, H. M., Chow, A. H. L., Wan, Y. K. Y., Williams, I.
3426 D., Shek, F. L. Y., and Chan, C. K.: Process-Induced Phase Transformation of Berberine
3427 Chloride Hydrates, *J. Pharm. Sci.*, 99, 1942-1954, 2010a.
- 3428 Tong, H. J., Reid, J. P., Dong, J. L., and Zhang, Y. H.: Observation of the Crystallization and
3429 Supersaturation of Mixed Component NaNO₃-Na₂SO₄ Droplets by FTIR-ATR and Raman
3430 Spectroscopy, *J. Phys. Chem. A*, 114, 12237-12243, 2010b.
- 3431 Tong, H. J., Reid, J. P., Bones, D. L., Luo, B. P., and Krieger, U. K.: Measurements of the
3432 timescales for the mass transfer of water in glassy aerosol at low relative humidity and
3433 ambient temperature, *Atmos. Chem. Phys.*, 11, 4739-4754, 2011.
- 3434 Tong, H. J., Ouyang, B., Nikolovski, N., Lienhard, D. M., Pope, F. D., and Kalberer, M.: A
3435 new electrodynamic balance (EDB) design for low-temperature studies: application to
3436 immersion freezing of pollen extract bioaerosols, *Atmos. Meas. Tech.*, 8, 1183-1195, 2015.
- 3437 Torrent, J., Barron, V., and Schwertmann, U.: Phosphate Adsorption and Desorption by
3438 Goethites Differing in Crystal Morphology, *Soil Science Society of America Journal*, 54,
3439 1007-1012, 1990.
- 3440 Treuel, L., Butler, J. R., Hargreaves, G., and Reid, J. P.: Probing the Equilibrium Size and
3441 Hydrogen Bonding Structure in Aqueous Aerosol Droplets, *Zeitschrift Fur Physikalische
3442 Chemie-International Journal of Research in Physical Chemistry & Chemical Physics*, 224,
3443 1185-1204, 2010.
- 3444 Tritscher, T., Juranyi, Z., Martin, M., Chirico, R., Gysel, M., Heringa, M. F., DeCarlo, P. F.,
3445 Sierau, B., Prevot, A. S. H., Weingartner, E., and Baltensperger, U.: Changes of
3446 hygroscopicity and morphology during ageing of diesel soot, *Environ. Res. Lett.*, 6,
3447 10.1088/1748-9326/6/3/034026, 2011.



- 3448 Trunk, M., Lubben, J. F., Popp, J., Schrader, B., and Kiefer, W.: Investigation of a phase
3449 transition in a single optically levitated microdroplet by Raman-Mie scattering, *Appl. Optics*,
3450 36, 3305-3309, 1997.
- 3451 Tsionsky, V., and Gileadi, E.: Use of the Quartz Crystal Microbalance for the Study of
3452 Adsorption from the Gas Phase, *Langmuir*, 10, 2830-2835, 1994.
- 3453 Twomey, S.: The identification of individual hygroscopic particles in the atmosphere by a
3454 phase-transition method, *J. Appl. Phys.*, 24, 1099-1102, 1953.
- 3455 Twomey, S.: The composition of hygroscopic particles in the atmosphere, *Journal of*
3456 *Meteorology*, 11, 334-338, 1954.
- 3457 Vainio, E., Kinnunen, H., Lauren, T., Brink, A., Yrjas, P., DeMartini, N., and Hupa, M.:
3458 Low-temperature corrosion in co-combustion of biomass and solid recovered fuels, *Fuel*, 184,
3459 957-965, 2016.
- 3460 Vali, G., DeMott, P. J., Möhler, O., and Whale, T. F.: Technical Note: A proposal for ice
3461 nucleation terminology, *Atmos. Chem. Phys.*, 15, 10263-10270, 2015.
- 3462 Varma, R. M., Ball, S. M., Brauers, T., Dorn, H. P., Heitmann, U., Jones, R. L., Platt, U.,
3463 Pohler, D., Ruth, A. A., Shillings, A. J. L., Thieser, J., Wahner, A., and Venables, D. S.:
3464 Light extinction by secondary organic aerosol: an intercomparison of three broadband cavity
3465 spectrometers, *Atmos. Meas. Tech.*, 6, 3115-3130, 2013.
- 3466 Veghte, D. P., Bittner, D. R., and Freedman, M. A.: Cryo-Transmission Electron Microscopy
3467 Imaging of the Morphology of Submicrometer Aerosol Containing Organic Acids and
3468 Ammonium Sulfate, *Anal. Chem.*, 86, 2436-2442, 2014.
- 3469 Virtanen, A., Joutsensaari, J., Koop, T., Kannosto, J., Yli-Pirila, P., Leskinen, J., Makela, J.
3470 M., Holopainen, J. K., Poschl, U., Kulmala, M., Worsnop, D. R., and Laaksonen, A.: An
3471 amorphous solid state of biogenic secondary organic aerosol particles, *Nature*, 467, 824-827,
3472 2010.
- 3473 Vittorias, E., Kappl, M., Butt, H. J., and Johannsmann, D.: Studying mechanical
3474 microcontacts of fine particles with the quartz crystal microbalance, *Powder Technology*,
3475 203, 489-502, 2010.
- 3476 Vlasenko, A., Sjogren, S., Weingartner, E., Gaggeler, H. W., and Ammann, M.: Generation
3477 of submicron Arizona test dust aerosol: Chemical and hygroscopic properties, *Aerosol Sci.*
3478 *Technol.*, 39, 452-460, 2005.
- 3479 Vlasenko, S. S., Su, H., Pöschl, U., Andreae, M. O., and Mikhailov, E. F.: Tandem
3480 configuration of differential mobility and centrifugal particle mass analysers for investigating
3481 aerosol hygroscopic properties, *Atmos. Meas. Tech.*, 10, 1269-1280, 2017.
- 3482 Wagner, C., Hanisch, F., Holmes, N., de Coninck, H., Schuster, G., and Crowley, J. N.: The
3483 interaction of N₂O₅ with mineral dust: aerosol flow tube and Knudsen reactor studies, *Atmos.*
3484 *Chem. Phys.*, 8, 91-109, 2008.
- 3485 Walker, J. S., Wills, J. B., Reid, J. P., Wang, L. Y., Topping, D. O., Butler, J. R., and Zhang,
3486 Y. H.: Direct Comparison of the Hygroscopic Properties of Ammonium Sulfate and Sodium
3487 Chloride Aerosol at Relative Humidities Approaching Saturation, *J. Phys. Chem. A*, 114,
3488 12682-12691, 2010.
- 3489 Wang, F., Zhang, Y. H., Li, S. H., Wang, L. Y., and Zhao, L. J.: A strategy for single
3490 supersaturated droplet analysis: Confocal Raman investigations on the complicated
3491 hygroscopic properties of individual MgSO₄ droplets on the quartz substrate, *Analytical*
3492 *Chemistry*, 77, 7148-7155, 2005.
- 3493 Wang, G. H., Zhang, R. Y., Gomez, M. E., Yang, L. X., Zamora, M. L., Hu, M., Lin, Y.,
3494 Peng, J. F., Guo, S., Meng, J. J., Li, J. J., Cheng, C. L., Hu, T. F., Ren, Y. Q., Wang, Y. S.,
3495 Gao, J., Cao, J. J., An, Z. S., Zhou, W. J., Li, G. H., Wang, J. Y., Tian, P. F., Marrero-Ortiz,
3496 W., Secrest, J., Du, Z. F., Zheng, J., Shang, D. J., Zeng, L. M., Shao, M., Wang, W. G.,
3497 Huang, Y., Wang, Y., Zhu, Y. J., Li, Y. X., Hu, J. X., Pan, B., Cai, L., Cheng, Y. T., Ji, Y.



- 3498 M., Zhang, F., Rosenfeld, D., Liss, P. S., Duce, R. A., Kolb, C. E., and Molina, M. J.:
3499 Persistent sulfate formation from London Fog to Chinese haze, *Proc. Natl. Acad. Sci. U. S.*
3500 *A.*, 113, 13630-13635, 2016.
- 3501 Wang, H. C., Chen, J., and Lu, K. D.: Development of a portable cavity-enhanced absorption
3502 spectrometer for the measurement of ambient NO₃ and N₂O₅: experimental setup, lab
3503 characterizations, and field applications in a polluted urban environment, *Atmos. Meas.*
3504 *Tech.*, 10, 1465-1479, 2017a.
- 3505 Wang, L., Huang, D. D., Chan, C. K., Li, Y. J., and Xu, X. J. G.: Nanoscale spectroscopic
3506 and mechanical characterization of individual aerosol particles using peak force infrared
3507 microscopy, *Chem. Commun.*, 53, 7397-7400, 2017b.
- 3508 Wang, Q. Q., Jacob, D. J., Spackman, J. R., Perring, A. E., Schwarz, J. P., Moteki, N.,
3509 Marais, E. A., Ge, C., Wang, J., and Barrett, S. R. H.: Global budget and radiative forcing of
3510 black carbon aerosol: Constraints from pole-to-pole (HIPPO) observations across the Pacific,
3511 *J. Geophys. Res.-Atmos.*, 119, 195-206, 2014a.
- 3512 Wang, X., Ye, X., Chen, H., Chen, J., Yang, X., and Gross, D. S.: Online hygroscopicity and
3513 chemical measurement of urban aerosol in Shanghai, China, *Atmos. Environ.*, 95, 318-326,
3514 2014b.
- 3515 Wang, X. M., Ye, X. N., Chen, H., Chen, J. M., Yang, X., and Gross, D. S.: Online
3516 hygroscopicity and chemical measurement of urban aerosol in Shanghai, China, *Atmos.*
3517 *Environ.*, 95, 318-326, 2014c.
- 3518 Ward, A. D., Zhang, M., and Hunt, O.: Broadband Mie scattering from optically levitated
3519 aerosol droplets using a white LED, *Optics Express*, 16, 16390-16403, 2008.
- 3520 Washenfelder, R. A., Flores, J. M., Brock, C. A., Brown, S. S., and Rudich, Y.: Broadband
3521 measurements of aerosol extinction in the ultraviolet spectral region, *Atmos. Meas. Tech.*, 6,
3522 861-877, 2013.
- 3523 Washenfelder, R. A., Attwood, A. R., Flores, J. M., Zarzana, K. J., Rudich, Y., and Brown, S.
3524 S.: Broadband cavity-enhanced absorption spectroscopy in the ultraviolet spectral region for
3525 measurements of nitrogen dioxide and formaldehyde, *Atmos. Meas. Tech.*, 9, 41-52, 2016.
- 3526 Wasisto, H. S., Uhde, E., and Peiner, E.: Enhanced performance of pocket-sized nanoparticle
3527 exposure monitor for healthy indoor environment, *Build. Environ.*, 95, 13-20, 2016.
- 3528 Weingartner, E., Burtscher, H., and Baltensperger, U.: Hygroscopic properties of carbon and
3529 diesel soot particles, *Atmos. Environ.*, 31, 2311-2327, 1997.
- 3530 Weingartner, E., Gysel, M., and Baltensperger, U.: Hygroscopicity of Aerosol Particles at
3531 Low Temperatures. 1. New Low-Temperature H-TDMA Instrument: Setup and First
3532 Applications, *Environ. Sci. Technol.*, 36, 55-62, 2002.
- 3533 Wendt, S., Matthiesen, J., Schaub, R., Vestergaard, E. K., Laegsgaard, E., Besenbacher, F.,
3534 and Hammer, B.: Formation and splitting of paired hydroxyl groups on reduced TiO₂(110),
3535 *Phys. Rev. Lett.*, 96, 066107, DOI: 10.1103/PhysRevLett.066107, 2006.
- 3536 Wex, H., Kiselev, A., Stratmann, F., Zoboki, J., and Brechtel, F.: Measured and modeled
3537 equilibrium sizes of NaCl and (NH₄)₂SO₄ particles at relative humidities up to 99.1%, *J.*
3538 *Geophys. Res.-Atmos.*, 110, doi:10.1029/2004JD005507, 2005.
- 3539 Wex, H., Petters, M. D., Carrico, C. M., Hallbauer, E., Massling, A., McMeeking, G. R.,
3540 Poulain, L., Wu, Z., Kreidenweis, S. M., and Stratmann, F.: Towards closing the gap between
3541 hygroscopic growth and activation for secondary organic aerosol: Part 1 – Evidence from
3542 measurements, *Atmos. Chem. Phys.*, 9, 3987-3997, 2009a.
- 3543 Wex, H., Petters, M. D., Carrico, C. M., Hallbauer, E., Massling, A., McMeeking, G. R.,
3544 Poulain, L., Wu, Z., Kreidenweis, S. M., and Stratmann, F.: Towards closing the gap between
3545 hygroscopic growth and activation for secondary organic aerosol: Part 1-Evidence from
3546 measurements, *Atmos. Chem. Phys.*, 9, 3987-3997, 2009b.



- 3547 Wex, H., Augustin-Bauditz, S., Boose, Y., Budke, C., Curtius, J., Diehl, K., Dreyer, A.,
3548 Frank, F., Hartmann, S., Hiranuma, N., Jantsch, E., Kanji, Z. A., Kiselev, A., Koop, T.,
3549 Mohler, O., Niedermeier, D., Nillius, B., Rosch, M., Rose, D., Schmidt, C., Steinke, I., and
3550 Stratmann, F.: Intercomparing different devices for the investigation of ice nucleating
3551 particles using Snomax (R) as test substance, *Atmos. Chem. Phys.*, 15, 1463-1485, 2015.
3552 Whitehead, J. D., Irwin, M., Allan, J. D., Good, N., and McFiggans, G.: A meta-analysis of
3553 particle water uptake reconciliation studies, *Atmos. Chem. Phys.*, 14, 11833-11841, 2014.
3554 Wills, J. B., Knox, K. J., and Reid, J. P.: Optical control and characterisation of aerosol,
3555 *Chem. Phys. Lett.*, 481, 153-165, 2009.
3556 Winkler-Heil, R., Ferron, G., and Hofmann, W.: Calculation of hygroscopic particle
3557 deposition in the human lung, *Inhal. Toxicol.*, 26, 193-206, 2014.
3558 Winkler-Heil, R., Pichelstorfer, L., and Hofmann, W.: Aerosol dynamics model for the
3559 simulation of hygroscopic growth and deposition of inhaled NaCl particles in the human
3560 respiratory tract, *J. Aerosol. Sci.*, 113, 212-226, 2017.
3561 Wise, M. E., Surratt, J. D., Curtis, D. B., Shilling, J. E., and Tolbert, M. A.: Hygroscopic
3562 growth of ammonium sulfate/dicarboxylic acids, *J. Geophys. Res.-Atmos.*, 108, 4638, DOI:
3563 4610.1029/2003JD003775, 2003.
3564 Wise, M. E., Biskos, G., Martin, S. T., Russell, L. M., and Buseck, P. R.: Phase transitions of
3565 single salt particles studied using a transmission electron microscope with an environmental
3566 cell, *Aerosol Sci. Technol.*, 39, 849-856, 2005.
3567 Wise, M. E., Semeniuk, T. A., Bruintjes, R., Martin, S. T., Russell, L. M., and Buseck, P. R.:
3568 Hygroscopic behavior of NaCl-bearing natural aerosol particles using environmental
3569 transmission electron microscopy, *J. Geophys. Res.-Atmos.*, 112, 2007.
3570 Wittmaack, K., and Strigl, M.: Novel Approach to Identifying Supersaturated Metastable
3571 Ambient Aerosol Particles, *Environ. Sci. Technol.*, 39, 8177-8184, 2005.
3572 Wu, H. B., Chan, M. N., and Chan, C. K.: FTIR Characterization of Polymorphic
3573 Transformation of Ammonium Nitrate, *Aerosol Sci. Technol.*, 41, 581-588, 2007.
3574 Wu, Z. J., Nowak, A., Poulain, L., Herrmann, H., and Wiedensohler, A.: Hygroscopic
3575 behavior of atmospherically relevant water-soluble carboxylic salts and their influence on the
3576 water uptake of ammonium sulfate, *Atmos. Chem. Phys.*, 11, 12617-12626, 2011.
3577 Wu, Z. J., Poulain, L., Henning, S., Dieckmann, K., Birmili, W., Merkel, M., van Pinxteren,
3578 D., Spindler, G., Müller, K., Stratmann, F., Herrmann, H., and Wiedensohler, A.: Relating
3579 particle hygroscopicity and CCN activity to chemical composition during the HCCT-2010
3580 field campaign, *Atmos. Chem. Phys.*, 13, 7983-7996, 2013.
3581 Wu, Z. J., Zheng, J., Shang, D. J., Du, Z. F., Wu, Y. S., Zeng, L. M., Wiedensohler, A., and
3582 Hu, M.: Particle hygroscopicity and its link to chemical composition in the urban atmosphere
3583 of Beijing, China, during summertime, *Atmos. Chem. Phys.*, 16, 1123-1138, 2016.
3584 Wu, Z. J., Wang, Y., Tan, T. Y., Zhu, Y. S., Li, M. R., Shang, D. J., Wang, H. C., Lu, K. D.,
3585 Guo, S., Zeng, L. M., and Zhang, Y. H.: Aerosol Liquid Water Driven by Anthropogenic
3586 Inorganic Salts: Implying Its Key Role in Haze Formation over the North China Plain,
3587 *Environ. Sci. Tech. Lett.*, 5, 160-166, 2018.
3588 Xue, H., Khalizov, A. F., Wang, L., Zheng, J., and Zhang, R.: Effects of dicarboxylic acid
3589 coating on the optical properties of soot, *Phys. Chem. Chem. Phys.*, 11, 7869-7875, 2009.
3590 Yamamoto, S., Kendelewicz, T., Newberg, J. T., Ketteler, G., Starr, D. E., Mysak, E. R.,
3591 Andersson, K. J., Ogasawara, H., Bluhm, H., Salmeron, M., Brown, G. E., and Nilsson, A.:
3592 Water Adsorption on α -Fe₂O₃(0001) at near Ambient Conditions, *J. Phys. Chem. C*, 114,
3593 2256-2266, 2010a.
3594 Yamamoto, S., Kendelewicz, T., Newberg, J. T., Ketteler, G., Starr, D. E., Mysak, E. R.,
3595 Andersson, K. J., Ogasawara, H., Bluhm, H., Salmeron, M., Brown, G. E., and Nilsson, A.:



- 3596 Water Adsorption on alpha-Fe₂O₃(0001) at near Ambient Conditions, *J. Phys. Chem. C*, 114,
3597 2256-2266, 2010b.
- 3598 Yang, L. T., Pabalan, R. T., and Juckett, M. R.: Deliquescence relative humidity
3599 measurements using an electrical conductivity method, *J. Solution Chem.*, 35, 583-604, 2006.
- 3600 Ye, X., Tang, C., Yin, Z., Chen, J., Ma, Z., Kong, L., Yang, X., Gao, W., and Geng, F.:
3601 Hygroscopic growth of urban aerosol particles during the 2009 Mirage-Shanghai Campaign,
3602 *Atmos. Environ.*, 64, 263-269, 2013.
- 3603 Ye, X. N., Ma, Z., Hu, D. W., Yang, X., and Chen, J. M.: Size-resolved hygroscopicity of
3604 submicrometer urban aerosols in Shanghai during wintertime, *Atmos. Res.*, 99, 353-364,
3605 2011.
- 3606 Yeşilbaş, M., and Boily, J.-F.: Particle Size Controls on Water Adsorption and Condensation
3607 Regimes at Mineral Surfaces, *Sci. Rep.*, 6, 32136, doi: 32110.31038/srep32136, 2016.
- 3608 Yeung, M. C., Lee, A. K. Y., and Chan, C. K.: Phase Transition and Hygroscopic Properties
3609 of Internally Mixed Ammonium Sulfate and Adipic Acid (AS-AA) Particles by Optical
3610 Microscopic Imaging and Raman Spectroscopy, *Aerosol Sci. Technol.*, 43, 387-399, 2009.
- 3611 Yeung, M. C., and Chan, C. K.: Water Content and Phase Transitions in Particles of
3612 Inorganic and Organic Species and their Mixtures Using Micro-Raman Spectroscopy,
3613 *Aerosol Sci. Technol.*, 44, 269-280, 2010.
- 3614 Yeung, M. C., Ling, T. Y., and Chan, C. K.: Effects of the Polymorphic Transformation of
3615 Glutaric Acid Particles on Their Deliquescence and Hygroscopic Properties, *J. Phys. Chem.*
3616 *A*, 114, 898-903, 2010.
- 3617 Yeung, M. C., Lee, B. P., Li, Y. J., and Chan, C. K.: Simultaneous HTDMA and HR-ToF-
3618 AMS measurements at the HKUST Supersite in Hong Kong in 2011, *J. Geophys. Res.-*
3619 *Atmos.*, 119, 9864-9883, 2014a.
- 3620 Yeung, M. C., Lee, B. P., Li, Y. J., and Chan, C. K.: Simultaneous HTDMA and HR-ToF-
3621 AMS measurements at the HKUST Supersite in Hong Kong in 2011, *J. Geophys. Res.-*
3622 *Atmos.*, 119, 9864-9883, 2014b.
- 3623 You, Y., Renbaum-Wolff, L., Carreras-Sospedra, M., Hanna, S. J., Hiranuma, N., Kamal, S.,
3624 Smith, M. L., Zhang, X. L., Weber, R. J., Shilling, J. E., Dabdub, D., Martin, S. T., and
3625 Bertram, A. K.: Images reveal that atmospheric particles can undergo liquid-liquid phase
3626 separations, *Proc. Natl. Acad. Sci. U. S. A.*, 109, 13188-13193, 2012.
- 3627 You, Y., Smith, M. L., Song, M. J., Martin, S. T., and Bertram, A. K.: Liquid-liquid phase
3628 separation in atmospherically relevant particles consisting of organic species and inorganic
3629 salts, *Int. Rev. Phys. Chem.*, 33, 43-77, 2014.
- 3630 Zardini, A. A., Sjogren, S., Marcolli, C., Krieger, U. K., Gysel, M., Weingartner, E.,
3631 Baltensperger, U., and Peter, T.: A combined particle trap/HTDMA hygroscopicity study of
3632 mixed inorganic/organic aerosol particles, *Atmos. Chem. Phys.*, 8, 5589-5601, 2008.
- 3633 Zawadowicz, M. A., Proud, S. R., Seppäläinen, S. S., and Cziczo, D. J.: Hygroscopic and
3634 phase separation properties of ammonium sulfate/organics/water ternary solutions, *Atmos.*
3635 *Chem. Phys.*, 15, 8975-8986, 2015.
- 3636 Zelenay, V., Ammann, M., Krepelova, A., Birrer, M., Tzvetkov, G., Vernooij, M. G. C.,
3637 Raabe, J., and Huthwelker, T.: Direct observation of water uptake and release in individual
3638 submicrometer sized ammonium sulfate and ammonium sulfate/adipic acid particles using X-
3639 ray microspectroscopy, *J. Aerosol. Sci.*, 42, 38-51, 2011a.
- 3640 Zelenay, V., Huthwelker, T., Krepelova, A., Rudich, Y., and Ammann, M.: Humidity driven
3641 nanoscale chemical separation in complex organic matter, *Environ. Chem.*, 8, 450-460,
3642 2011b.
- 3643 Zeng, G., Kelley, J., Kish, J. D., and Liu, Y.: Temperature-Dependent Deliquescent and
3644 Efflorescent Properties of Methanesulfonate Sodium Studied by ATR-FTIR Spectroscopy, *J.*
3645 *Phys. Chem. A*, 118, 583-591, 2014.



- 3646 Zhang, L., Sun, J. Y., Shen, X. J., Zhang, Y. M., Che, H., Ma, Q. L., Zhang, Y. W., Zhang, X.
3647 Y., and Ogren, J. A.: Observations of relative humidity effects on aerosol light scattering in
3648 the Yangtze River Delta of China, *Atmos. Chem. Phys.*, 15, 8439-8454, 2015.
- 3649 Zhang, Q., Jimenez, J. L., Canagaratna, M. R., Allan, J. D., Coe, H., Ulbrich, I., Alfarra, M.
3650 R., Takami, A., Middlebrook, A. M., Sun, Y. L., Dzepina, K., Dunlea, E., Docherty, K.,
3651 DeCarlo, P. F., Salcedo, D., Onasch, T., Jayne, J. T., Miyoshi, T., Shimojo, A., Hatakeyama,
3652 S., Takegawa, N., Kondo, Y., Schneider, J., Drewnick, F., Borrmann, S., Weimer, S.,
3653 Demerjian, K., Williams, P., Bower, K., Bahreini, R., Cottrell, L., Griffin, R. J., Rautiainen,
3654 J., Sun, J. Y., Zhang, Y. M., and Worsnop, D. R.: Ubiquity and dominance of oxygenated
3655 species in organic aerosols in anthropogenically-influenced Northern Hemisphere
3656 midlatitudes, *Geophys. Res. Lett.*, 34, L13801, DOI: 13810.11029/12007GL029979, 2007.
- 3657 Zhang, Q. N., Zhang, Y., Cai, C., Guo, Y. C., Reid, J. P., and Zhang, Y. H.: In Situ
3658 Observation on the Dynamic Process of Evaporation and Crystallization of Sodium Nitrate
3659 Droplets on a ZnSe Substrate by FTIR-ATR, *J. Phys. Chem. A*, 118, 2728-2737, 2014a.
- 3660 Zhang, X. L., Massoli, P., Quinn, P. K., Bates, T. S., and Cappa, C. D.: Hygroscopic growth
3661 of submicron and supermicron aerosols in the marine boundary layer, *J. Geophys. Res.-*
3662 *Atmos.*, 119, 2013JD021213, doi: 10.1029/2013JD021213, 2014b.
- 3663 Zhang, Y.-H., and Chan, C. K.: Understanding the Hygroscopic Properties of Supersaturated
3664 Droplets of Metal and Ammonium Sulfate Solutions Using Raman Spectroscopy, *J. Phys.*
3665 *Chem. A*, 106, 285-292, 2002a.
- 3666 Zhang, Y. H., and Chan, C. K.: Study of contact ion pairs of supersaturated magnesium
3667 sulfate solutions using raman scattering of levitated single droplets, *J. Phys. Chem. A*, 104,
3668 9191-9196, 2000.
- 3669 Zhang, Y. H., and Chan, C. K.: Understanding the hygroscopic properties of supersaturated
3670 droplets of metal and ammonium sulfate solutions using Raman spectroscopy, *J. Phys. Chem.*
3671 *A*, 106, 285-292, 2002b.
- 3672 Zhang, Y. H., and Chan, C. K.: Observations of water monomers in supersaturated NaClO₄,
3673 LiClO₄, and Mg(ClO₄)₂ droplets using Raman spectroscopy, *J. Phys. Chem. A*, 107, 5956-
3674 5962, 2003.
- 3675 Zhao, D. F.: Gas-aqueous-solid Multiphase Reaction of NO₂ with Individual CaCO₃ Particles
3676 and relevant hygroscopicity and CCN activity, PhD. Thesis, Peking University, Beijing,
3677 2010.
- 3678 Zhao, D. F., Buchholz, A., Kortner, B., Schlag, P., Rubach, F., Fuchs, H., Kiendler-Scharr,
3679 A., Tillmann, R., Wahner, A., Wahner, A., Wahner, A. K., Hallquist, M., Flores, J. M., Rudich, Y.,
3680 Kristensen, K., Hansen, A. M. K., Glasius, M., Kourtev, I., Kalberer, M., and Mentel, T.
3681 F.: Cloud condensation nuclei activity, droplet growth kinetics, and hygroscopicity of
3682 biogenic and anthropogenic secondary organic aerosol (SOA), *Atmos. Chem. Phys.*, 16,
3683 1105-1121, 2016.
- 3684 Zhao, H., Liu, X. F., and Tse, S. D.: Effects of pressure and precursor loading in the flame
3685 synthesis of titania nanoparticles, *J. Aerosol. Sci.*, 40, 919-937, 2009.
- 3686 Zhao, L. J., Zhang, Y. H., Wei, Z. F., Cheng, H., and Li, X. H.: Magnesium sulfate aerosols
3687 studied by FTIR spectroscopy: Hygroscopic properties, supersaturated structures, and
3688 implications for seawater aerosols, *J. Phys. Chem. A*, 110, 951-958, 2006.
- 3689 Zhao, W., Xu, X., Dong, M., Chen, W., Gu, X., Hu, C., Huang, Y., Gao, X., Huang, W., and
3690 Zhang, W.: Development of a cavity-enhanced aerosol albedometer, *Atmos. Meas. Tech.*, 7,
3691 2551-2566, 2014.
- 3692 Zhao, W. X., Xu, X. Z., Fang, B., Zhang, Q. L., Qian, X. D., Wang, S., Liu, P., Zhang, W. J.,
3693 Wang, Z. Z., Liu, D., Huang, Y. B., Venables, D. S., and Chen, W. D.: Development of an
3694 incoherent broad-band cavity-enhanced aerosol extinction spectrometer and its application to
3695 measurement of aerosol optical hygroscopicity, *Appl. Optics*, 56, E16-E22, 2017.



- 3696 Zhou, L., Wang, W. G., and Ge, M. F.: Temperature Dependence of Heterogeneous Uptake
3697 of Hydrogen Peroxide on Silicon Dioxide and Calcium Carbonate, *J. Phys. Chem. A*, 116,
3698 7959-7964, 2012.
- 3699 Zieger, P., Fierz-Schmidhauser, R., Gysel, M., Strom, J., Henne, S., Yttri, K. E.,
3700 Baltensperger, U., and Weingartner, E.: Effects of relative humidity on aerosol light
3701 scattering in the Arctic, *Atmos. Chem. Phys.*, 10, 3875-3890, 2010.
- 3702 Zieger, P., Fierz-Schmidhauser, R., Weingartner, E., and Baltensperger, U.: Effects of
3703 relative humidity on aerosol light scattering: results from different European sites, *Atmos.*
3704 *Chem. Phys.*, 13, 10609-10631, 2013.
- 3705 Zieger, P., Vaisanen, O., Corbin, J. C., Partridge, D. G., Bastelberger, S., Mousavi-Fard, M.,
3706 Rosati, B., Gysel, M., Krieger, U. K., Leck, C., Nenes, A., Riipinen, I., Virtanen, A., and
3707 Salter, M. E.: Revising the hygroscopicity of inorganic sea salt particles, *Nature Comm.*, 8,
3708 15883, doi: 15810.11038/ncomms15883, 2017.
- 3709 Zielinski, A. T., Gallimore, P. J., Griffiths, P. T., Jones, R. L., Seshia, A. A., and Kalberer,
3710 M.: Measuring Aerosol Phase Changes and Hygroscopicity with a Microresonator Mass
3711 Sensor, *Anal. Chem.*, 90, 9716-9724, 2018.
- 3712 Zobrist, B., Soonsin, V., Luo, B. P., Krieger, U. K., Marcolli, C., Peter, T., and Koop, T.:
3713 Ultra-slow water diffusion in aqueous sucrose glasses, *Phys. Chem. Chem. Phys.*, 13, 3514-
3714 3526, 2011.
- 3715 Zuberi, B., Johnson, K. S., Aleks, G. K., Molina, L. T., and Laskin, A.: Hydrophilic
3716 properties of aged soot, *Geophys. Res. Lett.*, 32, L01807, doi: 01810.01029/02004GL021496,
3717 2005.
- 3718 Zuend, A., Marcolli, C., Booth, A. M., Lienhard, D. M., Soonsin, V., Krieger, U. K.,
3719 Topping, D. O., McFiggans, G., Peter, T., and Seinfeld, J. H.: New and extended
3720 parameterization of the thermodynamic model AIOMFAC: calculation of activity coefficients
3721 for organic-inorganic mixtures containing carboxyl, hydroxyl, carbonyl, ether, ester, alkenyl,
3722 alkyl, and aromatic functional groups, *Atmos. Chem. Phys.*, 11, 9155-9206, 2011.
- 3723